Reviews of Geophysics

REVIEW ARTICLE
10.1029/2020RG000706

**Key Points:**
- Most known OFG is located at water depths of <100 m within 55 km of the coast, hosted in siliciclastic aquifers in passive margins
- Key gaps in knowledge include the extent and function of OFG systems, as well as the mechanism and timing of emplacement
- Isotopic tracers, jointly inverted geophysical data and 3-D hydrological models can help address these knowledge gaps

**Supporting Information:**
- Supporting Information S1

**Correspondence to:**
A. Micallef,
amicallef@geomar.de

**Citation:**
Micallef, A., Person, M., Berndt, C., Bertoni, C., Cohen, D., Dugan, B., et al. (2020). Offshore freshened groundwater in continental margins. *Reviews of Geophysics*, *58*, e2020RG000706. https://doi.org/10.1029/2020RG000706

Received 15 JUN 2020
Accepted 15 NOV 2020
Accepted article online 20 NOV 2020



# Offshore Freshened Groundwater in Continental Margins

**Aaron Micallef[1,2], Mark Person[3], Christian Berndt[1], Claudia Bertoni[4], Denis Cohen[2], Brandon Dugan[5], Rob Evans[6], Amir Haroon[1], Christian Hensen[1], Marion Jegen[1], Kerry Key[7], Henk Kooi[8], Volker Liebetrau[1], Johanna Lofi[9], Brian J. Mailloux[10], Renée Martin-Nagle[11], Holly A. Michael[12], Thomas Müller[1,13], Mark Schmidt[1], Katrin Schwalenberg[14], Elizabeth Trembath-Reichert[15], Bradley Weymer[1], Yipeng Zhang[2], and Ariel T. Thomas[16]**

[1]Helmholtz Centre for Ocean Research, GEOMAR, Kiel, Germany, [2]Marine Geology and Seafloor Surveying, Department of Geosciences, University of Malta, Msida, Malta, [3]Hydrology Program, New Mexico Institute of Mining and Technology, Socorro, NM, USA, [4]Department of Earth Science, University of Oxford, Oxford, UK, [5]Department of Geophysics, School of Mines, Golden, CO, USA, [6]Geology and Geophysics, Woods Hole Oceanographic Institution, Woods Hole, MA, USA, [7]Lamont-Doherty Earth Observatory, Columbia University, New York, NY, USA, [8]Deltares Research Institute, Utrecht, Netherlands, [9]University of Montpellier, CNRS, University of the Antilles, Montpellier, France, [10]Barnard College, Columbia University, New York, NY, USA, [11]A Ripple Effect, Rockville, Maryland, USA, [12]Departments of Earth Sciences and Civil and Environmental Engineering, University of Delaware, Newark, DE, USA, [13]Helmholtz Centre for Environmental Research, UFZ, Leipzig, Germany, [14]Federal Institute for Geosciences and Natural Resources (BGR), Hannover, Germany, [15]School of Earth and Space Exploration, Arizona State University, Tempe, AZ, USA, [16]Institute for Applied Geophysics and Geothermal Energy, RWTH, Aachen University, Aachen, Germany

**Abstract** First reported in the 1960s, offshore freshened groundwater (OFG) has now been documented in most continental margins around the world. In this review we compile a database documenting OFG occurrences and analyze it to establish the general characteristics and controlling factors. We also assess methods used to map and characterize OFG, identify major knowledge gaps, and propose strategies to address them. OFG has a global volume of $1 \times 10^6$ km$^3$; it predominantly occurs within 55 km of the coast and down to a water depth of 100 m. OFG is mainly hosted within siliciclastic aquifers on passive margins and recharged by meteoric water during Pleistocene sea level lowstands. Key factors influencing OFG distribution are topography-driven flow, salinization via haline convection, permeability contrasts, and the continuity/connectivity of permeable and confining strata. Geochemical and stable isotope measurements of pore waters from boreholes have provided insights into OFG emplacement mechanisms, while recent advances in seismic reflection profiling, electromagnetic surveying, and numerical models have improved our understanding of OFG geometry and controls. Key knowledge gaps, such as the extent and function of OFG, and the timing of their emplacement, can be addressed by the application of isotopic age tracers, joint inversion of electromagnetic and seismic reflection data, and development of three-dimensional hydrological models. We show that such advances, combined with site-specific modeling, are necessary to assess the potential use of OFG as an unconventional source of water and its role in sub-seafloor geomicrobiology.

**Plain Language Summary** This review paper considers offshore freshened groundwater (OFG), which is water hosted in sediments and rocks below the seafloor, with a total dissolved solid concentration lower than seawater. We have compiled >300 records to demonstrate that freshened groundwater occurs offshore on most continents around the world and has a global volume of $1 \times 10^6$ km$^3$. The majority of OFG was deposited when sea level was lower than today and is hosted in sandy sub-seafloor layers that are located within 55 km of coasts in water depths less than 100 m. We present a range of geochemical, geophysical, and modeling approaches that have successfully been used to investigate OFG systems. We also propose approaches to address key scientific questions related to OFG, including whether it may be used as an unconventional source of potable water in coastal areas.

## 1. Introduction

Offshore freshened groundwater (OFG) is water stored in pores of sediments and fractures of rocks in the sub-seafloor and with a total dissolved solid (TDS) concentration below that of seawater. OFG was first

**Table 1**
*List of Review Studies Focusing on Various Aspects of Marine Hydrogeology in a Range of Geological Settings*

| Process/topic | Environment | Reference |
|---|---|---|
| Clay dehydration and sediment compaction | Convergent margins | Kastner et al. (1991) |
| Hydrothermal circulation | Mid-ocean ridge and ridge flanks | Fisher (1998) |
| Geothermal convection | Passive margins | Wilson (2005) |
| Tools and techniques in marine hydrogeology | Spreading centers, mid-plate locations, continental margins | Fisher (2005) |
| Focused fluid flow | Passive margins | Berndt (2005) |
| Numerical modeling of flow and transport processes | Basement-sediment systems, subduction zones, and passive margins | Screaton (2010) |
| Overpressure generation | Passive margins | Dugan and Sheahan (2012) |
| Offshore freshened groundwater | Passive and convergent margins | Post, Groen, et al. (2013) |
| Submarine groundwater discharge | Passive and convergent margins | Moosdorf and Oehler (2017; Taniguchi et al. (2019) |

documented 60 years ago offshore of the Florida coast (Kohout, 1964). Twenty years later, during a petroleum resource assessment expedition of the U.S. Atlantic continental shelf, 19 wells were drilled in the seafloor offshore of Georgia to New England, in water depths of 20–300 m. While the shelf was found to host a small amount of hydrocarbons, OFG was found in many of these wells up to a distance of 100 km from the coastline (Hathaway et al., 1979). Since then, OFG has been documented in most continental margins, and there has been growing interest in the study of the architecture, flow, and emplacement dynamics of OFG systems (Post, Groen, et al., 2013). The estimated global volume of OFG is on the order of $10^5$ to $10^6$ km$^3$ (Adkins et al., 2002; D. Cohen et al., 2010; Post, Groen, et al., 2013). These estimates are highly uncertain, considering that they are entirely based on constant freshwater volume per unit width of shoreline, aquifer thickness, and porosity in passive continental margins. In comparison, the estimated global volume of groundwater in the upper 2 km of the continental crust onshore is $22.6 \times 10^6$ km$^3$ (Gleeson et al., 2016).

The interest in OFG systems is largely driven by their proposed use as an unconventional source of water in coastal areas, where groundwater resources are being rapidly depleted or contaminated (Bakken et al., 2012; UN-Water, 2020) or to improve recovery in the petroleum industry (Person et al., 2017). The mechanisms that lead to OFG, whether complex geologic structure or disequilibrium with present-day sea level due to slow transition since the Pleistocene, influence the past and future function of the systems and thus their potential for use. For systems in transition, an improved understanding of the evolution of OFG can provide better constraints on fluid migration histories in continental margins, which is relevant to offshore industries (e.g., resource exploration and carbon dioxide sequestration), as well as environmental change and human migration patterns in the past (Bailey & King, 2011; Morrissey et al., 2010). OFG also plays a key role in biogeochemical fluxes to the ocean (Michael et al., 2016; Wilson, 2003), and it has a direct impact on benthic and sub-seafloor ecology (W. S. Moore, 2010).

In the last 30 years, a number of review studies have considered different aspects of marine hydrogeology in a range of geologic settings (Table 1). The most comprehensive review of OFG was published by Post, Groen, et al. (2013). These authors demonstrated how OFG systems are a global phenomenon and reviewed the key mechanisms that promote the emplacement and preservation of these systems. Post, Groen, et al. (2013) also identified fields of research that would benefit from an improved understanding of OFG processes. Edmunds and Milne (2001), on the other hand, compiled a review of palaeowaters along European coastlines, some of which suggest potential extension offshore.

Our review paper is motivated by the significant advances in OFG research and the increasingly cross-disciplinary nature of OFG studies in the last decade. Here we update the global database of OFG records in Post, Groen, et al. (2013) and analyze this in the context of recent and past studies to (i) establish the current understanding of the general characteristics, emplacement mechanisms, and controlling factors of OFG in continental margins; (ii) present the geophysical, geochemical, and modeling approaches that are currently used to detect and characterize OFG; (iii) identify the major knowledge gaps and uncertainties that exist with respect to the above and make recommendations on how these should be addressed; and (iv) explore two frontier applications of OFG research (exploitation as a water resource and geomicrobiology) that will benefit from an improved understanding of OFG.

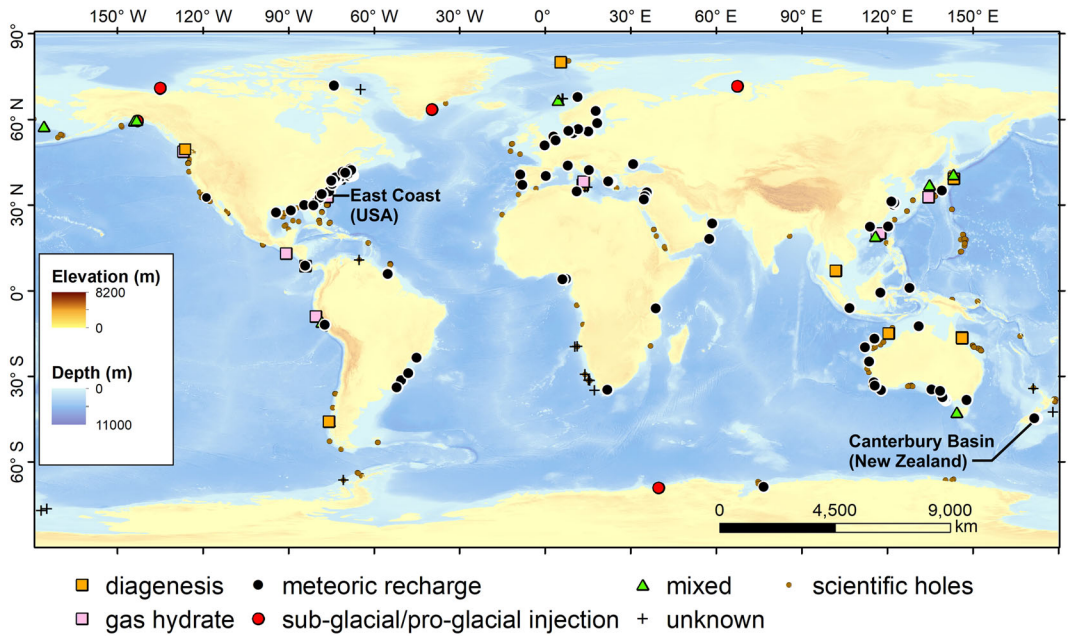


**Figure 1.** Map of OFG records and emplacement mechanisms. "Mixed" refers to two or more reported emplacement mechanisms. Scientific holes refer to sites drilled by the International Ocean Discovery Program (IODP), Ocean Drilling Program (ODP), and Deep Sea Drilling Project (DSDP) in continental margins with no record of OFG. Locations of case studies in section 3.5 are shown. Source of elevation and depth data: GEBCO.

In this study we use practical salinity units (PSU) to define groundwater TDS concentrations. PSU is analogous to parts per thousand TDS concentration. Brackish water has a concentration of 0.5–33 PSU. Majority refers to >50% occurrence.

## 2. Characteristics and Controls of OFG in Continental Margins

We establish the general characteristics, emplacement mechanisms, and controlling factors of OFG systems by compiling a database of 305 records of groundwater located in continental margins (Micallef, 2020). The criteria for including records in this database include salinities of ≤33 PSU, a location of ≥1 km away from the coast, and a distance of >10 km from other records (Figure 1). The majority of the information (84.6%) is sourced from borehole and core data. The rest is derived from marine electromagnetic (EM) surveys, observations of submarine groundwater discharge (SGD), and potential onshore indicators (e.g., fresh coastal groundwater dating to last glacial period; semi-confined coastal aquifers where [i] the onshore piezometric head is larger than the equivalent freshwater head or [ii] where the onshore freshwater is close to the shoreline despite the piezometric head being smaller than the equivalent freshwater head; Knight et al., 2018; Post, Groen, et al., 2013). For each record we extracted a number of characteristics (Micallef, 2020). The results of a statistical analysis of these characteristics are presented in Table 2.

### 2.1. Emplacement Mechanisms

Five main mechanisms are known to be responsible for the emplacement of OFG (Figure 1 and Table 2):

1. *Active, present-day meteoric recharge via permeable connections between offshore and onshore aquifers* (Bakalowicz, 2014; Hong et al., 2019; Johnston, 1983; Kooi & Groen, 2001; Michael et al., 2016; Varma & Michael, 2012). In these aquifers, fresh groundwater is prevented from discharging at the coastline due to confined conditions or geologic heterogeneity, which promote offshore flow and diffuse or focused SGD.
2. *Meteoric recharge during sea level lowstands*: Relict bodies of OFG have been documented in areas where active recharge is not possible, due to either a lack of a hydraulic connection with an onshore aquifer or a low onshore hydraulic head (Edmunds & Milne, 2001; Jiráková et al., 2011; Post, Groen, et al., 2013; Thomas et al., 2019; Zhang et al., 2018). Recharge occurs primarily during glacial periods via enhanced

**Table 2**

*Characteristics of OFG Bodies, Derived From a Statistical Analysis of Records in the Database (Micallef, 2020)*

| **Margin type (n = 305)** | | | | | | | | | |
|---|---|---|---|---|---|---|---|---|---|
| Passive | | | | Active | | | | | |
| 73% | | | | 27% | | | | | |
| **Minimum salinity of OFG (PSU; n = 258)** | | | | | | | | | |
| 0-4.9 | 5-9.9 | 10-14.9 | 15-19.9 | 20-24.9 | 25-29.9 | 30-33 | | | |
| 54.6% | 9.7% | 3.1% | 4.7% | 2.7% | 9.1% | 16.1% | | | |
| **Data source (n = 305)** | | | | | | | | | |
| Borehole | Core | Electromagnetic surveying | Onshore indicators | SGD observations | | | | | |
| 84.6% | 1.3% | 2.3% | 5.8% | 6.0% | | | | | |
| **Offshore distance (km; n = 239)** | | | | | | | | | |
| 0-24 | 25-49 | 50-74 | 75-99 | 100-124 | 125-149 | 150-174 | 175-199 | 200-750 | |
| 30.5% | 11.7% | 15.5% | 7.5% | 18.8% | 2.9% | 2.1% | 1.7% | 9.2% | |

*OFG with a gas hydrate and diagenetic origin has been recorded up to a distance of 720 km (388 nm; IODP Expedition 323 site 1343, Bering Sea); OFG with a meteoric origin has been documented up to a distance of 473 km (255 nm; ODP122 site 760, NW Australia).*

| **Seafloor depth (m; n = 284)** | | | | | | | | | | | |
|---|---|---|---|---|---|---|---|---|---|---|---|
| 0-24 | 25–49 | 50-74 | 75-99 | 100-124 | 125-149 | 150-499 | 500-999 | 1000-1499 | 1500-1999 | 2000-2499 | 2500-3100 |
| 11.3% | 4.2% | 28.2% | 4.2% | 21.5% | 0% | 10.2% | 8.5% | 5.4% | 2.5% | 2.2% | 1.8% |

*The deepest OFG record is at a depth of 3071 m (ODP112 site 683, offshore Peru) and is related to gas hydrate decomposition. For OFG with meteoric origin, the deepest record is 1970 m (ODP122 site 760, NW Australia).*

| **Sub-seafloor depth (top of OFG body/bodies, in m; n = 262) [a]** | | | | | | | | | | | |
|---|---|---|---|---|---|---|---|---|---|---|---|
| 0-24 | 25–49 | 50-74 | 75-99 | 100-199 | 200-499 | 500-999 | 1000-1499 | 1500-1999 | 2000-2499 | 2500-2999 | 3000-6000 |
| 19.8 % | 6.5% | 8.4% | 3.1% | 9.9% | 6.5% | 22.1% | 6.9% | 7.6% | 0.% | 0.4% | 8.8% |
| **Sub-seafloor depth (base of OFG body/bodies, in m; n = 238) [a]** | | | | | | | | | | | |
| 0-24 | 25–49 | 50-74 | 75-99 | 100-199 | 200-499 | 500-999 | 1000-1499 | 1500-1999 | 2000-2499 | 2500-2999 | 3000-6000 |
| 2.9% | 5.0% | 0% | 1.7% | 5.9% | 18.9% | 10.9 % | 2.1% | 0% | 4.2% | 2.5% | 27.3% |
| **Total thickness of OFG (in m; n = 242) [b]** | | | | | | | | | | | |
| 0-249 | 250-499 | 500-749 | 750-999 | 1000-1249 | 1250-1499 | 1500-1749 | 1750-1999 | 2000-2249 | 2250-2499 | 2500-2749 | 2750-3000 |
| 26.4 % | 12.4% | 6.6% | 1.7% | 18.2 % | 0.% | 2.5% | 4.1% | 23.6% | 0% | 4.5% | 0% |

| **Number of OFG bodies (n = 143)** | |
|---|---|
| One | Multiple |
| 43.4% | 56.6% |

| **Geology of aquifer hosting OFG (n = 267)** | | | | | | | |
|---|---|---|---|---|---|---|---|
| Clay | Crystalline | Diamict | Gravel | Limestone | Mixed [c] | Sand | Silt |
| 18.7% | 0.7% | 1.1% | 1.1% | 6.0% | 27.7% | 43.4% | 1.3% |

| **Porosity (%) of aquifer hosting OFG (n = 96) [d]** | | | | | | | | |
|---|---|---|---|---|---|---|---|---|
| 0-10 | 10.1-20 | 20.1-30 | 30.1-40 | 40.1-50 | 50.1-60 | 60.1-70 | 70.1-80 | 80.1-90 |
| 9.6% | 2.4% | 12.4% | 17.4% | 21.8% | 17.8% | 12.6% | 4.4% | 1.6% |

| **Emplacement mechanism inferred by author/s (n = 305)** | | | | | | | | | |
|---|---|---|---|---|---|---|---|---|---|
| Diagenesis | Gas hydrate decomposition | Meteoric | | | Glacial | | | Mixed [e] | Other | Unknown |
| 10.2 % | 3.0% | 72.8% | | | 3.6% | | | 3.9% | 0.7% | 5.9% |
| | | Undefined | Active recharge | Palaeo recharge | Active + palaeo recharge | Active recharge | Palaeo recharge | | | |
| | | 36.1 % | 3.3% | 33.4 % | 1.3% | 0.7% | 1.6% | | | |

*Note*. "*n*" represents number of records considered to estimate percentages.
[a]Top and base of an OFG body are delimited by peaks in the salinity profile; an OFG body comprises the lower salinity body in between. [b]Difference in depth between top and base of OFG body/bodies. [c]Refers to two or more types of rock or sediment. [d]Representative of the ranges of types/values of the borehole/core intervals in which OFG occurs. [e]Refers to two or more reported mechanisms.

topographically driven flow of freshwater from recharge areas located above sea level, due to higher hydraulic heads and steeper hydraulic gradients (D. Cohen et al., 2010; Essaid, 1990; Faure et al., 2002; Groen, Velstra, & Meesters, 2000; Meisler et al., 1984; Micallef et al., 2020; Person et al., 2003; Sanford & Buapeng, 1996), localized vertical recharge via gaps in confining units on exposed continental shelves (Bakker, 2006; Kooi et al., 2000; Kooi & Groen, 2001), and recharge from river and freshwater lake systems (Middelburg & de Lange, 1989; Southgate & Möller, 2000; Voris, 2000; Zamrsky et al., 2020).

3. *Sub-glacial and pro-glacial injection*: Groundwater dating, stable isotope data, and 3-D variable-density numerical model simulations have demonstrated that sub-ice-sheet recharge can re-organize sub-surface flow systems across a continental shelf via a number of mechanisms (DeFoor et al., 2011; Person et al., 2012; Siegel et al., 2014; van Geldern et al., 2014). These include sub-glacial melting, sub-glacial drainage networks, reversal of groundwater flow direction with respect to modern flow patterns, the formation of pro-glacial lakes in front of ice sheets, permeability reduction associated with permafrost formation, and the focusing of groundwater to ice-free discharge zones (Hooke, 1998; Lemieux et al., 2008a, 2008b, 2008c; Marksammer et al., 2007; Mulligan & Uchupi, 2003; Person et al., 2003; Person et al., 2012; Uchupi et al., 2001). Estimates of freshwater recharge rates in ice-covered continental shelves can be 2 to 10 times higher than modern values (Person et al., 2007).
4. *Diagenesis*: Post-sedimentary alteration processes can lead to the release of freshwater and the formation of freshened water fronts in deeply buried marine sediments or in high pressure and temperature conditions in convergent margins. Diagenesis of minerals such as silica (from Opal A to Opal CT; from Opal CT to quartz), gypsum (dehydration to anhydrite), and clay (transformation of smectite to illite) are responsible for pore water freshening in marine sediments (Bekins et al., 1994; Brown et al., 2001; Dählmann & De Lange, 2003; Hensen et al., 2004; Hupers & Kopf, 2012; Ijiri et al., 2018; Jowett et al., 1993; Kastner et al., 1991; Kastner & Gieskes, 1983; J. C. Moore & Saffer, 2001; Mora, 2005; Myhre et al., 1995; Swart et al., 1993).
5. *Decomposition of gas hydrates*: Gas hydrates are ice-like crystalline clathrate compounds made up of natural gas molecules encased in a lattice of water molecules. Formation of hydrates excludes salt ions from the crystal structure. When gas hydrates decompose as a result of changing temperatures or pressures, low salinity pore water is released (Hesse, 2003; Hesse & Harrison, 1981; Lin et al., 2010; Malinverno et al., 2008; Mora, 2005).

Meteoric recharge during sea level lowstands is the most common OFG emplacement process reported in the literature (33.4%), although 36.1% of the records do not distinguish between active and palaeo-meteoric recharge (Table 2). The second most common process emplacing OFG is diagenesis (10.2%). OFG emplaced by multiple mechanisms makes up 3.9% of our records.

Two additional mechanisms play a minor role in OFG emplacement. These include entrapment of connate water in subsiding basins (Haq et al., 1990; Ingle et al., 1989; Ruden, 2009) and landslides. There is one record of a coastal sediment slab hosting fresh to brackish water that slid into the Norwegian Basin 12–15 ka BP and that preserved the pore water composition (De Lange, 1983).

### 2.2. Spatial, Hydrological, and Geochemical Characteristics

The majority of OFG bodies in our database share the following characteristics: (i) They occur within 55 km of the coast and down to a water depth of 100 m, (ii) the top is located between 0 and 200 m below the seafloor, and (iii) they comprise multiple OFG bodies that collectively are <1 km thick (Figure 2 and Table 2).

OFG has been documented in most continental margins, with 73% of the records located in passive margins and 27% in active margins (Table 2). Passive margins tend to have thicker OFG bodies, whereas active margins have a larger fraction of OFG bodies in deeper waters. The deepest OFG occurrences in terms of seafloor depth (>1,750 m; $n = 15$) are predominantly in convergent margins, where they have minimum salinities of >15 PSU and were emplaced by diagenesis and/or gas hydrate decomposition. The U.S. Atlantic margin features the highest number of OFG records, followed by NW Europe and Australia. OFG has not been documented along the margins of NW Africa and the Indian sub-continent. This does not necessarily indicate an absence of OFG but is more likely a result of the spatial bias in drilling operations and geophysical surveys or the difficulty in accessing data in these regions.

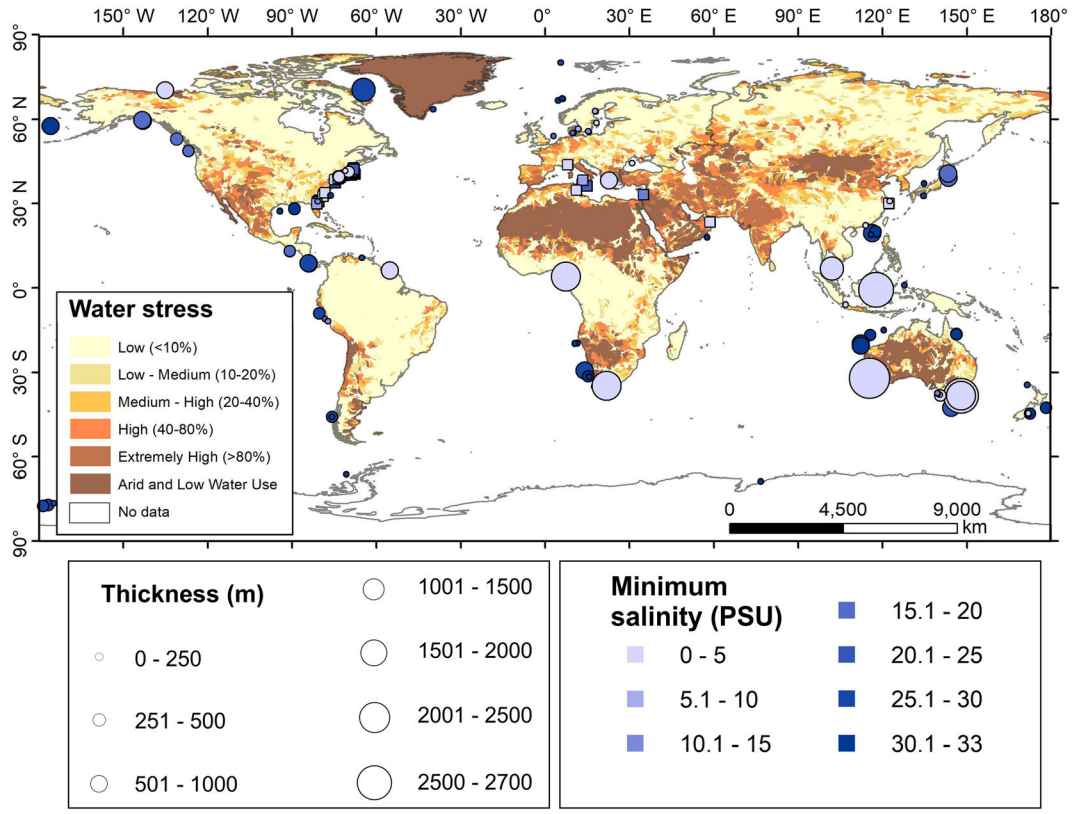


**Figure 2.** OFG thickness and minimum salinity plotted on a global map of water stress (source: Hofste et al., 2019). Square symbols denote sites where OFG thickness could not be determined.

The 54.6% of OFG records have minimum salinities of <5 PSU (Figure 2 and Table 2), and the majority of these are meteoric in origin. For OFG bodies <1 km thick, the minimum salinity ranges between 0 and 33 PSU, with a mean of 15 PSU. The transition from high salinities to the lower salinities at the top of OFG bodies is commonly characterized by higher gradients (0.16 PSU/m ± 0.36) than the transition from low salinities to higher salinities at the base (0.08 PSU/m ± 0.09). Chloride and sodium are generally the most important contributors to salinity change.

## 2.3. Controlling Factors

### 2.3.1. Geological Factors

The lithology and tectonic setting play an important role in the evolution of offshore hydrogeological systems.

OFG bodies occur in both siliciclastic and carbonate systems (Table 2 and Figure 3). The majority of OFG bodies are hosted in siliciclastic aquifers (sands to clays, with the majority in sands) with porosities between 30% and 60%. The thickest OFG bodies occur in sandy and mixed aquifers. The depositional environment of these aquifers is predominantly clastic sedimentary (especially shelf to slope settings).

The original depositional architecture is very important for controlling the permeability distribution of the margin, and as a result the flow, distribution, and volume of OFG. The persistence of OFG, regardless of the emplacement mechanism, is promoted by a geologic feature that prevents nearshore discharge of freshwater. We generally observe that the top of most OFG bodies coincides with a permeability contrast associated with a change from fine- to coarse-grained sediments (predominantly clay to sand) in a downward direction, with the OFG hosted in the coarser material (Micallef, 2020) (Figure 3a). Extensive, low-permeability aquitards have trapped freshwater emplaced during periods of sea level lowstands in inner and middle shelf regions (Bratton, 2007; K. M. Cohen & Lobo, 2013; Ehlers & Gibbard, 2004; Groen, Kooi,

et al., 2000; Gustafson et al., 2019; Hanebuth et al., 2002; Jiao et al., 2015; Kwong & Jiao, 2016; Marksammer et al., 2007; Reijenstein et al., 2011; Thomas et al., 2019; Uchupi et al., 2001; Zamrsky et al., 2020). Analytical and modeling studies provide further support that such a sedimentary architecture is conducive to OFG preservation (Knight et al., 2018; Kooi & Groen, 2001; Langevin et al., 2008; Michael et al., 2016; Morgan et al., 2018; Solorzano-Rivas & Werner, 2018; Thomas et al., 2019; Van Engelen et al., 2018). The base of most OFG bodies coincides with a change from coarse- to fine-grained sediments (predominantly sand to clay) (Micallef, 2020).

The continuity or connectivity of permeable and confining strata are important constraints on the extent of OFG systems. Strong anisotropy in hydraulic conductivity, and well-connected high-permeability zones or preferential flow paths, can move the freshwater-saltwater interface offshore and facilitate the extension of OFG bodies tens to hundreds of kilometers from the coastline, even in steady state conditions (Houben et al., 2018; Li et al., 2016; Michael et al., 2016; Paldor et al., 2020). Clinoform structures may provide heterogeneous conduit systems for OFG flow (Gustafson et al., 2019), whereas buried palaeochannels infilled with high-permeability sediments are sometimes essential to explain OFG in the outer parts of the continental shelf (Groen, Kooi, et al., 2000; Krantz et al., 2004; Micallef et al., 2020) (Figure 3a). Where such palaeochannels incise an aquitard, freshwater-saltwater mixing via saltwater intrusion or SGD is facilitated (Lofi, Pezard, et al., 2013; Mulligan et al., 2007). Seafloor erosion (e.g., submarine canyons) may expose offshore freshwater aquifers and promote fresh SGD (Lin et al., 2010; Paldor et al., 2020) or facilitate saltwater intrusion (Foyle et al., 2002).

Permeable faults can provide preferential pathways for OFG flow and emplacement (Grasby et al., 2009; Stakes et al., 1999; Varma & Michael, 2012) (Figure 3). On the other hand, faults can act as a source of salinization of shallow groundwater due to the flow of saline water along faults from underlying overpressured sediment (Gustafson et al., 2019; van Geldern et al., 2013). Faults can also act as barriers to lateral flow, as a result of displacement and steepening of the permeable strata, and/or clay smearing, and reduce the extent of OFG bodies and the rate of inland interface movement (Bense & Van Balen, 2004; Edwards et al., 2009; Morgan et al., 2018).

Facies distribution and sedimentary processes in siliciclastic margins have direct implications for offshore hydrogeology (Figure 3a). Especially in their proximal part, siliciclastic margins comprise gravels to muds that are predominantly delivered by fluvial discharge and glaciers, deposited from suspension and gravity flows. Past sea level changes modulate the offshore reach of topographically driven groundwater, and this can be reconstructed by mapping the offshore extent of buried continental and nearshore facies (Figure 3a). There is a general increase in low-permeability sediments from nearshore to offshore, and this plays an important role in the connectivity of aquifers, their offshore extent, and the preservation of OFG (e.g., Micallef et al., 2020; Siegel et al., 2014). Overpressures may develop due to linkages to onshore topography (artesian conditions) and glacial loading and by compaction in unconsolidated sediments with high compressibility and low permeability. Compaction-driven, overpressure-related flow can dominate over nearshore topographically driven meteoric flow in low-permeability offshore units during periods of rapid sedimentation, driving flow shoreward (Dugan & Flemings, 2000; Kooi et al., 2000) and generating artesian groundwater heads in deep coastal aquifers (Groen, 1998; Kooi, 1999).

Whereas carbonate margins dominated by autochthonous and biologically constructed limestones have a strong degree of stratigraphic heterogeneity, carbonate margins dominated by allochtonous sediments tend to be more similar to siliciclastic margins (Figure 3). Predominantly consisting of calcite precipitated by biotic and abiotic processes, sediments in carbonate margins vary from boulders to mud (Tucker & Wright, 1990). Water-rock interactions can create a permeability architecture that is highly heterogeneous, with permeability varying over many orders of magnitude (e.g., Legrand & Stringfield, 1971; Mazzullo, 2004; Sanford & Konikow, 1989). Dissolution, for example, can generate preferential flow paths that enhance groundwater exchange and its extension offshore (Back et al., 1979; Dimova et al., 2012; Evans & Lizarralde, 2003; Johnston, 1983; Lofi et al., 2012; Paull et al., 1990; Spechler, 1994; Swarzenski & Reich, 2000; Xu et al., 2016) (Figure 3b). Other diagenetic processes, such as micritization and dolomitization, as well as breccia emplacement by slope failure, can also significantly influence porosity and permeability variability in carbonate margins (Armitage et al., 2018; Moshier, 1989) (Figure 3b). Lava tubes can provide similar preferential flow pathways to karst conduits in volcanic settings (Attias et al., 2020; Kreyns et al., 2020).

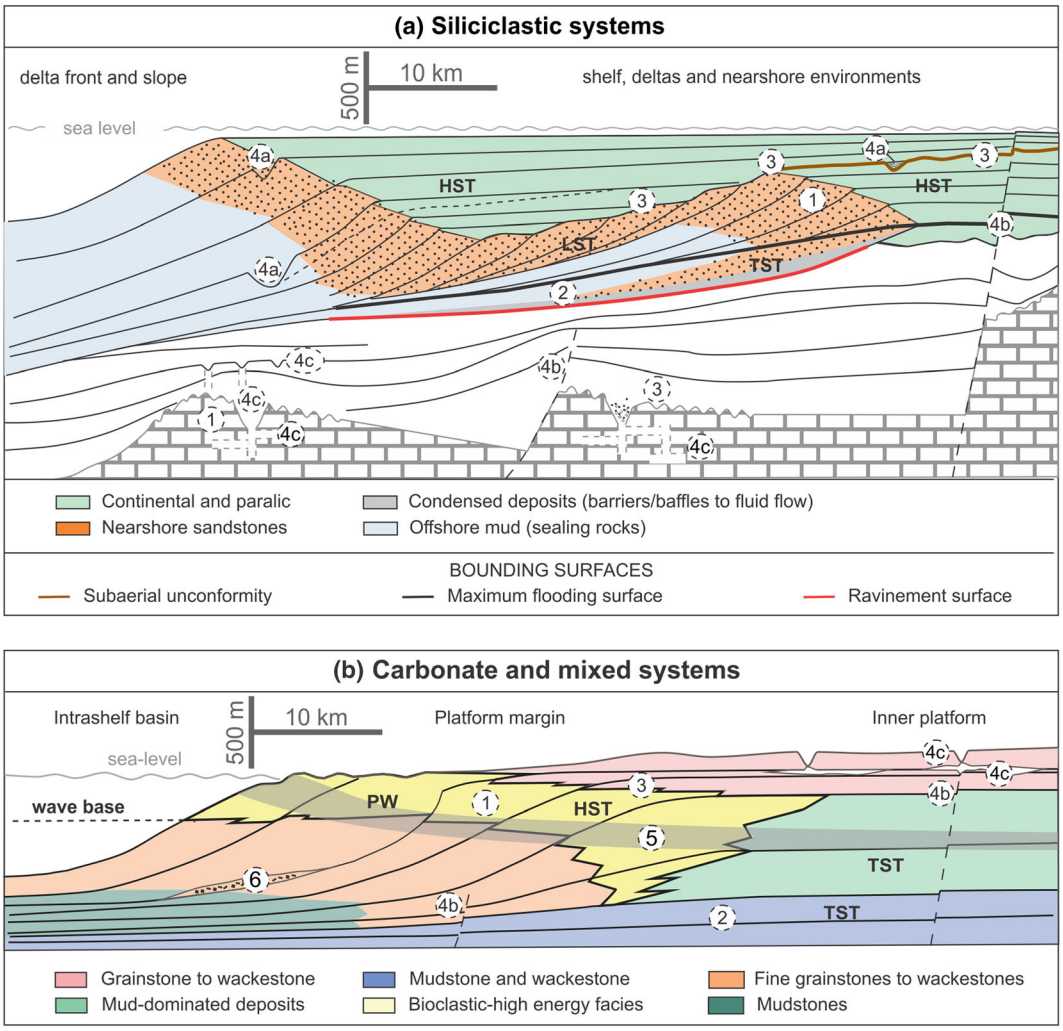


**Figure 3.** Simplified diagram of facies distribution and sedimentary processes in siliciclastic and carbonate margins, with a focus on structures that have hydrogeological relevance (modified after Bertoni et al., 2020). Sequence stratigraphic surfaces, facies contacts, and systems tracts for a (a) siliciclastic shelf setting (modified from Zecchin & Catuneanu, 2013), overlying a deeper carbonate basement, and (b) carbonate margin (modified from Razin et al., 2010). An indicative scale is included. 1: high-permeability sediments (aquifer); 2: low-permeability aquitard, such as fine-grained sediments or condensed deposits; 3: palaeo-continental environments or subaerial exposure, palaeo-coastline; 4: flow pathways: 4a: valleys or canyons on the shelf or slope, 4b: faults, and 4c: karstic caves, pockmarks, and collapse structures; 5: mixed-zone diagenesis; 6: slope failure breccia. Sequence stratigraphic systems tracts: HST: Highstand systems tract, TST: Transgressive systems tract, PW: Prograding wedge, LST: Lowstand systems tract.

### 2.3.2. Hydrological Factors

Topography-driven flow is one of the most important mechanisms driving freshwater offshore; its impact is determined by topographic gradients and modulated by the amplitude of sea level fluctuations (Kooi, 1999; Meisler et al., 1984; Voss & Souza, 1987). During sea level lowstands, shore-normal hydraulic gradients are enhanced. Seafloor exposure during sea level lowstands extended areas for terrestrial groundwater recharge (by up to 5% globally for the Last Glacial Maximum; Adkins et al., 2002). Meisler et al. (1984) show that the position of the mixing zone off New England reflects sea levels that were 50–100 m lower than at present, which corresponds to the mean Pleistocene sea level.

Large-scale groundwater systems are slow to adapt to rapid sea level changes (Edmunds & Milne, 2001). As sea level rose after the Last Glacial Maximum, seawater overtopped OFG bodies because the landward migration of the freshwater-seawater interface was slower (<10 km per 10 ka) than the sea level rise

(>35 km per 10 ka) (Cronin, 2012; Harrar et al., 2001; Meisler et al., 1984; Person et al., 2003; Post, Groen, et al., 2013). As a result, relict OFG bodies have been slowly salinizing via haline convection—defined as circulation driven by density gradients created by salinity variations—as a result of the landward movement of the freshwater-seawater interface and diffusion of salt from adjacent and overlying strata (Adkins et al., 2002; D. Cohen et al., 2010; Groen, Velstra, & Meesters, 2000; Hathaway et al., 1979; Kooi et al., 2000; Post, Groen, et al., 2013; Post & Kooi, 2003). A mixing zone affected by buoyancy forces separates OFG bodies from seawater (D. Cohen et al., 2010; Essaid, 1990; Groen, Velstra, & Meesters, 2000; Kohout, 1965; Kooi et al., 2000; Laattoe et al., 2013; Middelburg & de Lange, 1989; Post, Groen, et al., 2013). Development of such a mixing zone is hampered if the OFG is overlain by an aquitard (Morgan et al., 2018), although salinization of the aquitard can lead to salinization of the underlying OFG (Kooi et al., 2000; Kooi & Groen, 2001; Solorzano-Rivas & Werner, 2018). OFG contamination rates by saltwater can be slow, and diffusion time depends on the thickness and permeability of the confining unit and its solute diffusivity. As an example, the salinity of a 100-m-thick aquitard full of freshwater was modeled to increase to 20% of modern seawater salinity over 1 Ma by vertical diffusive transport (Harrar et al., 2001). In a density-driven system, upwelling freshwater discharge driven by buoyancy forces is balanced by downwelling fingers of saltwater (Greskowiak, 2014). Density-driven flow of saltwater via salt fingering has an estimated velocity of 2 m per 1 ka (Bakken et al., 2012). Faster speeds and convective mixing are expected for more permeable strata.

Geothermal convection, which involves regional circulation of groundwater due to thermally induced buoyancy, plays an important role in driving groundwater flow and seawater recirculation (Bratton, 2010; Caspard et al., 2004; Hughes et al., 2009, 2007; Kohout, 1965; Wilson, 2003, 2005). Although geothermal convection tends to be stronger beneath the continental slope, it may interact with topographically driven meteoric systems in narrow continental shelves (Wilson, 2005).

As mentioned in section 2.1, glacial loading is another driver of hydraulic head that may extend freshened groundwater bodies up to 100 km offshore. The latter depends on the local distribution of connected aquifers and low-permeability confining units (e.g., Hong et al., 2019).

### 2.4. Global Volume of OFG

We have used the database (Micallef, 2020) and the approach described in the supporting information to calculate the global volume of OFG at 1,094,000 $km^3$. This is slightly higher than earlier estimates but on the same order of magnitude (Adkins et al., 2002; D. Cohen et al., 2010; Post, Groen, et al., 2013). The actual OFG volume is expected to be larger because the records in the database are not always located in the distalmost part of the OFG bodies, and we have only considered records where the emplacement mechanism is meteoric recharge. Almost 20% of the calculated OFG volume (212,000 $km^3$) is estimated to have a salinity of <10 PSU.

## 3. Investigating OFG Systems

In this section we present and assess methods used to detect and characterize OFG systems. We also include two case studies of OFG systems investigated with some of these methods.

### 3.1. Drilling, Coring, and Logging

Unconsolidated seafloor sediment samples between 0.3 and 30 m in length can be acquired using remotely operated vehicle (ROV)-guided push cores, video-guided multicorer, box corer, gravity corer, and hydraulic piston corer systems operated from research vessels (Abegg et al., 2017; Lunne & Long, 2006). Offshore drilling technologies, on the other hand, allow kilometers of unconsolidated and consolidated sediments and rocks to be recovered (Spagnioli et al., 2015; Talwani, 2009). Where core recovery is good, the sediments can be assessed in terms of granulometry and hydraulic properties, whereas their pore waters are analyzed geochemically (see section 3.2). Where core recovery is incomplete, measurements of in situ parameters—for example, formation resistivity, porosity, density, sonic velocities, gamma ray content, temperature, and flow meter measurements—provide a way to characterize aquifer architecture at several scales, as well as constrain the distribution and salinity of the saturating fluids (Garing et al., 2013; Lofi, Inwood, et al., 2013; Oteri, 1988; Serra, 1984). Borehole wall imaging tools, on the other hand, can be used to identify structural and sedimentological features down to a scale of a few millimeters. These features include open faults, fractures, dissolution features, gravel beds, and cemented horizons, all of which could play a role in controlling

**Table 3**
*Geochemical Analytical Methods That Have Been Used to Characterize OFG*

| Tracer | Laboratory method | Sample volume | Age range | Reference |
|---|---|---|---|---|
| Total dissolved solid (TDS) | Gravimetry and conductivity | Bulk parameter | — | Hem (1970) |
| Chlorinity | Titration | Up to 1 ml | — | Grasshoff et al. (2009) |
| $\delta^{18}O$-$H_2O$ and $\delta^{2}H$-$H_2O$ | IRMS | 1 µl | — | Gehre et al. (2004) |
| | IRIS PICARRO | 1,8 µl (at once, but multiple injections necessary) | | van Geldern and Barth (2012) |
| Dissolved noble gases He, Ne, Ar, Kr, and Xe | Noble gas MS | ~3 ml | — | Strassmann et al. (2005) and Tomonaga et al. (2013) |
| $CH_4$ and $\delta^{13}C/\delta D$-$CH^4$ | GC; IRMS | ~3 ml of sediment | — | Sommer et al. (2009) |
| Rn, Ra activity concentration | Liquid scintillation counting | <500 ml; 50 L | — | Cable et al. (1996), W. S. Moore (1996, 1976), Purkl and Eisenhauer (2004), and Schubert et al. (2014)) |
| Nutrients ($NO_3$, $NH_4$, and $PO^4$) | Auto analyzer | Up to 1 ml | — | Grasshoff et al. (2009) |
| Anions (Br, I, and $SO_4$) | Ion chromatography | 10 µl | — | Hensen et al. (2007) and Scholz et al. (2009) |
| Rare earth elements | ICP-MS | 20 ml | — | Deng et al. (2017) |
| Sr, Sr isotope (water) | MC-ICP-MS and TIMS | 1–5 ml | | Beck et al. (2013) |
| U-Th and Sr isotope systematics (geochronology and source identification, authigenic mineral) | MC-ICP-MS and TIMS | 5 to 100 mg | characteristic age range (U-Th): decades to 350 ka before present (BP) | Bard et al. (1990), Bayon et al. (2009), Hong et al. (2019), and Liebetrau et al. (2014) |
| $^3H$, CFC, and SF6 | GC and MS | ~3 ml; 2 L (SF6) | <100 a | Böhlke and Krantz (2003) and Bratton et al. (2009) |

sub-surface fluid distribution and circulation (e.g., Manda & Gross, 2006; Pezard & Lovell, 1990). Downhole logs measure properties on a scale in-between that of core samples and surface geophysical surveys and thus provide a one-dimensional direct tie of physical properties between the two data types (Dugan & Flemings, 2000; Lofi, Inwood, et al., 2013).

### 3.2. Geochemical Methods

#### 3.2.1. Sampling Technologies

The geochemical sampling and detection technologies used for the identification of OFG are mostly ex situ methods, where sediment and pore water samples are recovered by coring/drilling (see section 3.1) and sub-samples are analyzed in offshore and onshore laboratories. Pore water can be extracted at the seafloor or from recovered sediment by various techniques, depending on grain size and permeability of the sample. On site techniques include (i) "peeper" and Rhizon sampling, which is operated by divers or ROV, and achieves a few decimeters of seafloor penetration depth (Linke, 2011; Teasdale et al., 1995); Rhizon sampling extracts about 10 ml of pore water, depending on porosity and permeability of sediment (Schrum et al., 2012; Seeberg-Elverfeldt et al., 2005); (ii) long-term in situ pore water sampler, which achieves up to 5 m of seafloor penetration depth (Beck et al., 2007); and (iii) the "Barnes" sampler, in its different versions, where the sampling device is connected to the drill bit and pushed into undisturbed sediments below the previous hole bottom (Barnes, 1973; Barnes, 1988). Techniques used to sample from recovered sediments include (i) Rhizon sampling; (ii) high-pressure squeezing, which yields a high yield of pore water from clay sediments (Bender et al., 1987; Brennwald et al., 2003; Jahnke, 1988; Siever, 1962); and (iii) centrifugation, which is ideal for sandy sediments (Rittenberg et al., 1963; Saager et al., 1990; Steiner et al., 2018; Tomonaga et al., 2013).

#### 3.2.2. Geochemical Characterization

Table 3 lists chemical tracers that have been used in OFG investigations, the relevant measurement technique, the required sample volume, and the range of residence time (where applicable).

Chloride analysis or TDS determination of separated pore water is the main conservative tracer indicating freshening of submarine groundwater (e.g., Johnston, 1983; Schlüter et al., 2004; Szymczycha et al., 2018; van Geldern et al., 2013). Chlorinity or TDS changes are also indicators for hydrological changes in the past (Soulet et al., 2010), as well as diagenetic processes (e.g., clay mineral dehydration) or gas hydrate dissociation (Dählmann & De Lange, 2003). TDS is indicative of any ratio of mixing between freshwater, seawater

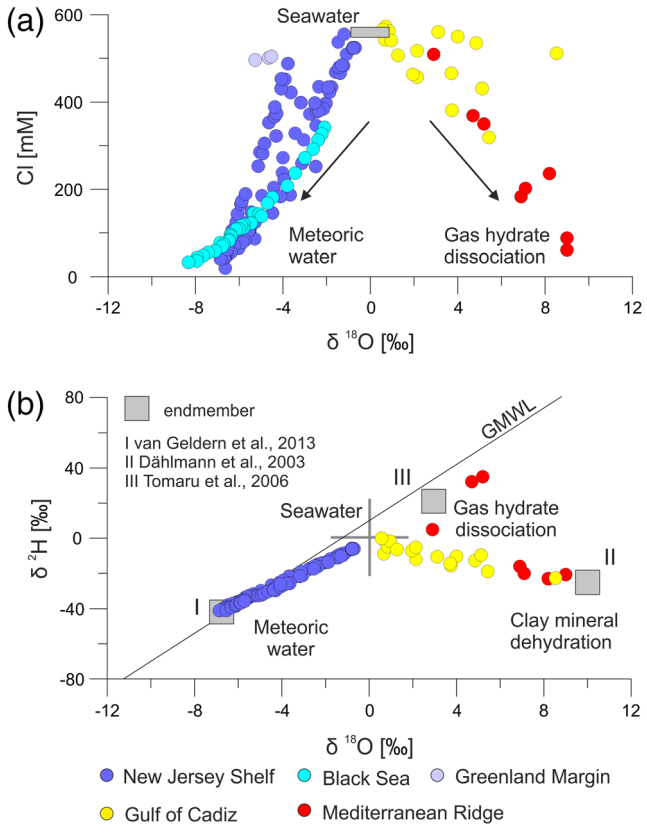


**Figure 4.** (a) Plot of $\delta^{18}O$ with Cl for sub-sea pore waters indicating mixing between meteoric water, seawater, and water from gas hydrate destabilization. (b) Plot of $\delta^{18}O$ and $\delta^{2}H$ for subsea pore waters of different origin. GMWL: Global Meteoric Water Line ($\delta^{2}H = \delta^{18}O + 10‰$).

and brine (e.g., Post, Groen, et al., 2013). The $\delta^{18}O$ and $\delta^{2}H$ values of pore water can be used as constraints for the origin of freshwater (e.g., aquifer recharge by glacial meltwater, Hong et al., 2019; recent or fossil meteoric water, van Geldern et al., 2013).

To further constrain the origin of OFG, a combination of diagnostic parameters can be used, especially by integrating chlorinity with stable isotope characteristics of water samples (i.e., $\delta^{2}H$-$H_2O$ and $\delta^{18}O$-$H_2O$) (Figure 4). Most of the data published by van Geldern et al. (2013) for the New Jersey shelf indicate mixing between seawater and modern or fossil (emplaced at a time with climatic and hydrologic conditions similar to modern) meteoric freshwater (−7‰ V-SMOW [$\delta^{18}O$] and −41‰ V-SMOW [$\delta^{2}H$]). In contrast, freshening due to clay mineral dehydration leads to highly enriched $\delta^{18}O$ values and highly depleted $\delta^{2}H$ values (cf. data from the Gulf of Cadiz and the Eastern Mediterranean Sea, Dählmann & De Lange, 2003; Hensen et al., 2007). Dählmann and De Lange (2003) provide an end-member of +10‰ ($\delta^{18}O$) and −32‰ ($\delta^{2}H$) for clay mineral dehydration. In contrast, freshwater release by the decomposition of gas hydrates results in a shift to more positive values for both isotopes, for example, +2.5‰ ($\delta^{18}O$) and +22‰ ($\delta^{2}H$) (estimated from Tomaru et al., 2006). Mixing ratios between possible fluid end-members in Figure 4 can be derived by using specific isotope mixing calculations after Hoefs (2009).

As methanogenesis may also occur in submerged anoxic aquifers, potentially leading to methane bubble formation and elevated gas and freshwater fluxes along pressure gradients (Hoffmann et al., 2020; Whiticar, 2002), pore water is typically analyzed for dissolved gas. This is carried out by sediment gas extraction procedures and head space gas analysis (Brennwald et al., 2003; Sommer et al., 2009). In addition, authigenic carbonates formed by subsequent methane oxidation provide archives of fluid transport processes and chemistry (Buchardt et al., 2001; Hong et al., 2019; Karaca et al., 2010; Stakes et al., 1999, and references therein). Specifically, the measurements of stable oxygen/carbon isotopes and trace element composition of carbonates provide information about formation temperature and interstitial fluid composition during growth.

### 3.3. Geophysical Methods

#### 3.3.1. Reflection Seismic Methods

As highlighted in section 2.3.1, the present-day distribution and flow of groundwater in the offshore domain relates closely to the geological heterogeneity across a continental margin. Seismic reflection data analysis can provide indirect constraints on the main factors controlling this heterogeneity—from the lithology and permeability of the sediments, to the geometry of depositional units and faults (Bertoni et al., 2020)—as well as image bottom-simulating reflectors, which allow detection of hydrate and thus indicate if pore water freshening associated to hydrate dissociation is feasible (Berndt et al., 2004). Seismic and sequence stratigraphy (Mitchum et al., 1977; Vail et al., 1977) have traditionally been used to identify the type of depositional environment and provide insights into the changes in sea level in a basin through time and the palaeogeographic evolution of a sedimentary margin (Miller et al., 1998; Mitchum et al., 1977; Zecchin & Catuneanu, 2015). Seismic facies analyses are used to estimate lithologies (Barnes, 2001). These types of seismic reflection analyses can provide indications on the vertical and lateral extent of aquifers and aquitards, as well as their connectivity, at a scale ranging from meters to hundreds of kilometers (Lofi, Inwood, et al., 2013).

Seismic reflection data can image sub-seafloor discontinuities that influence OFG flow, such as faults (Alcalde et al., 2019), which appear as offset seismic reflections, or focused fluid flow structures such as pipes, which are characterized by columnar zones of reduced seismic amplitude or warped seismic reflections (Cartwright & Santamarina, 2015). Specific geomorphic features, such as karst-related collapse and

dissolution structures, are frequently imaged as down-warped seismic reflections that form sub-circular structures in map view (Bertoni & Cartwright, 2005; Lofi et al., 2012; Swarzenski et al., 2001). These karstic features are sometimes associated with active resurgences visible in the water column as a result of water density contrasts (Swarzenski et al., 2001). Buried palaochannels on continental shelves, which can enhance vertical and horizontal fluid exchange, can be identified from laterally constrained, irregular, high-amplitude reflections (e.g., Micallef et al., 2020). Diagenetic processes are indirectly revealed by anomalous features such as prominent crosscutting reflections (e.g., Morley et al., 2017).

Seismic reflection data therefore constitute an excellent tool to map 2-D and 3-D aquifer properties at multiple scales. Due to their response to compressible media, seismic reflection data can directly detect gas in sediments (Castagna et al., 2003), but they cannot image salinity variations in pore water. Therefore, seismic reflection data cannot be used on their own to detect OFG. A workflow aimed at OFG identification requires integration of seismic reflection data analysis with other methods such EM surveying.

#### 3.3.2. EM Surveying

The electrical resistivity of water depends on its salinity. Measurements of seafloor bulk resistivity using EM methods can thus discriminate between regions that are saturated with saline water (less resistive) from those that contain fresh groundwater (more resistive). Since bulk resistivity also depends on porosity, there is ambiguity in differentiating between porosity and salinity variations using resistivity alone. However, EM methods are a powerful tool for understanding the distribution of OFG if additional constraints of the local hydrology and geology are available. EM methods offer the only non-invasive geophysical technique that is directly sensitive to the presence of freshwater in the sub-surface and they have been used successfully to map near-surface freshened groundwater in diverse continental shelf environments (Attias et al., 2020; Evans, 2007; Evans & Lizarralde, 2011; Gustafson et al., 2019; Micallef et al., 2020; H. Müller et al., 2011; Mulligan et al., 2007; Russoniello et al., 2013), shore-based or nearshore regions (Dimova et al., 2012; Haroon, Lippert, et al., 2018; Levi et al., 2018; Lippert & Tezkan, 2020), and shoreline-crossing regions with airborne methods (Siemon et al., 2009). Here, we focus on high-resolution, marine controlled-source electromagnetic (CSEM) methods, with a review of the principles, instrumentation, and data interpretation. Additional electrical resistivity background measurements to larger depths can be obtained using the magnetotelluric (MT) method. The MT method uses natural EM waves as a source signal, which are generated by the interaction of the Earth's magnetic field with the sun's radiation and plasma emissions, and through lightning activity. Damping of the high-frequency source signal by the conductive ocean, however, can result in a decreased resolution of the marine MT method in comparison to its terrestrial counterpart or marine CSEM.

##### 3.3.2.1. Salinity, Porosity, and Bulk Electrical Resistivity

Seafloor sediment electrical resistivity is dominated by the matrix porosity and the pore fluid resistivity, which depends on salinity (PSU), temperature (°C), and pressure (dB) (Perkin & Lewis, 1980). In most continental shelf environments, seawater forms a saturated, interconnected network through the sediment, and the relationship between host-rock porosity $\Phi$, pore fluid resistivity $\rho_f$, and measured bulk seafloor resistivity $\rho_m$(in Ωm) can be expressed using the empirical Archie's law (Archie, 1942):

$$\rho_m = \Phi^{-m}\rho_f. \tag{1}$$

The cementation or shape factor $m$ generally increases as sediment particles become less spherical, with lower values of $m$ describing a well-connected fluid network (Archie, 1942; Jackson et al., 1978). Values of $m$ between 1.2 and 3.0 have been reported from core samples of different lithologies (Salem & Chilingarian, 1999), but typically, $m$ ranges between 1.5 and 2.5 for marine sediments. Archie's law implicitly postulates a non-conductive rock matrix. Sediments with a large clay fraction violate this assumption due to water trapped in the clay's internal mineral structure and the cation exchange capacity of clay. Clay-rich sediments are therefore more conductive than would be predicted by Archie's law, a fact that can be accounted for by using the Waxman Smits model (Waxman & Smits, 1968).

Figure 5 illustrates how freshened pore fluid in an aquifer produces a high resistivity anomaly that is a suitable target for EM mapping. However, decreased porosity in the deeper gravel layer creates a comparable resistivity anomaly; thus, the interpretation of resistivity anomalies in offshore EM data requires additional geological information to discriminate salinity from porosity variations. In contrast, seismic velocity is only

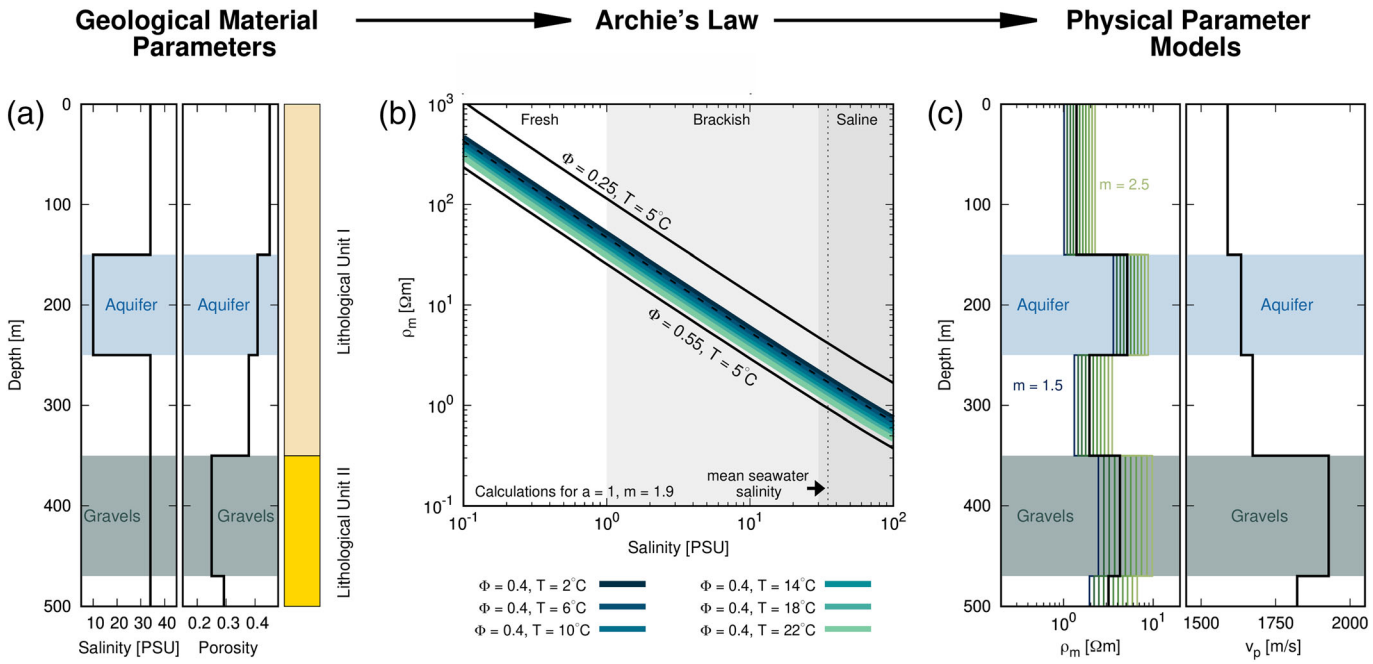


**Figure 5.** Relationship between seafloor porosity (Φ), pore fluid salinity, and bulk resistivity ($\rho_m$) using Archie's law (Equation 1) and for seismic velocity ($v_p$) using the Wood equation (Wood, 1941). (a) Pore fluid salinity and porosity depth models including a freshened aquifer (salinity of 10 PSU) contained within lithological unit I (salinity of 34 PSU). (b) Relationship between pore fluid salinity and bulk resistivity for porosity values of 0.25, 0.4, and 0.55 at 5°C. Colored lines depict temperature variations for Φ = 0.4. (c) Resistivity and velocity-depth models corresponding to the salinity and porosity models in (a). Colored lines in the resistivity models correspond to variations in cementation factor m between 1.5 and 2.5. The black line corresponds to the resistivity model for $m = 1.9$.

sensitive to porosity and lithological variations and is not affected by salinity changes. Combined seismic and EM surveys can therefore offer a powerful approach to map occurrences of offshore aquifers in various marine environments, with recent applications including siliciclastic sedimentary settings (Gustafson et al., 2019; Micallef et al., 2020), low porosity carbonate rocks (Evans & Lizarralde, 2011; Micallef, Mountjoy, et al., 2018), and volcanic settings (Attias et al., 2020).

#### 3.3.2.2. Offshore EM Surveying

EM data sensitive to OFG are primarily collected using CSEM systems consisting of an electric dipole transmitter and dipole receivers positioned at various distances from the transmitter (Gustafson et al., 2019; Micallef et al., 2020). The transmitter emits a time varying electric current that induces EM fields in the ocean and seafloor. As these fields diffuse away from the transmitter, attenuation is more pronounced in the less resistive ocean than in the more resistive sediments. Attenuation is further reduced in resistive brackish and fresh aquifers, which act as waveguides for the EM field. This results in higher-amplitude signals measured by receivers located above an aquifer compared to receivers located over saline or brine-filled sediments.

Commercial interest in CSEM for mapping resistive hydrocarbon reservoirs drove significant improvements in instrumentation over the past two decades (Constable, 2013), resulting in technological capabilities that can be readily applied to OFG exploration. The transmitter and receiver dipoles are oriented horizontally and inline, making the entire system practical to deploy using a cable towed from a ship (Figure 6). The depth sensitivity is primarily dictated by the frequency or time range of the signal and on the separation between the transmitter and receivers, with lower frequencies (or later time ranges) and longer offsets having sensitivity to deeper depths. Recent surveys used four receivers spaced to 650-m offset (Micallef et al., 2020) and to 1,380-m offset (Gustafson et al., 2019). Systems can be dragged on the seafloor and stopped at stations (Gehrmann et al., 2015; Yuan & Edwards, 2000) or continuously towed in the water column (Constable et al., 2016). Resolution is highest, and data noise levels are lowest, for the stationary seafloor data, but this slows down survey speed and requires robust instrumentation to avoid damages. In shallow water (up to about 200 m), CSEM streamer systems can be towed on the sea surface or in the

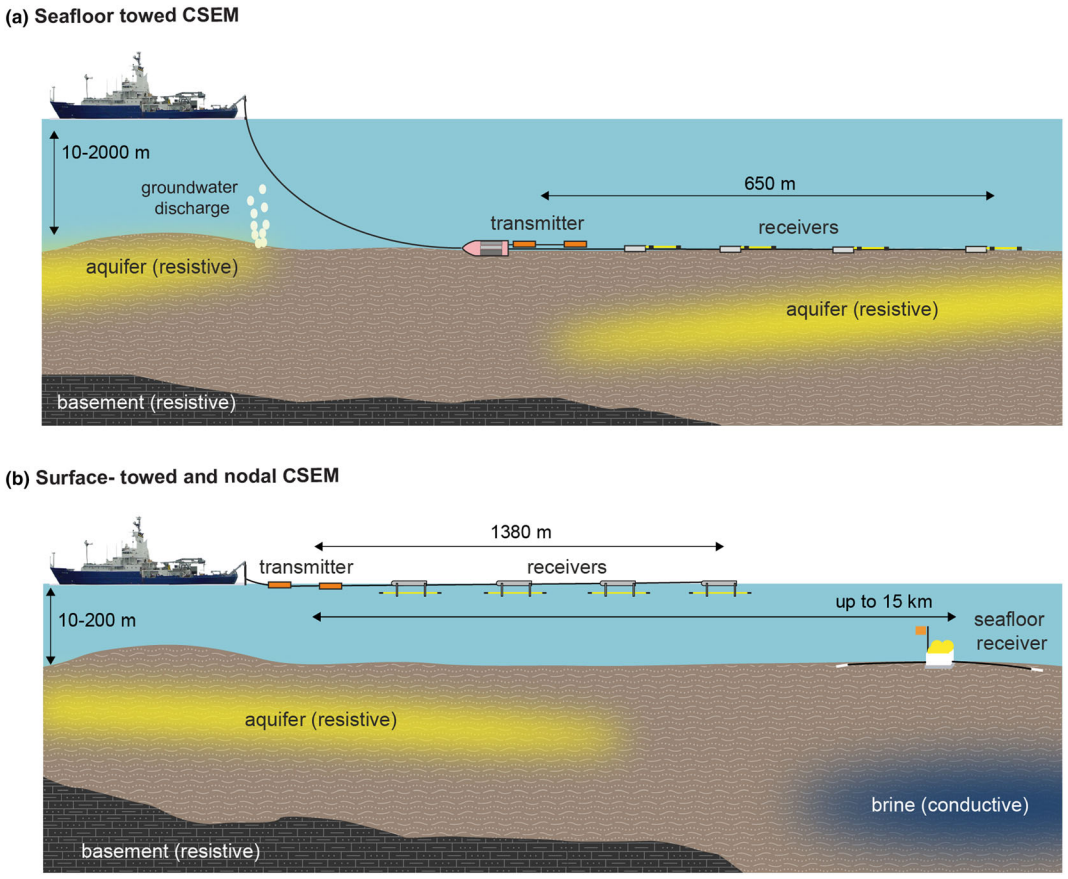


**Figure 6.** Marine EM systems for mapping OFG. (a) CSEM data collected off New Zealand (Micallef et al., 2020) used a system dragged along the seafloor for maximum coupling. A transmitter output of 20-A current on a 100-m dipole was used, whereas the signal was measured on four dipole receivers at up to 650-m offset. (b) A surface-towed CSEM system applied offshore of New Jersey (USA) (Gustafson et al., 2019), used a transmitter with 88-A current output on a 337-m dipole, with the EM signal recorded by four towed receivers at up to 1,380-m offset. Additional long-offset CSEM data and natural source MT data with greater depth penetration were recorded using nodal seafloor receivers.

water column for more rapid data acquisition (Gustafson et al., 2019; Sherman et al., 2017). CSEM data can also be augmented with natural-source MT data collected by stationary nodal EM receivers (Figure 6b) to significantly improve resolution of both resistive and conductive structures (Blatter et al., 2019; Gustafson et al., 2019).

#### 3.3.2.3. Best Practice Strategies

The choice of suitable EM instrumentation depends on the specific target layer and environmental conditions. The strong attenuation of EM fields in conductive seawater limits the usability of surface-towed EM systems to about 200-m water depth. Within this range, depth of penetration and resolution decrease with increasing water depth. An advantage of surface towing is faster surveying at speeds of ~4 kn. Deep towed (20–100 m above seafloor) and particularly seafloor-towed systems can have increased resolution and penetration depth, yet survey speed is reduced to 1–2 kn. Seafloor-towed systems also benefit from higher signal-to-noise ratios because it is possible to stack signals at stationary waypoints. Towed CSEM systems can be configured to have a sensitivity to a depth range of 500 m below seafloor, which encompasses the top of most OFG bodies of interest. Depth penetration limitations of all systems can be addressed by using larger transmitter-receiver offsets, although these also require larger transmitter moments and lower noise-level receivers. A commercial surface-towed system designed for deep hydrocarbon mapping has 44 receiver dipoles on a 7.7-km-long streamer and would be ideal for large-scale mapping of OFG (Du & Key, 2018).

The size of the expected salinity anomaly and the aquifer depth dictate which system is most suitable. A shallow and strong anomaly constitutes a target for surface-towed systems, while more subtle or deeper

anomalies might require deep or seafloor-towed systems. For detailed local or 3-D surveys, stationary seafloor nodes and a towed transmitter are a good alternative. Increased resolution is gained by a larger range of transmitter-receiver offsets, whereas transmitter tows in various directions yields additional 3-D information, data coverage, and information on conductivity anisotropy (Du & Key, 2018; Haroon, Hölz, Gehrmann, et al., 2018; Hölz et al., 2015).

### 3.4. Numerical Modeling

#### 3.4.1. Modeling Approaches

Hydrologic models have been developed to quantify SGD and coastal saltwater intrusion problems around the world (e.g., Bear et al., 1999; Cheng & Ouazar, 2003; Michael et al., 2005, 2016; Sanford & Pope, 2010). Such models are typically run on time scales of tides to decades, which is sufficient to capture processes relevant for management purposes, and the systems are assumed to be in equilibrium with present-day sea level. Under these conditions, the simulated freshwater-saltwater interfaces generally extend from the shoreline landward, and SGD occurs primarily in the nearshore environment. OFG can occur under these conditions in simulations that incorporate geologic heterogeneity, either explicitly (Yu & Michael, 2019a) or as upscaled anisotropy in permeability. On the small (~1 km) scale, simulations that include geologic features such as palaeochannels, which are buried beneath lower-permeability units that prevent shoreline discharge, show freshened groundwater plumes offshore (Mulligan et al., 2007). On larger (1–10 km) scales, simulated features such as karst conduits (Xu et al., 2018) and lava tubes (Kreyns et al., 2020) can lead to OFG flow. On the shelf (10–100 km) scale, analytical (Knight et al., 2018) and numerical (Paldor et al., 2019) simulations of layered coastal aquifers show OFG within confined aquifers, where active fresh SGD is either focused at outcrops or diffuse across confining units. Simulations on the shelf scale that incorporate geostatistical representations of aquifer heterogeneity, in which aquifers are not completely confined, show that such systems can also host large volumes of OFG. The latter can extend tens to hundreds of kilometers offshore, depending on the connectedness and degree of confinement of high-permeability preferential flow paths connecting onshore and offshore groundwater systems (Michael et al., 2016). Upscaling large-scale heterogeneity results in high degrees of permeability anisotropy, with ratios ($k_h/k_v$) reaching $10^4$ or more. Equilibrium simulations in such systems also produce freshwater-saltwater interfaces far offshore but with much less variability in the offshore extent and salinity distributions than corresponding heterogeneous models (Kreyns et al., 2020; Michael et al., 2016).

As scales become larger, hydrogeologic systems respond to hydrologic forcing more slowly, and the assumption of equilibrium with present-day sea level no longer holds. Thus, there is a need to capture longer-term transience in hydrological models to fully understand the emplacement and persistence of OFG in systems where equilibrium conditions cannot support it. The application of hydrologic models to study OFG emplacement over geologic time scales (Table 4) is less common. First developed in the 1980s, palaeo-hydrologic models have provided insights into the mechanisms of emplacement and distribution of OFG. Meisler et al. (1984) used a steady-state hybrid sharp-interface model to assess freshened groundwater offshore New Jersey, USA. More recent palaeo-hydrologic models of OFG, such as D. Cohen et al. (2010), Kooi et al. (2000), Thomas et al. (2019), and Micallef et al. (2020), have considered time-varying sea level conditions during the Pleistocene. A subset of these palaeo-hydrologic models have been developed to assess overpressure formation, which can deter seaward migration of OFG (Kooi, 1999), as well as continental shelf geomorphic processes (Table 5).

#### 3.4.2. Modeling Methods

Analytical methods that solve for the position of the freshwater-saltwater interface using sharp-interface theory were developed by Henry (1964), Hantush (1968), and more recently by Bakker (2006) (see section A.6). These schemes provide closed-form solutions predicting the position of the interface in space and time. Numerical solutions using sharp-interface theory have also been developed to consider multi-layered systems (Bakker et al., 2017; Essaid, 1990; Werner & Robinson, 2018). These have been widely used to study coastal aquifer systems around the world (Guswa & LeBlanc, 1985; Knight et al., 2018, 2019; Ledoux et al., 1990; Rivera et al., 1990).

Numerical methods are best suited to represent aquifer and confining unit heterogeneity, as well as coupled processes. Finite difference methods that approximate solutions to the variable-density groundwater flow and heat/solute transport equations such as *SEAWAT* (Langevin et al., 2008) are widely used today and

**Table 4**
*Marine Palaeo-Hydrogeologic Modeling Studies*

| Study area | Processes represented | Reference |
|---|---|---|
| New Jersey, USA | Shore normal topography-driven flow and sharp-interface models (2-D) | Meisler et al. (1984) and Thomas et al. (2019) |
| Suriname, SA | Shore normal topography-driven flow | Kooi et al. (2000) |
| Long Island, USA | Ice sheet loading (2-D), permafrost, and shore normal topography-driven flow | Person et al. (2003) |
| New Jersey to Maine, USA | Pleistocene glaciations and shore normal topography-driven flow (3-D) | D. Cohen et al. (2010) |
| Southeastern Greenland | Ice sheet loading (2-D), permafrost, and shore normal topography-driven flow | DeFoor et al. (2011) |
| Nantucket, USA | Ice sheet loading, permafrost, and shore normal topography-driven flow (2-D and 3-D) | Marksammer et al. (2007), Person et al. (2003, 2012), and Siegel et al. (2012, 2014) |
| Canterbury Bight, New Zealand | Shore normal topography-driven flow (2-D) and groundwater residence times | Micallef et al. (2020) |

*Note*. All of these studies considered solute transport and variable-density groundwater flow.

have been applied to studies of OFG (Michael et al., 2016; Yu & Michael, 2019a; Yu & Michael, 2019b). Finite element solutions schemes are better suited to represent irregular strata geometries and have also seen wide application (D. Cohen et al., 2010; Micallef et al., 2020; Person et al., 2003; Post & Kooi, 2003; Siegel et al., 2014; Voss & Souza, 1987). A few finite element codes have been parallelized (e.g., D. Cohen et al., 2010; Zwinger et al., 2019), which permits representation of fine scale features at the continental shelf scale. Select examples of model applications to study OFG are provided in section A.7.

Quantifying OFG emplacement in continental shelf environments over geologic time scales requires consideration of a number of coupled processes (Kooi (1999); Figure A1). These include variable-density fluid flow, heat transfer, solute transport, and mechanical loading and potentially lithosphere geodynamics (Figures A8–A11). The governing flow equations for coupled heat and mass transport are described in the sections A.1–A.3. The equations are coupled through equations of state relating temperature, pressure, and salinity to fluid density and viscosity (section A.4). Representation of mechanical loading due to sedimentation is another form of coupling and requires dynamic mesh generation (Dugan & Flemings, 2000; You & Person, 2008). Here, pore pressure, effective stress, porosity, and permeability are coupled, resulting in non-linear feedbacks. If the time steps are small enough (~1a), coupling between effective stress and porosity can also be evaluated in a sequential manner. Dimensionless number groups, including the Rayleigh number (*Ra*) (Post & Kooi, 2003), the Peclet Number (*Pe*), and scaling analysis parameters such as characteristic time for diffusion, have also seen wide application (section A.5). These have been used to characterize the importance of different fluid flow impelling mechanisms in layers of known thickness, distances, and permeability within continental shelf environments, as well as the time scales over which they operate. For example, the characteristic time constant for vertical diffusion is over 100,000 a for solute transport across a 10-m-thick bed, if a Fickian diffusion coefficient of $3 \times 10^{-11}$ $m^2/s$ is assumed (Equation A16). Relating the rates of sea level rise to diffusion time scales can provide insights into confining unit transport processes. Peclet number analysis helps to constrain the time required for advection dominated solutes to migrate

**Table 5**
*Marine Hydrogeologic Modeling Studies Focused on Overpressure Generation*

| Study area | Processes represented | Reference |
|---|---|---|
| Gulf of Mexico | Compaction-driven flow, aqua-thermal pressuring, porosity-permeability evolution, and clay dehydration | Bethke (1986), Gordon et al. (1999), Harrison and Summa (1991), and Stigall and Dugan (2010) |
| Barbados Accretionary Prism | Clay dehydration | Bekins et al. (1994) and Vrolijk et al. (1991) |
| New Jersey continental shelf | Compaction-driven flow, slope failure analysis | Dugan and Flemings (2000) |
| North Sea-Norwegian continental shelf | Glacial loading, lithosphere flexure, illite-smectite dewatering | Grollimund and Zoback (2000) and Schneider and Hay (2001) |
| Nankai accretionary prism | Subduction zone processes | Tobin and Saffer (2009) |

either laterally or vertically across a permeable bed by advective transport (Equation A15). The utility of dimensionless number analysis is less clear in heterogeneous geological settings where aquifer dimensions and properties are not well constrained (Gerdes et al., 1998).

#### 3.4.3. Value and Challenges of Numerical Modeling

Given the paucity and depth limitations of offshore wells and marine EM surveys, hydrologic modeling represents one of the most cost-effective methods for estimating OFG resources. Numerical models can also be used to guide data collection by indicating which system features may be diagnostic of the emplacement mechanism and which are the best sites to drill wells to obtain the most valuable data. Numerical models can integrate disparate and complementary data sets, identifying the most critical gaps (spatial, temporal, and conceptual), as well as agreements or discrepancies among independent data.

There are three primary challenges in numerically simulating OFG systems. First, there is considerable uncertainty in assigning petrophysical properties such as permeability, sediment compressibility, and porosity offshore (Thomas et al., 2019). Approaches for geologic property modeling in OFG systems can be either deterministic or geostatistical. Where sufficient data are available, the distribution of properties can be assigned directly, with interpolation/extrapolation of property observations supported by geophysical data and geologic knowledge (D. Cohen et al., 2010; Micallef et al., 2020; Paldor et al., 2019; Varma & Michael, 2012). Geostatistical methods can be used to represent property distributions where data are too sparse relative to the relevant geologic features to allow interpolation and where statistical distributions of properties or patterns can be obtained or inferred (Michael et al., 2016; Zamrsky et al., 2020).

A second challenge is that the long time scale required for palaeo-hydrological simulations presents difficulties in determining appropriate boundary conditions. Imposing recharge rates (Putnam & Broecker, 2017), land surface topography changes (Tarasov & Peltier, 2004), temperature variations, and sea level fluctuations over geologic time scales adds significant uncertainty to model predictions. Estimates of relative sea level change are available for the Holocene and Late Pleistocene in some locations, but they are uncertain for earlier epochs, especially in tectonically active areas with large vertical movements of the crust. Therefore, it is necessary to use ice sheet (Johnsen et al., 1995) and marine sediment climate proxies of eustatic sea level changes (Hansen et al., 2013) to extend models back to the middle to early Pleistocene.

Third, coupling of multiple processes over tens of thousands of years using a sufficiently resolved grid to accurately characterize transport processes is computationally intensive. This limits our ability to fully represent OFG systems. Most palaeo-hydrological simulations to date have been limited to 2-D, which can reduce onshore-offshore connectivity and understanding of alongshore variability. Haline convection (section A.7), for example, is an important mechanism salinizing shallow and permeable sand layers during periods of sea level rise (Post & Kooi, 2003; Thomas et al., 2019). In order to represent haline convection accurately, a numerical model requires highly resolved grids. Post and Kooi (2003) argued that grid discretization is permeability-dependent and a function of the Rayleigh number. These authors found that a hydraulic conductivity range between $10^{-4}$ and 10 m/day requires a vertical grid resolution that varied between ~276 m and 3 mm. Thus, a 100-m-thick sand unit having a permeability of 10 m/day and a 1-km lateral extent would require about $5 \times 10^9$ nodes, assuming a horizontal discretization of 6 mm. Clearly, even with high-performance computing, some type of upscaling algorithm needs to be considered in the development of regional continental shelf hydrogeologic models.

### 3.5. Case Studies

#### 3.5.1. East Coast, USA

The best studied example of OFG in continental shelves comes from offshore of New Jersey (USA), where drilling efforts in the 1970s detected significant low salinity layers at large distances from shore (Hathaway et al., 1979). A more recent mid-shelf drilling campaign (International Ocean Discovery Program [IODP] Expedition 313) found complex aquifer structures and salinity variations, with the freshest offshore groundwater being hosted in fine-grained sedimentary layers (Lofi, Inwood, et al., 2013; Mountain et al., 2010). Geochemical studies of sampled pore waters suggest emplacement of meteoric freshwater in modern times or at a time when climatic and hydrologic conditions were similar (Mottl & Hayashi, 2009; van Geldern et al., 2013). Additionally, IODP Expedition 313 Site M0029 documented increasing salinity at depth (twice the salinity of seawater), which is interpreted to result from upwelling brines via faults, suggesting that substantial mixing is occurring (Lofi, Inwood, et al., 2013). Seismic reflection data tied to the

borehole data show a good correlation between seismic facies and pore water salinity, with the exception of the zones under the influence of brines (Lofi, Inwood, et al., 2013). For example, the Miocene clinothems with gently dipping seaward topsets, composed of continuous, high-amplitude reflections, host thick OFG intervals (Figure 3c). Inversely, the upper part of the clinoform foresets, characterized by discontinuous to steeply dipping reflections, preferentially store saltier pore waters.

The spatial extent of the OFG system was revealed by a survey conducted in 2015, which combined surface-towed CSEM and seafloor MT soundings (Figure 6b). The resulting resistivity model from 2-D inversions shows two resistive zones (10–110 Ωm) within the upper 400 m, which are interpreted as submarine low salinity aquifers and generally agree with low salinity regions seen in co-located well logs (Gustafson et al., 2019; Key, 2016) (Figure 7a). The deeper conductive zones (0.4–1 Ωm) are associated with the brines that occur in IODP Expedition 313 Site M0029. Overlain seismic reflection data suggest that the seaward dip to the resistive aquifer is due to an overlying confining layer, while its offshore extent is limited by a sequence of clinoform structures. A similar, laterally continuous aquifer extending about 90 km offshore is also seen in an additional EM profile collected off Martha's Vineyard (Gustafson et al., 2019). Together, these profiles and well data suggest that the offshore aquifer may span at least 350 km of the U.S. Atlantic coast and could host ~2,800 $km^3$ of low-salinity groundwater.

D. Cohen et al. (2010) represented the hydrostratigraphy of the U.S. Atlantic continental shelf as a series of aquifers and confining units in 3-D using a lateral discretization of ($\Delta x$, $\Delta y$) of 4 km (Figure 8a) and considered time-varying sea level conditions for the past 2 Ma. The salinities computed with D. Cohen et al.'s (2010) model (Figure 8b) were in reasonable agreement with salinity variations in offshore wells (as reported in Hathaway et al., 1979). Thomas et al. (2019) developed a 2-D geostatistical model of hydrogeologic facies based on seismic reflection and well data (Figure 8c), by assigning a $\Delta x$ of 0.1 km and running the model for 12,000 a. With such a model they were able to closely match observed salinity data from the IODP Expedition 313 well data (Lofi, Inwood, et al., 2013; Thomas et al., 2019) (Figures 8d and 8e).

#### 3.5.2. Canterbury Bight, New Zealand

A pore water salinity anomaly indicating an OFG system is present at IODP Expedition 317 Site 1353 in the continental margin of the east coast of New Zealand's South Island (Fulthorpe et al., 2011). This OFG system was investigated in detail using marine CSEM, seismic reflection profiling, and numerical modeling (Micallef et al., 2020).

The geophysical data were used to determine the geometry and dimensions of the OFG system in 3-D and to identify the factors controlling salinity distribution (Micallef et al., 2020). Seafloor-towed CSEM data were acquired using the system shown in Figure 6a and interpreted to a depth of 350 m below seafloor using 2-D inversion (Haroon, Hölz, Weymer, et al., 2018). The CSEM resistivity data reveal one main resistivity anomaly and two smaller ones (>20 Ωm), which are interpreted as OFG bodies (Figure 7b). The main body extends up to 60 km from the coast, down to a water depth of 110 m and has a maximum thickness of at least 250 m. The minimum and maximum groundwater volumes, estimated for porosities of 20% and 40%, are 56 and 213 $km^3$, respectively. Interpretation of the seismic reflection data suggests that the OFG mainly occurs in silt and sand layers and occasionally in gravel and clay. Interpretations of the geophysical data also reveal spatial variability in groundwater salinity along the shelf, which is attributed to sedimentary structures (e.g., high-permeability conduits and corridors), normal faults, and river recharge during sea level low stands.

Based on the geochemical characteristics of the pore water in the borehole data ($Ca^2$, Na, and Cl concentrations lower than seawater; $HCO_3$ concentrations and $HCO_3$/Cl ratios higher than seawater; asymmetry of the salinity profile), the OFG is inferred to be meteoric in origin, whereas the young groundwater age at the coast suggests active recharge of the OFG at present (Fulthorpe et al., 2011; Micallef et al., 2020; Stewart et al., 2002). However, 2-D models of groundwater flow and solute transport, based on geologic interpretation of the seismic reflection data, indicate that active recharge can only account for a small fraction of the OFG volume. Transient models incorporating sea level variability in the past 1 Ma suggest that the majority of the OFG was emplaced during the last 300 ka (Micallef et al., 2020) (Figure 9). Topographically driven, shore-normal flow was enhanced during sea level lowstands due to an increase in hydraulic head gradients, which drove freshwater offshore and extended the OFG bodies toward the continental shelf break. Topographically driven flow declined with an increase in sea level, and lateral differences in salinity on the shelf drove groundwater laterally and shoreward.

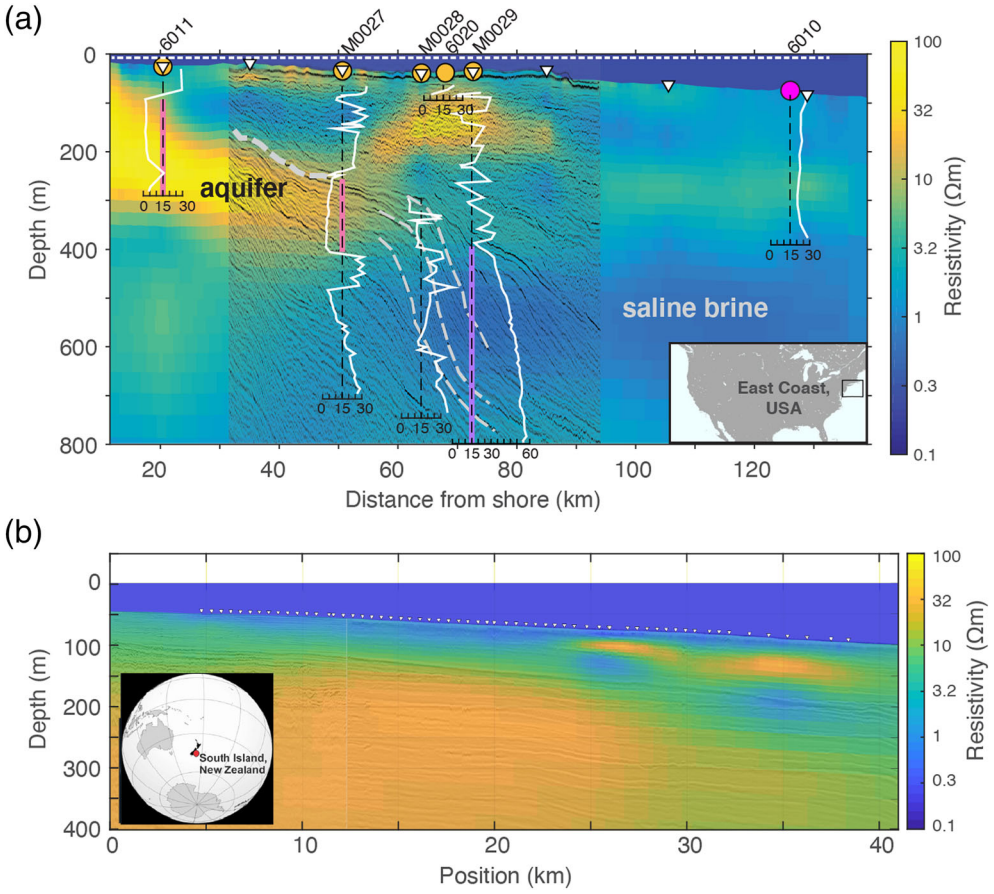


**Figure 7.** (a) Resistivity model (shaded colors) obtained offshore of New Jersey from 2-D joint inversion of surface-towed CSEM and seafloor MT data, overlain with corresponding seismic reflection data. The resistive zones (>10 Ωm) are interpreted as low salinity OFG. Pore water salinity data (white lines) are shown for boreholes AMCOR sites 6,010, 6,011 and 6,020, and IODP Expedition 313 Sites M0027–M0029, on a linear scale ranging from 0 to 60 PSU (Hathaway et al., 1979; Mountain et al., 2010). Salinity value of 15 PSU is represented by black dashed lines. Light gray dashed lines denote seismically imaged confining units and clinoform structures. Modified from Gustafson et al. (2019). (b) Resistivity model from 2-D inversion of CSEM data from the Canterbury Bight, along a line oriented perpendicular to the shoreline, and overlain with the corresponding seismic reflection section. The model contains an extended, seaward dipping, resistive body (>20 Ωm) at depths of 25–215 m below seafloor, which is interpreted as the main OFG body. The shallow resistive feature between 25 and 40 km (>20 Ωm) follows seismic reflectors and is interpreted as freshened groundwater within a fine sand unit. Stationary measurements were conducted at waypoints indicated by the white markers. Modified from Micallef et al. (2020).

## 4. Gaps in Knowledge and Recommendations for Future Work

Based on the information presented in the previous two sections, we identify the key challenges in our understanding of OFG systems and make recommendations for the most suitable approaches to address them.

### 4.1. Characteristics and Controls of OFG

As most of our knowledge related to OFG has been derived from data collected for other scientific projects, there are still many outstanding gaps in knowledge. Some of the most important of these include the following:

1. We have a poor understanding of the distribution, extent, and dimensions of OFG bodies, as well as their flow characteristics.
2. Direct observations of the aquifer structure and geochemical characteristics of OFG are rare (Lofi, Inwood, et al., 2013; van Geldern et al., 2013).

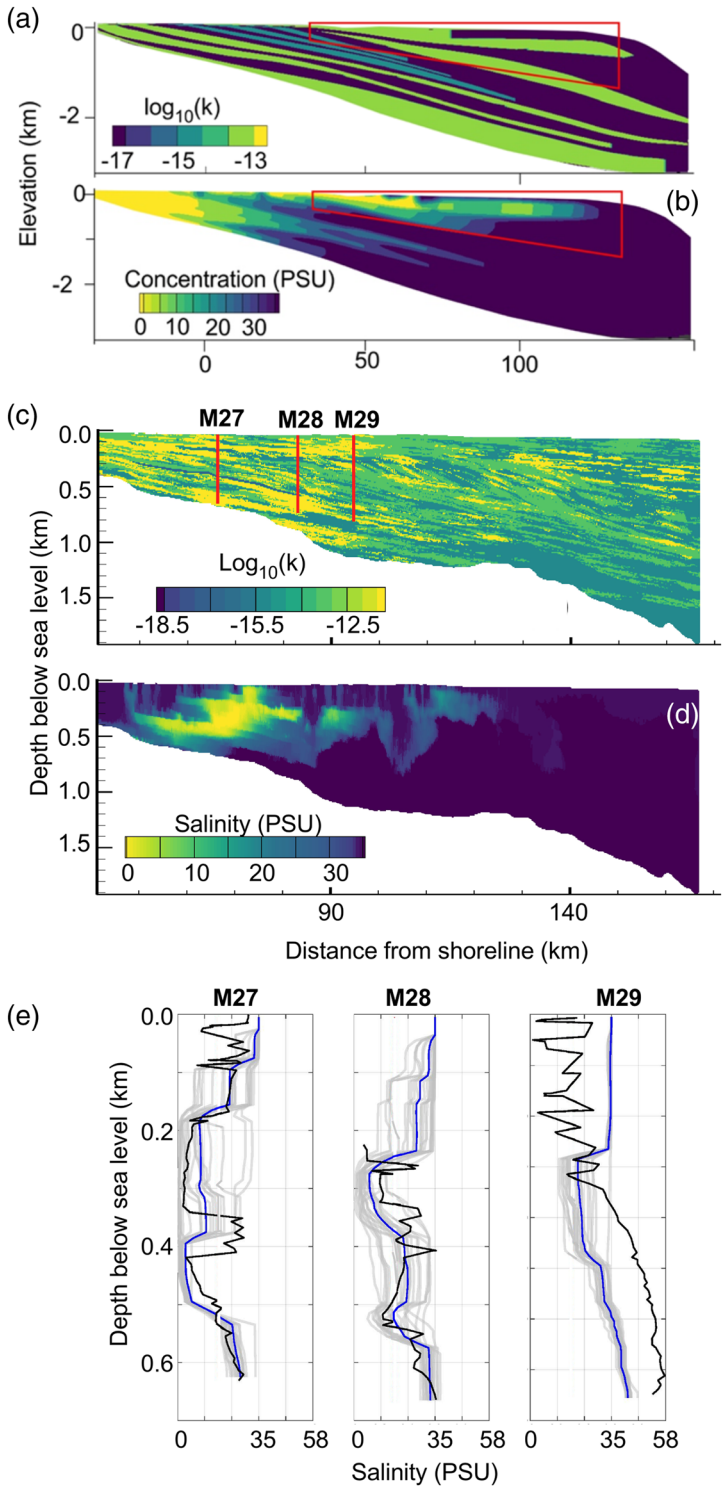


**Figure 8.** (a) $Log_{10}$ permeability ($m^2$) and (b) concentration model output for the New Jersey shelf (modified from D. Cohen et al., 2010). (c) Permeability distribution from one sequential indicator simulation of the New Jersey mid-shelf region. (d) Present-day simulated salinity distribution associated with (c). The location of the geostatistical model domain in (c) and (d) is indicated by a red polygon in (a). (e) Simulated salinity profiles from twenty different sequential indicator simulations (gray lines). The blue line presents the mean simulated salinity profile while the black line denotes observed conditions from IODP Expedition 313 Wells M0027, M0028, and M0029. Modified from Thomas et al. (2019).

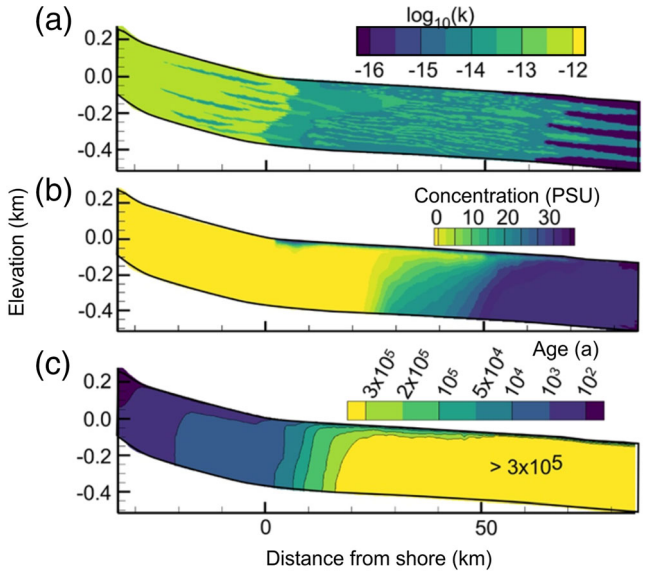


**Figure 9.** (a) $Log_{10}$ permeability ($m^2$), (b) concentration, and (c) mean residence time model outputs for the Canterbury Bight (modified from Micallef et al., 2020).

3. The control of the geological environment (e.g., stratigraphy and structures) on the spatial distribution and flow of OFG is poorly constrained. It is unclear how the evolution of a continental margin during multiple sea level cycles influences the emplacement and dynamics of OFG.
4. The mechanism and timing of OFG emplacement are often unknown. The emplacement mechanism of <10 records in Table 2 has been confirmed via geochemical analyses.
5. The function of OFG systems—whether they are actively recharging and discharging or slowly recovering from past hydrological conditions—is rarely well defined, yet it is critically important for predicting how they will respond to future use and environmental changes. One key difference is that actively recharging systems may be sustainable or even growing depending on recharge rate, fluid production rate and environmental changes, whereas relict bodies are progressively salinizing under modern sea level conditions. Future studies need to better characterize OFG systems by integrating improved constraints on hydrogeologic properties and driving forces, as well as groundwater age.
6. Drivers of OFG in convergent margins are poorly constrained, and it is not clear how OFG flow and emplacement interact with processes such as tectonically induced porosity reduction, sediment loading, thrust faults, and volcanic intrusions.
7. There is an urgent need for a more complete assessment of how OFG systems will respond to climate change, particularly in polar regions.
8. Apart from the two frontier applications of OFG research discussed in section 5, other research avenues that deserve attention include the impact of OFG flow on continental margin geomorphology (Micallef, Mountjoy, et al., 2018) and the role of periodic flushing of continental shelves in ocean cycling of many elements and species.

### 4.2. Drilling, Coring, and Logging

Scientific boreholes are still relatively rare in the upper few hundred meters of continental shelves due to challenges with drilling and sampling (Figure 1). The record in industry boreholes, on the other hand, generally starts hundreds of meters below the seafloor, missing most OFG bodies, and access may be limited by proprietary issues. Most drilling campaigns have implemented data acquisition programs that are not directly relevant to OFG studies. Where drill sites intersect OFG systems (Micallef, 2020) and appropriate data are available, additional insights may be gained with respect to the physical properties of aquifers and the geochemical structure of OFG.

No dedicated OFG drilling project has been completed to date through Ocean Drilling Program (ODP)/IODP. Future transformative discoveries within the OFG field of research will result from hydrogeologically focused drilling campaigns on the continental shelf. IODP Expedition 313, while not focused on marine hydrogeology, is illustrative of how drilling can advance understanding of OFG systems. The drilled wells provided important new insights into OFG distribution in the mid-shelf (Lofi, Inwood, et al., 2013), whereas data-driven modeling highlighted the importance of haline convection in OFG geometry (Thomas et al., 2019). Offshore wells that are designed and sampled to address hydrogeological properties and processes can be used to (i) determine the hydrogeological and petrophysical properties of the aquifer, thus reducing uncertainty in numerical models of OFG; (ii) provide the necessary ground truth to tie formation resistivity to salinity and decrease the ambiguity of geophysical data; (iii) conduct pumping tests, using a packer system (e.g., K. Becker & Fisher, 2008), to measure the bulk hydraulic conductivity of continental shelf stratigraphic units, and to collect geochemical tracers and environmental isotopes; (iv) make direct measurements of fluid pressures along shore normal borehole transects to assess hydraulic gradients and flow directions; and (v) monitor the type and time scale of changes in the physical and chemical characteristics of the OFG, especially with respect to changes in onshore recharge; within karst OFG systems, it may

**Table 6**
*Geochemical Analytical Methods That Can Be Used to Characterize OFG*

| Tracer | Laboratory method | Sample volume | Age range | Reference |
|---|---|---|---|---|
| $^{4}$He | AMS | <500 ml | 100 a to 1 Ma | Torgersen and Stute (2013) |
| $^{14}$C-DIC/DOC/carbonate | AMS $^{14}$C | 100-ml water or 200-mg sediment | 1 ka to 30 ka | Plummer and Glynn (2013) |
| $^{36}$Cl | AMS and IDMS | 1–10 L (10 mg Cl are needed) | 50 ka to 1 Ma | Desilets et al. (2006) and Phillips (2013) |
| $^{39}$Ar | Atom Trap Trace Analysis (ATTA) | several liters of pore water[a] | <1,000 a | Jiang et al. (2011) |
| $^{81}$Kr | Atom Trap Trace Analysis (ATTA) and AMS | several liters of pore water[a] | 50 ka to 1 Ma | Jiang et al. (2012), Purtschert et al. (2013), and Sturchio et al. (2004) |

*Note*. The listed references are for studies of onshore groundwater.
[a]Needed water volume depends on gas extraction method.

be possible to achieve this using borehole-borehole tracer tests. Recent developments in marine geophysical methods ensure that OFG bodies can be identified more accurately, which aids more focused, efficient drilling and sampling programs.

### 4.3. Geochemical Methods

Noble gas samples can provide indications on the temperature conditions during infiltration. If combined with other information (e.g., isotopic analyses discussed in section 3.2.2), they can help constrain the timing of recharge period. Comparison of observed residence times and those simulated by numerical models should help constrain mechanisms of OFG emplacement. Groundwater age dating along a shore normal transect of wells could provide crucial information on whether an OFG body is connected to an active meteoric aquifer (in which case, groundwater age should increase moving offshore) or whether the recharge occurred during sea level lowstands (in which case, groundwater ages would not show a systematic increase moving offshore). The OFG in large-scale systems is likely old, even in active systems, and dating techniques may not be entirely diagnostic of the emplacement mechanism.

Residence times of onshore groundwater have been estimated by $^{14}$C-DIC/DOC, $^{39}$Ar activity, radiogenic $^{4}$He concentrations, or $^{81}$Kr tracer ages (Gerber et al., 2017; T. Müller et al., 2016; Phillips, 2013; Ritterbusch et al., 2014; Sprenger et al., 2019; Strassmann et al., 2005; Tomonaga et al., 2013) (Table 6). These techniques have not yet been used offshore, however, for two reasons. First, the sample quantities required are higher than the pore water quantities usually obtained from sediment cores. Different horizons need to be isolated to minimize mixing of groundwater of different ages and depths. Packer systems and pumping tests in boreholes can provide the required volumes and isolation, but these techniques have seldom been employed as part of OFG studies (e.g., Johnston, 1983; Krantz et al., 2004). Second, noble gases in sediment pore waters can be strongly dominated by molecular diffusion (Strassmann et al., 2005), which does not allow conventional dating employed in onshore groundwater studies. Detailed knowledge of how different types of OFG systems function is needed to identify the best data collection and analytical approach.

Carbonate geochronology has the potential to fill important knowledge gaps in OFG research. Stable Sr systematics are promising tools for the identification of timelines for groundwater emplacement and reservoir host rock formation, as demonstrated by studies of marine Sr budget and influencing source variations (Beck et al., 2013; Krabbenhöft et al., 2010). This approach requires the application, transfer, and exploration of recent advances in U-Th geochronological approaches on calcite (Yehudai et al., 2017) for rather young time scales within last glacial/interglacial cycles, and in U-Pb geochronology of carbonate formation reaching back to hundreds of millions of years (Godeau et al., 2018; Roberts et al., 2020). The authigenic mineralization that accompanies fluid flow can be used to derive the age of pore water, for example, by analyzing $^{14}$C or U/Th (<350,000 a) of authigenic carbonates (Liebetrau et al., 2014). A survey of carbonate rock $^{18}$O composition collected from active and ancient continental shelf environments reveals important interactions with meteoric waters (Mozley & Burns, 1993), which may also help reveal meteoric flow system activity during sea level lowstands.

### 4.4. Geophysical Methods

The survey examples shown in Figure 7 demonstrate how offshore EM data can improve estimates of the extent of aquifer systems and the total volume of OFG. Similar marine EM campaigns have only been carried out at three locations (Attias et al., 2020; Gustafson et al., 2019; Micallef et al., 2020). Future surveys should either characterize OFG systems in broader regional contexts and link them to regional terrestrial hydrologic systems, or should be designed to more tightly constrain localized systems. Results from EM surveys can be coupled, where available, with geophysical well logs, allowing the characterization of pore water properties at a drill site and their lateral extrapolation. Resistivity and induction logs record the conductivities of the formations, from which pore water conductivity estimates can be derived (Archie, 1942; Waxman & Smits, 1968). Nuclear magnetic resonance logs, on the other hand, can determine rock porosity, fluid content and permeability.

The significant amount of seismic reflection data already acquired for hydrocarbon exploration on continental margins worldwide, where available for shallow sub-seafloor depths, provides a valuable database for locating and investigating OFG bodies, as shown in Australia and Suriname (Groen, Velstra, & Meesters, 2000; Varma & Michael, 2012). The application of techniques used in petroleum geology can ensure that the full potential of the seismic reflection data is exploited. Pre- and post-stack seismic attributes can be used to interpret lithology and provide quantitative estimates of porosity, which can be related to permeability in sub-surface rocks. Seismic inversion is commonly used in hydrocarbon exploration to transform seismic reflection data into quantitative rock properties (Avseth et al., 2009; Mavko et al., 2003). Via this method, seismic reflection data can be transformed into acoustic impedance and subsequently into density, which can be used to constrain porosity; ties with well logs can improve the confidence of these inversions. The accuracy of this method is strongly dependent on the quality of logs from well tie and the availability of boreholes intersecting the seismic line trace. Post-stack attributes, such as coherence and amplitudes, can provide an indication of the lateral extent of lithological units representing aquifers or aquitards and can be used to enhance the interpretation of fractures or faults, channels, pipes, or other discontinuous features that might represent a permeability boundary (e.g., Lofi, Inwood, et al., 2013). The presence of overpressures can be detected through indirect observations of fluid expulsion features on post-stack seismic data interpretation, AVO/AVA (amplitude vs. offset or amplitude vs. angle) (Castagna & Smith, 1994; Castagna & Swan, 1997) or seismic velocity analysis (Huffman, 2002; Sayers et al., 2002). Core-log-seismic integration allows extrapolating the 1-D information from boreholes (sub-millimeter to decimeter scales) into 2-D and 3-D Earth models from seismic reflection data (various meter scale). There is, however, a need to identify the measurable parameters and properties that can improve such correlations.

A fundamental question is how geophysical data can best constrain offshore aquifer thickness, porosity, and pore water salinity to provide estimations of total freshened groundwater volume. Marine geophysical data inversions for physical parameters (e.g., resistivity and velocity) are inherently non-unique, and these ambiguities propagate to the derived geological properties such as porosity. In Figure 10 we illustrate exploration limitations and their possible mitigations. Using the synthetic model in Figure 5a containing a freshened aquifer and a low porosity gravel layer, we calculate EM and seismic velocity data with added noise. Ambiguities of the model parameters (resistivity, velocity, and layer thicknesses) for the aquifer and gravel layer are illustrated in Figure 10a (black lines) and Figure 10b. When determining equivalent models (thickness and resistivity) for the gravel or aquifer layer, we assumed all other model parameters to be known. The responses to the resistivity models shown in Figures 10a and 10b are equivalent and thus cannot be distinguished from each other by the data. Figure 10c shows the equivalent geological models derived from the resistivity and velocity models. Resistivity data can be explained by a relatively large range of layer thickness, porosity, and salinity values. In contrast, seismic velocity data are unaffected by salinity and exhibit a tighter range in layer thickness and porosity. Thus, using structural information from seismic imaging in the geophysical inversion and porosity constraints from velocity data in the geological interpretation results in greatly reduced ambiguity and a more accurate characterization of the aquifer. Additional improvements in resolution and model reliability can be gained by jointly inverting seismic reflection and EM data using coupled parameterizations (Heincke et al., 2017; Moorkamp et al., 2013).

Understanding the evolution and sustainability of OFG requires imaging across the shoreline to establish connectivity between onshore and offshore aquifers. Airborne EM surveys have been used extensively for

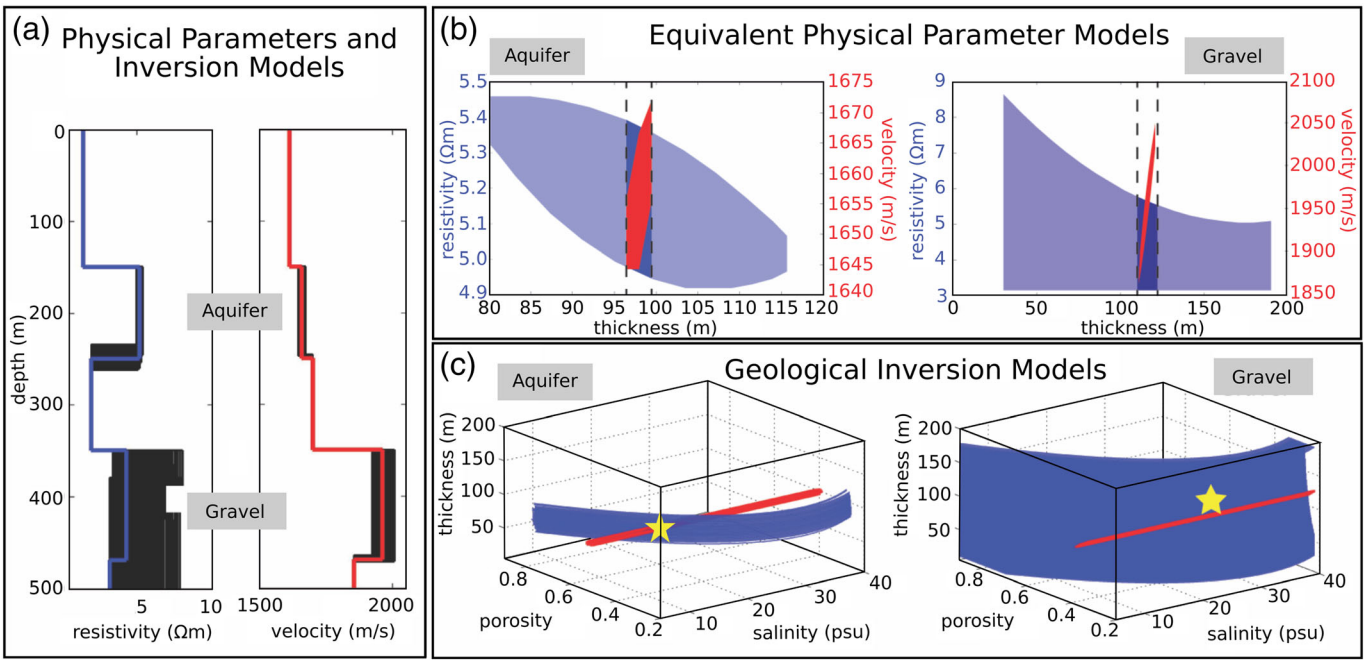


**Figure 10.** (a) Resistivity (left) and velocity (right) inversion models, which fit the synthetic noisy data generated by the true model (blue and red lines). (b) Equivalent velocity and resistivity models for the aquifer (left) and gravel layer (right). Blue area corresponds to equivalent resistivity and red to equivalent velocity models. The black lines outline the residual range of equivalent models when a common thickness of the layer is required. (c) Possible geological models (porosity, salinity, and thickness) derived from equivalent resistivity (blue) and velocity (red) models for the aquifer (left) and gravel (right) layer. The intersecting set of the red and blue models shows the plausible joint geological model range defined by seismic and electromagnetic data; yellow star denotes the true model parameters.

hydrogeological studies in coastal areas (Goebel et al., 2019; Kirkegaard et al., 2011; Siemon et al., 2009), but are limited to water depths of <10 m. As a result, additional geophysical techniques (e.g., terrestrial transient EM) are required to connect the geophysical image across the shoreline (Weymer et al., 2020). Given that the signature of an aquifer might change to a conductive anomaly on land (depending on level and type of water saturation) (Evans & Lizarralde, 2011), continuous imaging of an offshore-onshore aquifer can be challenging. In addition, the acquisition of seismic reflection data poses a technical challenge in shallow water areas. Offshore pumping in concert with 4-D EM surveys, on the other hand, can help assess seawater migration during OFG production.

### 4.5. Numerical Modeling

The discovery of significant variability in shore-parallel formation resistivities across the Canterbury Bight (Micallef et al., 2020) suggests that 3-D continental shelf heterogeneities need to be constrained in order to make numerical models informative. Lateral variations in permeability are likely due to avulsing river systems on an exposed continental shelf. An important next step would entail using heterogeneity information, derived from either 3-D seismic reflection data or laboratory simulations (Paola et al., 2001), to develop a 3-D stratigraphy of the shelf that can be used in numerical models. 3-D seismic reflection data may also be used to reconstruct past shelf morphologies and account for topographically driven flow in the past.

Geostatistical methods are now being used to construct stochastic realizations of representative geological models, along with the associated permeability heterogeneity (Thomas et al., 2019; Yu & Michael, 2019a; Zamrsky et al., 2020). Future geostatistical models must address regional geologic trends such as decreasing grain size in the offshore direction (e.g., Browne & Naish, 2003) and porosity compaction (Athy, 1930). Analog data sets or numerical models can be used to simulate sedimentary structures at a high resolution. Multiple-point geostatistics is another useful technique, where three or more points in space are used to characterize complex geological structures (Strebelle, 2002). Both the shape and geometry of the geological features to be modeled need to be taken into consideration when selecting the modeling approach (Seifert & Jensen, 1999).

Accurate numerical simulation of haline convection will require representation of lateral and vertical variations in permeability using geostatistical methods on highly resolved grids. On the other hand, continental shelf flow systems have natural lateral dimensions of hundreds of km and thicknesses of at least 1 km. This suggests that future continental shelf modeling projects will likely utilize high-performance computer (HPC) models. Community models such as *SEAWAT* will have to be parallelized.

Simulated groundwater residence times (e.g., Goode, 1996) for OFG systems represent an important future direction for OFG palaeo-hydrologic groundwater models. Post, Vandenbohede, et al. (2013) were the first to assess mean groundwater age for coastal mixing zone systems. More recently, groundwater residence time calculations under conditions of Pleistocene sea level variations were used to assess the timing of OFG emplacement offshore of New Zealand (Micallef et al., 2020).

The discovery of continental shelf groundwater having salinities higher than seawater at shallow depth (<1 km) on the continental shelf systems off New Jersey's continental margin (Gustafson et al., 2019; Mountain et al., 2010) and the Canterbury Bight (Fulthorpe et al., 2011) indicates that OFG models need to take upward brine migration into consideration. This can be done by: (i) extending the model to depths where evaporite layers occur, (ii) representing continental shelf salinity evolution on much longer time scales, (iii) including evolving grids to represent sedimentation, subsidence, and erosion, and (iv) incorporating compaction-driven flow and geothermal convection processes (Bratton, 2010; Caspard et al., 2004; Hughes et al., 2009, 2007; Kohout, 1965; Wilson, 2005, 2003). The latter will allow the identification of the most important process driving upward brine migration.

## 5. Frontier Applications of OFG Research

There are numerous fields of pure and applied research that are likely to see significant advances in the years to come as a result of recent and predicted advancements in our understanding of OFG systems. In the last section of this review we discuss two of the most promising: exploitation as a water resource, and sub-surface geomicrobiology.

### 5.1. Exploitation as a Water Resource

#### 5.1.1. Potential

Access to clean and safe water is at the core of sustainable socio-economic development, and it has been included in the United Nations' sustainable development goals (SDG6). Sixty percent of the global population lives in areas of water stress (Damania et al., 2017); water stress is defined as the ratio of total water withdrawals to available renewable surface and groundwater supplies. “High” to “extremely high” water stress levels are found in western North and South America, NW Europe, the Mediterranean Sea region, wide swathes of Africa and Australia, and the stretch of coastline from the Arabian Peninsula to the Indian sub-continent (Figure 2). Water stress in coastal communities is increasing due to climate change, rapid population growth, and urbanization (Aeshbach-Hertig & Gleeson, 2012; Bates et al., 2008; Hofste et al., 2019). Major coastal cities, such as Cape Town (South Africa) in 2018 and Chennai (India) in 2019, have already suffered extreme water shortages, and other large cities like Jakarta, Beijing, and Sao Paolo are likely to follow suit (BBC News, 2018). By 2030, we may fall 40% short of the amount of freshwater needed to support the global economy (United Nations, 2015).

OFG has been proposed as an alternative source of freshwater to relieve water scarcity, mitigate the adverse effects of groundwater depletion in coastal regions, and provide a buffer to increased demand during periods of intense drought (Bakken et al., 2012; UN-Water, 2020). At Atlantic City and Cape May, water is produced via onshore pumping from a brackish groundwater body that extends offshore (Barlow, 2003; McAuley et al., 2001). However, to our knowledge, contained OFG bodies have not been directly or intentionally exploited so far. Whether OFG can be used as an unconventional source of potable water in coastal regions is still uncertain. This is mainly due to difficulties with prospecting and quantification, and a resulting lack of information on the location, volume, and salinity of the OFG, and the properties of the aquifer where it is hosted and the overlying confining units. These difficulties can be addressed as described in section 4. Here we use the available information in the database (Micallef, 2020) to carry out a simple calculation of where OFG may be a source of freshwater and for how long. We consider those records where OFG is meteorically recharged, has a minimum salinity of <10 PSU, and is hosted in sandstone aquifers. Where information on offshore distance and thickness is available, we estimated the volume of OFG per km of

**Table 7**
*Estimation of Years of Available Freshwater Derived From OFG Systems for Selected Cities*

| OFG site | Offshore distance (km) | Thickness (m) | Volume of OFG in $km^3$ per km of shoreline | Volume of OFG in $km^3$ per km of shoreline after desalination | City | Daily water consumption per capita (L)[a] | Population[b] | Years of available freshwater |
|---|---|---|---|---|---|---|---|---|
| Baltic Sea | 70 | 23 | 0.72 | 0.29 | Stockholm | 180 | 975,000 | **45** |
| Beaufort McKenzie Basin | 100 | 1,000 | 45.00 | 18.00 | Whitehorse | 406 | 25,000 | **48,586** |
| Bredasdorp Basin (South Africa) | 100 | 2,000 | 90.00 | 36.00 | Cape Town | 173 | 430,000 | **13,259** |
| Canterbury Bight (New Zealand) | 60 | 250 | 6.75 | 2.70 | Christchurch | 450 | 363,000 | **453** |
| Gippsland (Australia) | 10 | 1,600 | 7.20 | 2.88 | Melbourne | 166 | 5,000,000 | **95** |
| Hong Kong | 2 | 40 | 0.04 | 0.01 | Hong Kong | 130 | 7,500,000 | **0.4** |
| Israel | 3.5 | 150 | 0.24 | 0.09 | Tel Aviv | 837 | 410,000 | **8** |
| Mahakam Basin | 20 | 2,130 | 19.17 | 7.67 | Balikpanan | 1,194 | 850,000 | **207** |
| Nantucket (USA) | 60 | 500 | 13.50 | 5.40 | Boston | 246 | 694,000 | **867** |
| Niger Delta | 40 | 1,840 | 33.12 | 13.25 | Port Harcourt | 230 | 1,000,000 | **1,578** |
| Perth Basin (Australia) | 50 | 2,700 | 60.75 | 24.30 | Perth | 340 | 2,000,000 | **979** |
| Suriname | 90 | 600 | 24.30 | 9.72 | Parambiro | 3,339 | 234,000 | **341** |

[a]Source: https://www.worldometers.info/water/ [b]Source: https://www.citypopulation.de/

shoreline by considering a rectangular profile and a porosity of 45%. We assume that 60% of the available OFG volume is lost as brine during desalination (Jones et al., 2019). The remaining OFG volume is used to estimate the number of years when freshwater would be available for the largest city located closest to the OFG record and by considering the current population and annual water consumption rates (Table 7). The cities where OFG has the highest potential to be used as a resource, also in consideration of water stress at present (Figure 2), are Cape Town, Melbourne, and Perth.

Additional limitations to the use of OFG as a resource are tied to the poorly quantified technological and economic feasibility of OFG utilization, the poorly constrained environmental impact of OFG extraction, and the unclear legal implications of OFG extraction are unclear. A brief consideration of the most recent developments related to these issues is presented in sections 5.1.2–5.1.4.

Another use of OFG may be water injection to enhance oil recovery (Person et al., 2017). The salinity of the water used in enhanced oil recovery can play a critical role in oil production. Low salinity groundwater (<5 PSU) can increase the recovery efficiency by 14% on average in comparison to higher salinity water (Lager et al., 2007). Person et al. (2017) demonstrated that offshore regions that contain OFG coincide with passive margin areas hosting proven hydrocarbon reserves. Other potential petroleum-related applications of OFG include enhanced oil recovery with polymer flooding, and as fracking fluid once hydro-fracking becomes more common offshore.

#### 5.1.2. Exploitation Strategies

Utilization of OFG may happen when the costs for exploring, pumping, transporting, and treating OFG will be lower than the costs of seawater desalination by reverse osmosis. Exploitation will require drilling, extraction and transportation of the groundwater from offshore aquifers to water processing plants. The capital costs of developing OFG are relatively high, exceeding $5 million for drilling and installing one offshore well. Bakken et al. (2012) had concluded that OFG could be a potential substitute for desalination of seawater, in terms of comparable or lower cost potential. This study was generic, however, and no site-specific data were used to evaluate the economic feasibility of OFG use. A thorough economic assessment requires detailed information on demands and costs (which depend on the offshore distance, sub-seafloor depth, and permeability of the offshore aquifer, among others) on a local and regional scale.

The technological requirements for OFG exploitation are still not well defined. The process could take advantage of technology and infrastructures installed by the oil and gas industry as well as existing desalination plants. A jack-up rig or a barge with a modular rig has been proposed to drill wells for OFG extraction (Bakken et al., 2012). For OFG production, a modular rig on an offshore platform (Bakken et al., 2012) or horizontal wells extending from existing offshore platforms (Person et al., 2017) could be utilized to extract OFG near hydrocarbon production sites. Transport of large volumes of OFG from offshore regions to

onshore plants needs pipelines, and existing ones used for the oil and gas industry may be converted for such a purpose. A single horizontal well is estimated to produce 16,366 $m^3$/day (3,000 gpm) (Person et al., 2017). If a general purpose tanker with a capacity of 18,900 $m^3$ (5 million gallons) were to be used to transport OFG, it would be filled in ~1 day. An idealized numerical model demonstrated that the salinity of brackish submarine groundwater could be maintained below 5 PSU at a production well after 30 years of continuous pumping at a rate of 19 $m^3$/day/m of well screen via a single 1,000-m-long horizontal well (Person et al., 2017). This generic study was conducted in a single-layered, relatively permeable confined aquifer system with a homogeneous permeability ($10^{-12}$ to $10^{-11}$ $m^2$) and sandwiched between lower-permeability ($10^{-15}$ $m^2$) confining units above and below. The effects of confining units and aquifer heterogeneity could greatly reduce the volume of freshwater production before seawater breakthrough. Site-specific modeling studies based on detailed characterization of regional hydrostratigraphy are thus needed to guide best practices of OFG exploitation by allowing testing of a wide range of pumping rates and well configurations.

Once the water has been transported onshore, the type of treatment for use as drinking water depends on the quality of the OFG. While brackish offshore groundwater does not satisfy drinking water standards, it is more economically favorable to desalinate than seawater (\$0.29/$m^3$ to \$0.66/$m^3$, Arroyo & Shirazi, 2012; in comparison \$0.79/$m^3$ to \$2.38/$m^3$, Water Reuse Association, 2012), which could spurn synergistic relationships between OFG production and coastal desalination facilities (Stein et al., 2016). Developing OFG sites located in proximity of existing desalination plants makes economic sense, especially when the OFG is connected to an onshore aquifer and it can be extracted via pre-existing onshore wells. The high capital costs associated to OFG production would be partially offset, and there are significant cost savings, as well as reduced greenhouse gas emission, associated to desalinating brackish water rather than seawater (Karagiannis & Soldatos, 2008).

Pumping of brackish offshore groundwater without recharge (e.g., extraction of palaeo-waters) may result in spatial and temporal salinity variations of the source water, which could lead to an adverse impact on the reverse osmosis process and the need for expensive infrastructural repairs. To provide source water with constant salinity, mixing OFG pumped from different wells with different salinities (both higher and lower than the desired salinity) may be an effective solution. Care needs to be taken to calculate the saturation index of different mineral species of the OFG mixture to avoid mineral precipitation and well/membrane clogging (Stuyfzand & Raat, 2010). The use of chemicals might be necessary when the solutes in the groundwater precipitate and clog the membrane of the desalination facility (Greenlee et al., 2009). It is also worth noting that there is the possibility that radium and boron concentrations of OFG could exceed permissible drinking water standards (Stuyfzand & Raat, 2010). Reduced groundwater frequently contains high concentrations of dissolved metals such as arsenic (Schaefer et al., 2016). These metals could potentially be removed by aeration systems prior to desalination.

#### 5.1.3. Environmental Impacts

The environmental impacts of OFG extraction depend primarily on the distribution of the aquifers, the emplacement mechanism, and the extent to which they are connected to active onshore aquifers. In actively recharging systems, OFG is a renewable resource as long as the extraction rate is lower than the rate at which the OFG is being recharged. If less water is extracted during dry seasons than is recharged during wet seasons, OFG may be used to allay water stress in dry seasons. Preferential flow conduits in actively recharging systems can conduct fresh groundwater offshore, yet those same conduits may provide a route for fast salinization due to onshore and offshore pumping (Geng & Michael, 2020; Kreyns et al., 2020; McAuley et al., 2001; Michael et al., 2016; Yu & Michael, 2019a; Yu & Michael, 2019b). Conversely, OFG systems that lack a direct land-sea connection may be more stable and resistant to saltwater intrusion. Their exploitation can still lead to drawdown and saltwater intrusion elsewhere. If the OFG in these systems is not being actively recharged and has predominantly been emplaced during lowstands, they are a limited resource and sustainable usage is not possible. However, if the systems are geologically young or have a strong connection to the seafloor (e.g., through SGD), extraction may still be preferable because the resource would be lost regardless due to leakage and salinization.

OFG bodies are already being actively and passively produced by onshore extractions (Geng & Michael, 2020; Knight et al., 2018; Werner et al., 2013; Yu & Michael, 2019b). Extraction of freshened groundwater from offshore aquifers that are connected to onshore systems may directly reduce the quantity of water that can be

pumped from onshore wells and result in loss in, or contamination of, SGD (Varma & Michael, 2012; Yu & Michael, 2019a). The latter can negatively impact benthic ecosystems (Amato et al., 2016), including microbial communities (Adyasari et al., 2019). If OFG extraction taps the mixed water from the transition zone, it can expose the onshore aquifer to seawater intrusion (Houben & Post, 2017). The more heterogeneous the aquifer structure is, the larger the magnitude of these impacts. In this regard, it is particularly important to understand the 3-D configuration of aquifers and confining units and the temporal variability of the OFG system.

Another unwanted collateral of OFG extraction is surface subsidence. Pumping of OFG will cause a volume deficit in the subsurface causing the seafloor to subside. This subsidence may extend onshore if drawdowns propagate (Yu & Michael, 2019a). This relative rise in sea level aggravates problems caused by eustatic sea level rise (Neumann et al., 2015; Nicholls & Cazenave, 2010). Oil and gas production in the Adriatic Sea, for example, threatened to worsen subsidence issues in the city of Venice (Gambolati et al., 1984). Coastal groundwater extraction has caused severe subsidence problems in places such as Jakarta (Chaussard et al., 2013), although there are also examples where the discontinuation of coastal groundwater extraction was able to halt and even reverse subsidence (Chen et al., 2007).

Additional environmental impacts associated to OFG extraction include (i) handling of brine, a by-product of the desalination process that needs to be disposed of; the salinity of the disposed brine from OFG desalination will be lower than that for seawater (Ghaffour et al., 2013); (ii) habitat degradation caused by well, pipeline, and treatment plant construction, which can result in a negative impact on faunal migration routes, spawning grounds, and an overall reduction in habitat quality; (iii) cultural noise during drilling operations, refuse left behind after shutting down wells, and artificial structures (e.g., rigs and platforms) that are associated with negative aesthetic impacts; and (iv) cross-contamination from existing exploration boreholes where drilling fluids and brines are re-injected into the surrounding seawater (Bakken et al., 2012).

A thorough assessment of the environmental impacts listed above needs to be made before OFG exploitation can commence. Since our understanding of such impacts is still limited, future research efforts should focus on their modeling and field monitoring.

#### 5.1.4. Legal Implications

Exploitation of natural resources requires clarity about rights to access, possess, and distribute those resources, and guidance for governance of offshore natural resources can be found in the 1982 UN Convention on the Law of the Sea, which has been adopted by the vast majority of nations and is almost universally followed. Pursuant to this convention, each coastal state has the exclusive sovereign right to all natural resources in its seabed and in the overlying water column for a distance of 370 km from the low tide shoreline, an area that is called the Exclusive Economic Zone. If a state can prove that its outer continental shelf extends beyond the Exclusive Economic Zone, then it can claim exclusive sovereign rights to seabed natural resources for up to another 278 km beyond the 200 nautical mile zone. However, pursuant to the UN Convention on the Law of the Sea, up to 7% of the value or volume of production of outer continental shelf seabed resources must be contributed to the International Seabed Authority for distribution to developing states. Natural resources lying beyond the Exclusive Economic Zone and the outer continental shelf are outside national jurisdiction and are considered to be the "common heritage of mankind". Under current legal regimes, land-locked nations have no rights to natural marine resources (Martin-Nagle, 2016).

Most OFG that has been discovered to date lies within domestic Exclusive Economic Zones, although higher salinity OFG has been detected in the outer continental shelf and in areas beyond national jurisdiction. While deposits of OFG will almost certainly be found straddling maritime boundaries, the UN Convention on the Law of the Sea provides no guidance on transboundary resources. Given this governance void, states will probably follow customary patterns that have evolved for transboundary reserves of offshore oil and gas (Martin-Nagle, 2020). Many states sharing hydrocarbon deposits establish joint development agreements, wherein they agree to cooperate in exploration and exploitation by appointing a single operator and negotiating allocation of expenses and production (Ong, 2002). Joint development agreements, also known as participation agreements, are adopted by many private organizations as well (Villarreal & LeVoy, 2010).

Allocation and distribution of OFG and other natural resources is left to the discretion of the sovereign state or states, with no obligation to ensure equitable dissemination. Concerns about water scarcity have

produced a growing chorus for establishment of a human right to adequate quantities of potable water (Morgera et al., 2020). Further, ecosystems depending on OFG are not guaranteed an adequate supply of freshwater for their survival, although some governments have passed laws giving legal rights to rivers and to nature generally (Martin-Nagle, 2020).

Extraction of freshened groundwater from its offshore environs would not proceed without usage conflicts with, for example, fishing, shipping, mining, cable placement, marine research, and military exercises. Often, each sector has its own laws, rules, regulations, and principles and its own governing body. The nascent practices of integrated ocean management, integrated coastal zone management, and marine spatial planning attempt to organize and harmonize the plethora of marine activities, impacts, and obligations, but for the moment any nation or organization wishing to exploit OFG will have to navigate a labyrinth of domestic, regional and international requirements and restrictions (Scott, 2015).

While the UN Convention on the Law of the Sea provides an overall framework for ocean management, and regional agreements may impose additional obligations on state signatories, those obligations are enacted through national laws. Therefore, exploration and exploitation of OFG found in domestic Exclusive Economic Zones and outer continental shelves must comply with the laws of the country in whose jurisdiction the resource is located. Rules and laws regarding prospecting, drilling, spatial planning, and environmental protections for that country's marine area generally, and for its seabed in particular, must be consulted and observed. In some countries, such as the United States, sub-national units have their own legal rights and requirements regarding coastal activities that must also be observed (e.g., 1953 Submerged Lands Act, 43 U.S.C. 1301 et seq). Where they exist, statutes and regulations governing offshore hydrocarbon development may provide guidance regarding administrative requirements. Exploration and development of any transboundary OFG will require coordination with and between the nations in whose jurisdictions the deposit lies.

### 5.2. Sub-Surface Geomicrobiology of OFG Systems

Microbes are ubiquitous and found in all aquifers that are within the thermal constraints for life. There have been substantial efforts to estimate the total abundance of sub-surface microbes based on scientific drilling operations over the past few decades (Bar-On et al., 2018; Magnabosco et al., 2018). Such studies suggest that there are an order of $10^{29}$ to $10^{30}$ cells in total and that the deep biosphere is dominated by a diverse array of microbes that includes bacteria, archaea microeukaryotes (Edgcomb et al., 2011; Liu et al., 2017), and viruses (Engelhardt et al., 2014; Nigro et al., 2017; Pan et al., 2019).

Little is known about the microbial communities that inhabit the sub-surface interface between freshwater and marine aquifers. Even in sub-surface systems where microbial samples have been collected, there remain many unknowns due to the overall paucity of data. For example, microbial communities could contain organisms that are capable of generating their own inorganic carbon (autotrophs), or heterotrophs that utilize organic carbon from the environment. Autotrophs may be dominant in areas with mixing of reduced and oxidized inorganic compounds, thereby providing the energy sources they need to grow. Reduced inorganic species could enter the aquifers via flow into a less reduced region, from low-permeability units that are more reducing, or an active zone at the margin. Heterotrophs may be dominant in zones where a source of organic carbon exists (e.g., entry via freshwater recharge, autochthonous carbon from within the aquifers, carbon from low-permeability units, and carbon recharging from the seaward side).

In order to infer the biogeochemical processes that might be occurring offshore, it is useful to examine onshore systems with similar geology and flow paths. Of the studies that have analyzed microbial communities in sedimentary coastal aquifers, the majority has been from a pollution-tracking perspective (e.g., studies on contaminated aquifers on Cape Cod; Harvey & George, 1987) and/or focused on relatively shallow zones (Santoro et al., 2006, 2008). Coastal core transects intersecting a shallow (~10 m) groundwater body have shown that microbial communities, interrogated based on their nitrogen cycling genes, appear to differ across geochemical gradients in coastal groundwater (Santoro et al., 2006, 2008). The authors are unaware of any deep (>100 m) studies of OFG microbial communities. Modeling of nutrient profiles have also suggested that microbial processes in marine sediments alone cannot account for observations without additional inputs from advective submarine groundwater transport (Jahnke et al., 2003).

It is an open question how, and under what conditions, microbes travel through sub-surface aquifers. Based on the low recoveries from tracer experiments, it is likely that most microbes entering an aquifer remain retained in constricted flow paths or biofilms. For example, studies in diverse groundwater systems (M. W. Becker et al., 2003; Cumbie & McKay, 1999; Harvey et al., 1993) showed <4% recovery of cells or microspheres injected in well tracer experiments. One study also compared types of cells and found the highest recovery from non-motile rods (3.5%) and small cocci (2.3%), compared to 91% of the deuterated water added as a chemical tracer (M. W. Becker et al., 2003). In addition, the discovery that non-motile cells had the highest recovery suggests that motile bacteria may have been able to move out of the main flow paths or were possibly more effective at establishing biofilms. There is also evidence that, in low nutrient environments, motile microbes will selectively collect in protected biofilm enclaves (Park et al., 2003) and can access mineral bound nutrients (Bennett et al., 2001).

The combination of evidence of diverse and abundant sub-surface life from terrestrial and marine studies, and the evidence for ample nutrient fluxes from geochemical studies, points to opportunities for discovery along this geochemical fringe. Key questions in sub-surface geomicrobiology of OFG can be addressed by (i) scientific drilling campaigns, which can directly access microbial communities, in both sediments and fluids, across geochemical gradients, and (ii) characterization of the OFG flow rates and pathways, and associated nutrient fluxes, by geochemical, geophysical, and numerical modeling methods. These approaches would provide cell density estimates, help understand the connectivity between terrestrial and marine sub-surface life, improve models of biogeochemical cycling in shelf environments, and inform on potential effects from alteration of OFG systems by human activity. The latter may be particularly important from a microbial perspective, since microbes are known to play an active role in the mobility of geogenic contaminants (e.g., arsenic; Fendorf et al., 2010) in groundwater quality for human consumption.

## 6. Summary

The majority of known OFG is located in passive margins, within 55 km of the coast, down to a water depth of 100 m and a sub-seafloor depth of 200 m. OFG predominantly occurs as multiple bodies that are up to 1 km thick, having mean salinities of 15 PSU, and hosted in siliciclastic aquifers with porosities of 30–60%. With an estimated global volume of ~$1 \times 10^6$ $km^3$, OFG has been documented up to a distance of 720 km from the coast and water depths of ~3,000 m. Meteoric recharge during sea level lowstands is the most common emplacement mechanism reported in the literature. The depositional architecture of continental margins is a key factor controlling OFG occurrence. The most important geological elements include a permeability contrast along the top of the OFG body, continuity/connectivity of permeable and confining strata, clinoform structures, buried palaeochannels, and faults. Dissolution and other diagenetic processes are additional elements in carbonate margins. Topography-driven flow and salinization due to sea level rise are key hydrological factors influencing OFG distribution.

Incidental discoveries during scientific and industry drilling have provided the most fundamental information on OFG thus far. Integration of chlorinity with stable isotope characteristics of water samples has been used to constrain the origin of OFG, although such analyses remain rare. Recent improvements in marine EM systems have provided the geoscience community with a non-invasive technique that can resolve electrically resistive sub-seafloor freshwater. Inversion and interpretation of EM and seismic reflection data provide important constraints on lithologies, geologic structures and palaeo-environmental evolution. Numerical modeling has been used since the 1980s to map OFG systems at the shelf scale. Analytical methods, numerical solutions using sharp-interface theory, and finite different and element methods have provided a cost-effective method for estimating OFG volumes and emplacement. These models are limited by uncertainties in petrophysical properties and boundary conditions, such as fluctuations in sea level and ice sheet thickness over geologic time scales. The shelf off the East Coast of the United States and Canterbury (New Zealand) provide the best examples of the application of the above methods for the investigation of OFG globally.

Numerous first-order questions on OFG remain unanswered. We have a poor understanding of the distribution, dimensions, flow characteristics, and function of OFG systems, while the mechanism and timing of OFG emplacement are rarely corroborated by geochemical data. Crucial to addressing these questions is the (i) application of isotopic tracers (such as $^{81}Kr$ and $^{4}He$) and carbonate geochronology to determine

OFG residence times, (ii) joint inversion of EM and seismic reflection data, and (iii) utilization of 3-D continental shelf hydrological models. However, a step change in our understanding of OFG will primarily require dedicated drilling campaigns in geophysically characterized OFG systems that include specialized in situ testing and sampling for hydrogeological properties, groundwater age, geochemistry, and biogeochemical processes and activity.

OFG has been proposed as an alternative source of freshwater in coastal regions. We have identified Cape Town, Melbourne, and Perth as the cities where OFG has the highest potential to be used as a resource. However, prospecting and quantification are still problematic, the technological and economic feasibility of OFG use is poorly quantified, the environmental impacts of OFG extraction are not well constrained, and the legal implications are unclear. Future studies should focus on addressing these issues by employing site-specific modeling and monitoring studies. Another frontier application of OFG research is sub-surface geomicrobiology. Sampling of microbial communities in OFG systems and characterization of the fluid flow rates and pathways can help update cell density estimates and understand the connectivity between terrestrial and marine sub-surface life.

## Appendix A: Mathematical Modeling of OFG—Fundamental Principles and Parameters

### A.1 Groundwater Flow

A complete mathematical description of continental shelf flow transport systems requires consideration of a number of coupled processes. These include groundwater flow, solute transport, fluid-rock geochemical reactions, heat transport, sedimentation, erosion, glaciations, changes in porosity, and permeability (Figure A1). Assuming one-dimensional (vertical) loading, the governing groundwater flow equation is given by

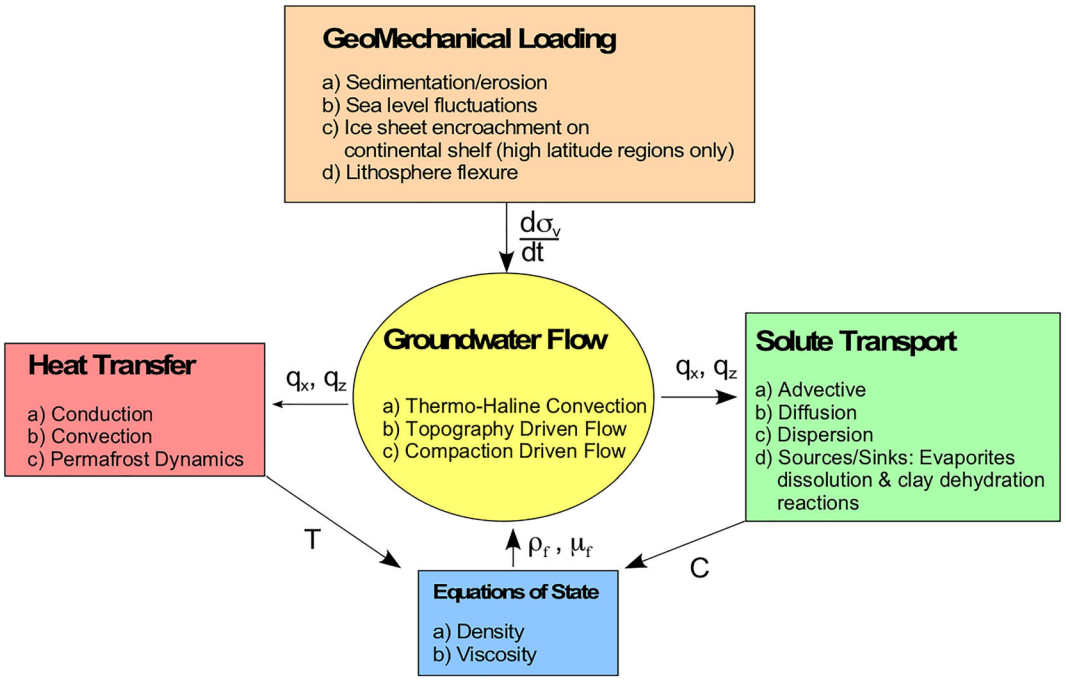


**Figure A1.** Schematic diagram depicting coupled transport processes influencing the emplacement of freshwater in continental shelf environments. Variables include vertical geomechanical load $\sigma_v$, time ($t$), Darcy flux in the horizontal and vertical directions ($q_x$, $q_z$), temperature ($T$), and solute concentration ($C$), fluid density ($\rho_f$), and fluid viscosity ($\mu_f$).

$$S_s\left[\frac{Dh}{Dt}+\zeta\frac{\partial\eta}{\partial t}-\frac{\zeta}{\rho_f g}\frac{\partial\sigma_z}{\partial t}\right]=\nabla\cdot[\mathbf{K}u_r\nabla(h+\rho_r z)]+f_{wt}\frac{\rho_s}{\rho_f}\frac{\partial s}{\partial t}(1-\varnothing)+\alpha_T\frac{\partial T}{\partial t} \quad \text{(A1)}$$

where $\zeta$ is the one-dimensional loading efficiency, $\partial\sigma_z/\partial t$ are the change in the vertical load through time resulting from sedimentation, erosion, or glaciations, $\partial\eta/\partial t$ is loading related to sea level fluctuations, $\mathbf{K}$ is the hydraulic conductivity tensor, $h$ is the equivalent freshwater hydraulic head, $\boldsymbol{\rho_r}$ the relative fluid density ($\rho_r = [\rho_f - \rho_o]/\rho_o$), $\rho_o$ is the base density at standard temperature, concentration, and pressure (10°C, 0 mg/L, atmospheric pressure), $z$ is elevation, $\rho_f$is fluid density, and $\rho_s$is the sediment density, $f_{wt}$ is the fraction of water in the clay (constant), $\frac{\partial s}{\partial t}$ is the temperature-dependent, illite-smectite transformation rate (Bekins et al., 1994), and $\alpha_T$ is the aquathermal expansion coefficient. Gas hydrates transformations and other $H_2O$ geochemical source terms are not represented in Equation A1.

The Darcy flux ($\vec{q}$) for variable-density groundwater flow is given by:

$$\vec{q}=-\nabla[\boldsymbol{\mu_r}\,\mathbf{K}(h+\rho_r z)] \quad \text{(A2)}$$

where $\boldsymbol{\mu_r}$ is the relative viscosity ($\boldsymbol{\mu_r = \mu_o/\mu_f}$), $\mu_o$ is the base viscosity at standard state conditions, (10°C, 0 mg/L, atmospheric pressure), and $\mu_f$ is the fluid viscosity at elevated temperatures and concentrations.

Hydraulic conductivity is a function of both fluid and rock properties:

$$K=\frac{\rho_o g k}{\mu_o} \quad \text{(A3a)}$$

$$log_{10}(k)=-a+b\phi \quad \text{(A3b)}$$

where $k$ is permeability and $a$, $b$ are empirical porosity $\log_{10}$ permeability fit coefficients. In the remainder of this text, we will refer to permeability rather than hydraulic conductivity when describing how transmissive a sediment/rock formation is. Permeability in marine environments can vary over a wide range (up to 9 orders of magnitude (Figures A2 and A3) and plays a critical role in the formation and preservation of OFG and anomalous pressure generation. Poorly consolidated marine sediments typically display a log-linear relationship between permeability and porosity:

$$\log_{10}(k)=\phi b-a \quad \text{(A4)}$$

where $a$ and $b$ are empirical fit coefficients. Porosity tends to decrease with depth due to the effects of mechanical compaction, with most porosity decrease occurring in the upper 500 m. A widely used equation to represent changes in porosity with depth is given by

$$\phi=\phi_o\exp(-\beta\sigma_e) \quad \text{(A5)}$$

where $\sigma_e$ is effective stress ($\sigma_e = \sigma_v - P$), $\beta$ is sediment compressibility, $\phi$ is porosity, $\phi_o$ is porosity at the sediment-water interface (i.e., $\sigma_e = 0$), and $\sigma_v$is the weight of the overlying sediment column. Note that there are other, more fundamental forms of compressibility than represented by Equation A5. Equation A5 is a simplified form of a more complex, multi-dimensional stress-strain analysis (Neuzil, 2003).

In order to solve the groundwater flow Equation A1, boundary and initial conditions must be specified. For two- or three-dimensional problems, the bottom and sides of the solution domain are typically set to be no-flux boundary conditions. A specified head (or on-shore recharge) is typically assigned to all nodes above sea level. For nodes below sea level, the sea level should be treated as a specified head boundary. Because Equation A1 solves for equivalent freshwater heads. The effects of seawater density must be included when sub-seafloor specified head boundary conditions are imposed:

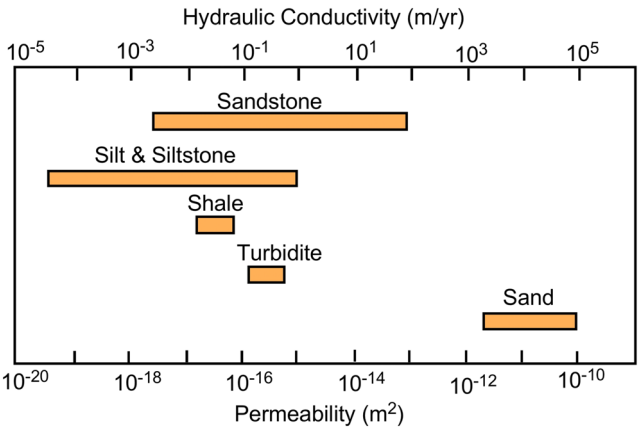


**Figure A2.** Range of measured permeability and hydraulic conductivity from sediment cores for passive margin deposits. (Sources: Janssen et al., 2005; Lofi, Pezard, et al., 2013; Meissl & Behrmann, 2010).

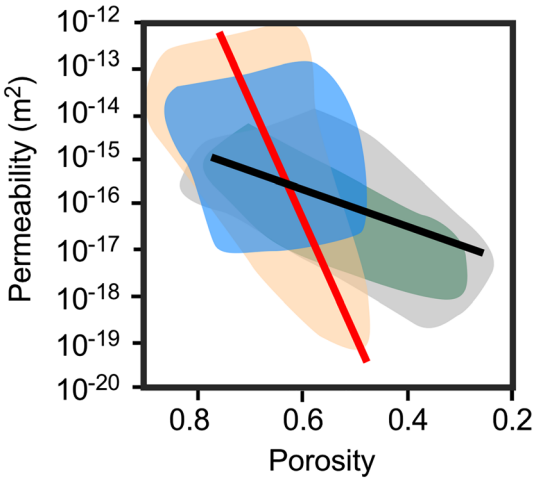


**Figure A3.** Plot of log permeability versus porosity for select marine sedimentary facies including turbidities (gray), calcareous (blue), and siliclastic (orange) sediments. (Source: Spinelli et al., 2004). The black and red lines are examples of application of Equation A3b. Note that there are at least four to six orders of magnitude in variability for a given porosity value. The black line used a = −32 and b = 26. The red line used a = −18.2 and b = 4.

$$h_{bc}(x,\ t) = \eta(t) + \frac{\rho_f - \rho_o}{\rho_o} d\ (x,\ t) \tag{A6}$$

where $h_{bc}(x,\ t)$ is the specified head for nodes below sea level, $d(x,\ t)$ is the water depth below sea level at a given location and time, and $\eta$ (t) is sea level elevation. During the Pleistocene, sea level varied by up to 120 m (Hansen et al., 2013). Hydrostatic initial conditions are typically imposed. For the continental shelf-slope boundary, a specified head can be set using Equation A6.

## A.2 Solute Transport

The governing solute transport equation through porous media due to advection, diffusion and dispersive processes (Konikow & Grove, 1977) is given by

$$\phi\frac{\partial C}{\partial t} + C\frac{\partial \phi}{\partial t} = \nabla\cdot[\phi \mathbf{D}\nabla C] - \nabla\left[C\overleftarrow{q}\right] + \gamma(C - C_{max}) \tag{A7}$$

where $C$ is concentration, $\gamma$ is a rate constant for evaporite dissolution, $C_{\max}$ is the equilibrium solubility of halite, and $\boldsymbol{D}$ is the hydrodynamic dispersion-diffusion tensor. The components of the hydrodynamic dispersion-diffusion tensor (in two dimensions: $D_{xx}$, $D_{zx}$, $D_{xz}$, and $D_{zz}$) are given by Bear (2012):

$$D_{xx} = \alpha_L\frac{v_x^2}{|v|} + \alpha_T\frac{v_z^2}{|v|} + D_d \tag{A8a}$$

$$D_{zz} = \alpha_T\frac{v_x^2}{|v|} + \alpha_L\frac{v_z^2}{|v|} + D_d \tag{A8b}$$

$$D_{xz} = D_{zx} = (\alpha_L - \alpha_T)\frac{v_x v_z}{|v|} \tag{A8c}$$

where $D_d$ is the solute diffusivity (~$10^{-10}$ to $10^{-11}$ $m^2/s$), $\alpha_L$ and $\alpha_T$ are the longitudinal (typically in the range of 10–100 m) and transverse dispersivities (typically $\alpha_T = 0.1\alpha_L$), and $v_x$ ($v_x = q_x/\phi$) and $v_z$ ($v_z = q_z/\phi$) are the seepage velocities in the $x$ and $z$ directions respectively, which are related to the Darcy flux ($\overrightarrow{q}$). Temporal porosity changes ($\frac{\partial\phi}{\partial t}$) are typically neglected in Equation A7 in all but the lowest-permeability environments (<$10^{-19}$ $m^2$) because of the dominant role advection plays. Evaporite dissolution can play an important role in continental shelf environments on increasing salinity beyond 35 PSU. Evapo-concentration of seawater in restricted marine environments can also account for elevated salinities as well (Sanford & Wood, 2001). Equation A7 does not include a sink term to account for the freshening of seawater due to clay dewatering (Saffer & McKiernan, 2009).

Boundary conditions for Equation A7 typically include a specified concentration along the top of the solution domain and no flux boundaries on the sides and base. Above sea level, a concentration of 0 PSU is specified and 35 PSU for areas below sea level. Studies focused on SGD sometimes impose a spring boundary condition ($dc/dz = 0$) wherever flow is upward at the seafloor in the offshore environment. This assumes the system is advection dominated.

Initial conditions are very important and potentially problematic for simulations on Pleistocene to Holocene time scales. In most cases, it is important to ensure that the initial salinity conditions do not influence modern calculated salinity conditions. Probably the most appropriate initial condition would be to spin the model up using Pleistocene temporal variations in sea level for at least 1 Ma (Hansen et al., 2013). A computationally less expensive initial condition would be to to compute steady-state salinity conditions for all cell. For all offshore cells, the local bathymetry of which is below 40 m (i.e., mean Pleistocene sea level, Meisler et al., 1984), the salinity would be set to 35 PSU. All cells where the local bathymetry is above 40 m should be set at 0 PSU (freshwater).

## A.3 Heat Transport

The governing flow equation accounting for conductive and convective components of heat transfer (Bethke, 1985) are given by:

$$\left[\phi c_f \rho_f + (1-\phi) c_s \rho_s\right] \frac{\partial T}{\partial t} + \frac{\rho_f h_f}{(1-\phi)} \frac{\partial \phi}{\partial t} = \nabla \cdot [\phi \boldsymbol{\lambda} \nabla T] - \nabla \left[T \overleftarrow{c_f \rho_f q}\right] \tag{A9}$$

where $\boldsymbol{\lambda}$ is the thermal dispersion-conduction tensor, $T$ is temperature, $c_S$ is the specific heat capacity of the solid phase, $c_f$ is the specific heat capacity of the fluid phase, $h_f$ is the fluid enthalpy, and $\rho_s$ is the density of the solid phase. Effects of transverse and lateral thermal dispersion in heat transport (de Marsily, 1986) are accounted for in the components of $\lambda_{xx}$, $\lambda_{zx}$, $\lambda_{xz}$, $\lambda_{zz}$which are given by:

$$\lambda_{xx} = \alpha_L \frac{q_x^2}{|v|} + \alpha_T \frac{q_z^2}{|q|} + \lambda_f \phi + (1-\phi)\lambda_f \tag{A10a}$$

$$\lambda_{zz} = \alpha_T \frac{q_x^2}{|q|} + \alpha_L \frac{q_z^2}{|q|} + \lambda_f \phi + (1-\phi)\lambda_f \tag{A10b}$$

$$\lambda_{xz} = \lambda_{zx} = (\alpha_L - \alpha_T) \frac{q_x q_z}{|q|} \tag{A10c}$$

where $\lambda_{xx}$, $\lambda_{xz}$, $\lambda_{zx}$, $\lambda_{zz}$are the components of the thermal conduction-dispersion tensor, $\alpha_L$ and $\alpha_T$ are the longitudinal and transverse dispersivities, $q_x$ and $q_z$ are Darcy fluxes in the $x$ and $z$ directions, and $\lambda_f$ and $\lambda_s$ are the thermal conductivity of the fluid and solid phases, which are assumed to be isotropic scalar quantities. $|q|$ is the absolute value of the Darcy flux, given by $|q| = \sqrt{q_x^2 + q_z^2}$. Equation A10a implicitly assumes that the solid phase is in thermal equilibrium with the fluid phase, which is reasonable for most basin environments.

In continental settings, land surface temperatures have varied globally by up to 6–15°C during the past 2.5 Ma. During the Pleistocene, permafrost formed at latitudes >48°N (Pewe, 1983). The largest continental temperature variations have occurred at high latitudes away from the coastline. Nevertheless, in regions where continental shelf aquifer systems crop out at the land far from the coastline, permafrost conditions have may have had an important effect on onshore recharge (Kleinberg & Griffin, 2005; McKenzie & Voss, 2013).

Boundary conditions should include a specified basal heat flux (~0.06 W/m$^2$), no flux sides, mean annual temperature above sea level and mean ocean temperature (~4°C) below sea level. A conductive vertical temperature gradient of 30°C/km is typically used as an initial condition.

## A.4 Equations of State

Equations for state are needed to formally couple the groundwater flow equation to the heat and solute transport equations. Density and viscosity changes are calculated based on second order polynomial expressions using temperature, concentrations, and pressure (e.g., Batzle & Wang, 1992; Kestin et al., 1981). In coastal aquifer settings within the upper 4 km, salinity typically varies between 0 and 35 PSU, temperature ranges between 4°C and 120°C, and pressure increases from 0 to 40 MPa (Figure A4). The presence of evaporite beds at depth can result in salinity exceeding 35 PSU. Figure A4 presents density and viscosity variations assuming linear increases in salinity (11.25 PSU/km), temperature 30°C/km), and pressure (10 MPa/km). For these conditions, fluid densities range between ~1,000 and 1,025 kg/m$^3$ and viscosity between ~0.00077 and 0.00125 kg/(m·s). Figure A4 was created using the equation of state of Batzle and Wang (1992) (Equations A11a–A12).

$$\rho_w^{TP} = 1 + 10^{-6}\left[-80T - 3.3T^2 + 0.00175T^3 + P - 2TP + 0.016T^2P - 1.3\times10^{-5}T^3P - 0.333P^3 - 0.002P^2T\right] \tag{A11a}$$

$$\rho_f = \rho_w^{TP} + C\left\{0.668 + 0.44C + 10^{-6}[300P - 2,400PC + T(80 + 3T - 3,300C - 13P + 47PC)]\right\} \tag{A11b}$$

$$\mu_f = 0.1 + 0.333\mathrm{C} + \left(1.65 + 91.9C^3\right)\exp\left\{-\left[0.42\left(C^{0.8} - 0.17\right)^2 + 0.045\right]T^{0.8}\right\} \tag{A12}$$

where $T$ is temperature (°C), $P$ is pressure (Pa), and $C$ is concentration (mass fraction, seawater is 0.035).

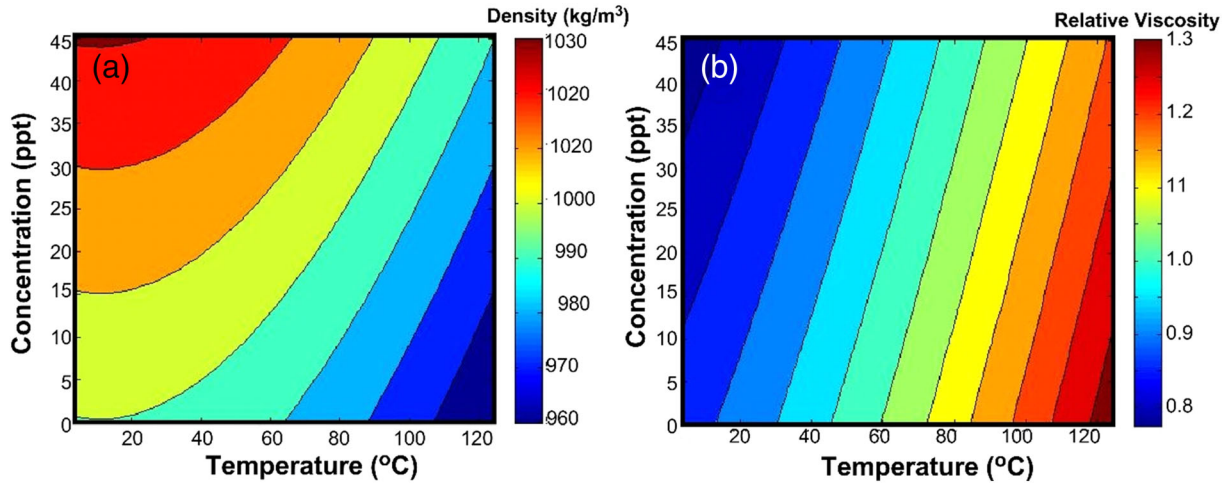


**Figure A4.** Changes in density and relative viscosity ($\mu_o/\mu$) over a depth range of 0–4 km due to temperature and salinity changes. The base viscosity ($\mu_o$) is 0.001 Pa-s. Note that it is assumed that pore pressure increased from 0 to 40 MPa, concurrently with temperature and salinity. Equation of state used to compute density and viscosity from Batzle and Wang (1992) (see Equations A11a and A12).

## A.5 Dimensionless Number Groups

Dimensionless number groups and scaling analysis are very useful tools for assessing the dominant flow mechanisms and characteristic time scales over which various transport processes operate on the continental shelf. Perhaps the most important dimensionless number for characterizing fluid flow in continental shelf environments is the Rayleigh number (*Ra*):

$$R_a = \frac{kHg\left(\rho_s - \rho_f\right)}{\mu_f D} \tag{A13}$$

where $g$ is gravity, $k$ is permeability, $D$ is solute diffusivity, and $H$ is thickness of the aquifer, for sea level rise across a permeable sand layer. The *Ra* number represents convective processes in the numerator and viscous and diffusive processes in the denominator (both of which oppose haline convection). Equation A13 helps to characterize whether or not a solute plume will form and descend from the seafloor resulting mixing and salinity increases. Post and Kooi (2003) reported various estimates of the critical *Ra* (when haline convection begins), from 400 to $3.6 \times 10^5$. These critical *Ra* number estimates assume Fickian diffusion. Incorporation of hydrodynamic dispersion into the Ra would modify these estimates (Duffy & Al-Hassan, 1988). Duffy and Al-Hassan (1988) proposed a modified Ra expressed by Equation A14, which considers the effects of lateral flow and dispersion associated with shore normal recharge:

$$R_a = \frac{kHg\ \Delta\rho}{\mu r_e\ \alpha_T} \tag{A14}$$

where $g$ is gravity, $k$ is permeability, $D$ is solute diffusivity, $\alpha_T$ is the transverse dispersivity, and $r_e$ is the average recharge rate per unit area. The numerator defines density-driven flow, which promotes haline convection while the denominator describes viscous and dispersive processes that retard haline convection.

An advective time scale for the solute front to reach the bottom of a layer of thickness H can be estimated as follows (Post & Kooi, 2003):

$$\tau_{Adv} = \frac{H}{v_z} = \frac{4H\phi\mu_f}{k\left(\rho_s - \rho_f\right)\mathrm{g}} \tag{A15}$$

where $v_z$ is the spatially averaged vertical velocity of a series of descending saline fingers, $H$ is the thickness of the sand bed, $\phi$ is porosity, and $\tau_{Adv}$ is the characteristic time scale for advection. Using a bed

thickness of 200 m, a permeability of $10^{-11}$ m$^2$, a porosity of 0.2, and a density difference of 25 kg/m$^3$, the characteristic diffusion time is about 51 a.

In low permeability clay units, solute diffusion may control the rate of solute transport and the characteristic time of diffusion; it is given by:

$$\tau_{Dif} \cong \frac{H^2}{D_d} \tag{A16}$$

where $\tau_{Dif}$ is the diffusive time scale. Using relatively thin clay layers (10 m) and a solute diffusivity of $3 \times 10^{-11}$ m$^2$/s, the diffusion time is about $10^5$ a, which is the same time scale of Milankovitch-driven sea level fluctuations over the past 1 Ma (Hansen et al., 2013).

## A.6 Sharp-Interface Models

Seawater and freshwater have densities of about 1,025 and 1,000 kg/m$^3$, respectively. In a permeable ($<10^{-14}$ m$^2$) coastal aquifer system, these relatively small density contrasts result in freshwater essentially floating on saltwater. The isostatic force balance in an aquifer between freshwater and seawater was first described by Ghyben-Herzberg (Wentworth, 1939) and is schematically illustrated in Figure A5. The pressure of a column of seawater of depth "$b$" is given by:

$$P_s = \rho_s b g \tag{A17}$$

Glover (1959) proposed a modification of the Ghyben-Herzberg principle at the coastline to allow freswater to discharge into the ocean across an interface of thickness.

At the interface between saltwater and freshwater, we can assume a pressure balance with the overlying freshwater lens. The pressure of the freshwater lens is given by:

$$P_f = (\Delta h + b)\rho_f g \tag{A18}$$

Equating the seawater and freshwater pressures at the interface yields:

$$P_f = P_s \tag{A19}$$

Substituting Equations A17 and A18 into A19 and solving for $\Delta h$:

$$\Delta h = \frac{\left(\rho_s - \rho_f\right) b}{\rho_f} \sim 40b \tag{A20}$$

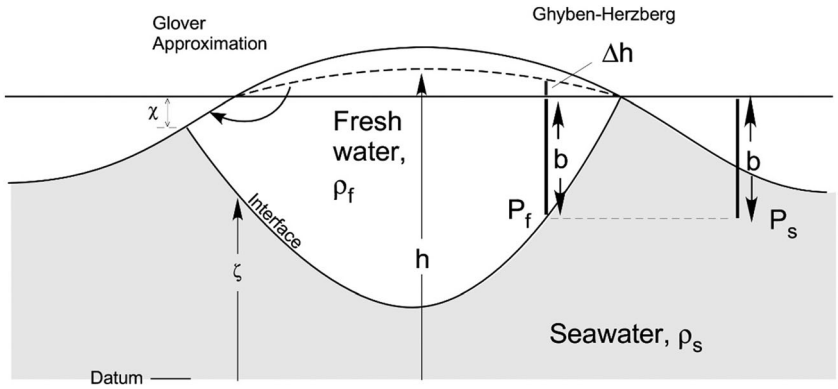


**Figure A5.** Schematic diagram illustrating the Ghyben-Herzberg principle used to estimate the depth to the interface between saltwater and freshwater (b) in a coastal aquifer system. The interface position represents a force balance between a lens of freshwater floating on seawater.

The relationship expressed in Equation A20 indicates that for every meter of water table elevation above sea level there is 40 m of freshwater below (Figure S5). At the coastline, however, where $\Delta h = 0$, the freshwater lens thickness is predicted to be 0, which is incorrect. Shoreward freshwater discharge must leave the coastline beneath the seafloor as SGD. Glover (1959) proposed an approximation for estimating the freshwater lens thickness at the shoreline:

$$\chi = -\frac{T_f}{K_f}\frac{\rho_f}{\Delta\rho}\frac{\partial h}{\partial n} \tag{A21}$$

Hydrogeologists have embedded the Ghyben-Herzberg approximation into transmissivity-based groundwater flow equations (Bakker, 2006; Ledoux et al., 1990). This assumption neglects vertical variations in hydraulic head and only represents lateral flow. The variable hydraulic conductivity is replaced by transmissivity (the product of saturated thickness and hydraulic conductivity). In the present application to coastal settings, two plan-view-based groundwater flow equations are developed for the freshwater and saltwater phases. The unknowns are the water table elevation ($h$) and the position of the freshwater saltwater interface ($\xi$). For a quasi-two-dimensional system, the two transport equations are given by:

$$\frac{\partial}{\partial x}\left(T_x^f\frac{\partial h}{\partial x}\right) = S_y\frac{\partial h}{\partial t} - \phi\frac{\partial \xi}{\partial t} - R + Q_p \tag{A22a}$$

$$\frac{\partial}{\partial x}\left(T_x^s\frac{\rho_s - \rho_f}{\rho_s}\frac{\partial \xi}{\partial x} + T_x^s\frac{\rho_f}{\rho_s}\frac{\partial h}{\partial x}\right) = \phi\frac{\partial \xi}{\partial t} \tag{A22b}$$

where $T_x^f$ is the freshwater transmissivity ($T_x^f = [K^f(h - \xi)]$), $T^s$ is the saltwater transmissivity ($T_x^s = K^s\xi$), $\rho_s$ is salt water density, $\rho_f$ is freshwater density, $h$ is water table elevation, $\xi$ is interface elevation, $x$ is lateral distance, $Q_p$ is the pumping rate of a municipal well, and $R$ is the recharge rate. The two dependent variables are $h$ and $\xi$. Note that both variables appear in each of the equations. Steady-state forms of these equations are given by:

$$\frac{\partial}{\partial x}\left(T_x^f\frac{\partial h}{\partial x}\right) = R - Q_p \tag{A23a}$$

$$\frac{\partial}{\partial x}\left(T_x^s\frac{\rho_s - \rho_f}{\rho_s}\frac{\partial z}{\partial x} + T_x^s\frac{\rho_f}{\rho_s}\frac{\partial h}{\partial x}\right) = 0 \tag{A23b}$$

Figure A6 compares steady-state solutions with the sharp-interface (Equations A23a and A23b) equations, finite element solutions, variable-density groundwater flow (Equation A1), and solute transport (Equation A7) equations. The parameters used in this model inter-comparison are listed in Table A1. The steady state sharp-interface equations were solved numerically using MATLAB. The two unknowns were solved for simultaneously using the finite difference method. About six iterations were required to converge at a solution. The maximum water table height was about 10.5 m above sea level along the right side of the model. Using the Glover equation (Equation A21), the freshwater lens thickness at the shoreline was 39.1 m. The variable-density groundwater flow and solute transport equations were solved sequentially using the finite element model *RIFT2D* (Wieck et al., 1995). We imposed a specified head boundary condition along seaward edge of the model domain. The model was run for 1 Ma to approach steady-state conditions using a grid composed of 161 nodal columns and 81 nodal rows. Equivalent freshwater heads are shown in Figure A6a. Comparison between computed salinities and the sharp-interface are shown Figure A6b. Groundwater flow patterns are not orthogonal to equivalent freshwater head contours due to variable-density effects in Figure A6.

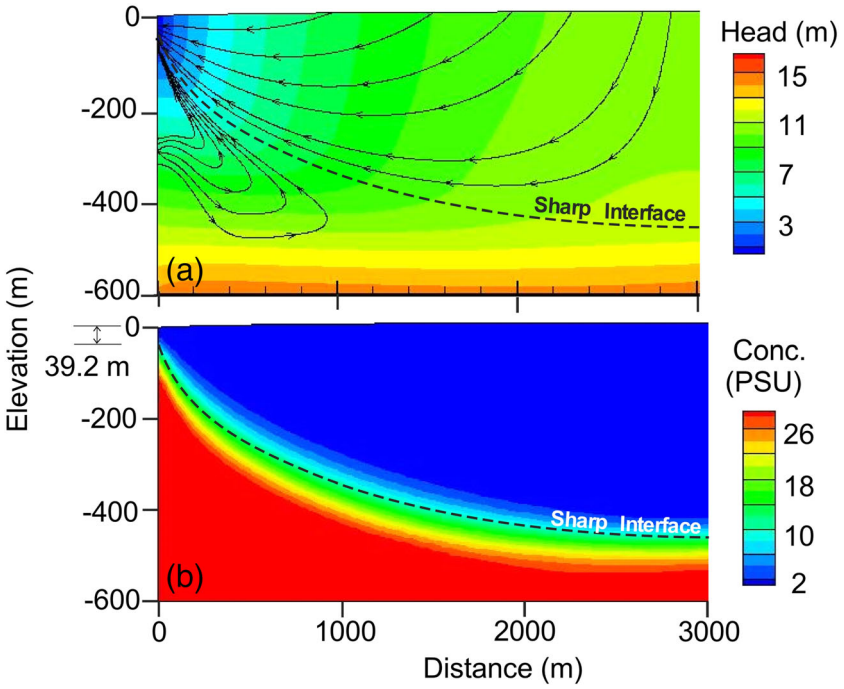


**Figure A6.** (a) Comparison between computed equivalent freshwater heads (contours, flow directions indicated by lines with arrows) and (b) solute concentrations and the position of the freshwater-seawater interface (dashed line) for an idealized coastal aquifer system. The lines with arrows in panel (a) represent streak lines depicting groundwater flow trajectories.

## A.7 Survey of Model Applications to Study OFG

The transport equations presented in sections A.1–A.4 have been solved both analytically and numerically. Analytical methods that solve for the position of the freshwater-saltwater interface using sharp-interface theory were originally developed by Henry (1964), Hantush (1968), Edelman (1972), and more recently by Bakker (2006). Numerical approximations to the flow and transport equations include Bear et al. (1999), Essaid (1990), Galeati et al. (1992), and Souza and Voss (1987). These studies focused on water resources investigations and seawater intrusion.

Some of the first studies to address groundwater flow conditions in coastal aquifers over geologic time scales and freshwater emplacement were by Kooi (1999) and Kooi and Groen (2003). These authors analyzed the relative importance of topography and compaction-driven flow in continental shelf aquifer systems using analytical methods. Kooi (1999) presented the following groundwater flow equation developed for a rectangular aquifer of thickness $H_a$ overlain by a confining unit of thickness $H_s$ (Figure A7):

$$k_a\frac{\partial^2 h}{\partial x^2}-\frac{k_s h}{H_s H_a}+Q=S_s\frac{\partial h}{\partial t} \tag{A24a}$$

$$Q=\alpha_r\left(\rho_r-\rho_f\right)(1-\phi)g v_{sed}-\phi\alpha_f\rho_f g v_z \tag{A24b}$$

where $h$ is hydraulic head, $k_a$ is the aquifer hydraulic conductivity, $Q$ is the sediment loading term, $v_{sed}$ is the sedimentation rate, $v_z$ is the subsidence rate, for head dissipation due to shore normal topography-driven flow through an aquifer having a permeability of $k_a$ across a thin confining unit having a permeability of $k_s$. In this model, head changes along the aquifer are controlled by vertical leakage across the upper confining unit.

**Table A1**
*Parameters Used in Sharp-Interface and Variable-Density Groundwater Flow/Solute Transport Equations Model Comparison*

| Parameter | Value |
|---|---|
| Permeability ($k$) | $10^{-11}$ m$^2$ |
| Freshwater density ($\rho_f$) | 1,000 kg/m$^3$ |
| Seawater density ($\rho_s$) | 1,025 kg/m$^3$ |
| Recharge ($R$) | 0.005 m/day |
| Number of nodes | 101 |
| $\Delta x$ | 60 m |

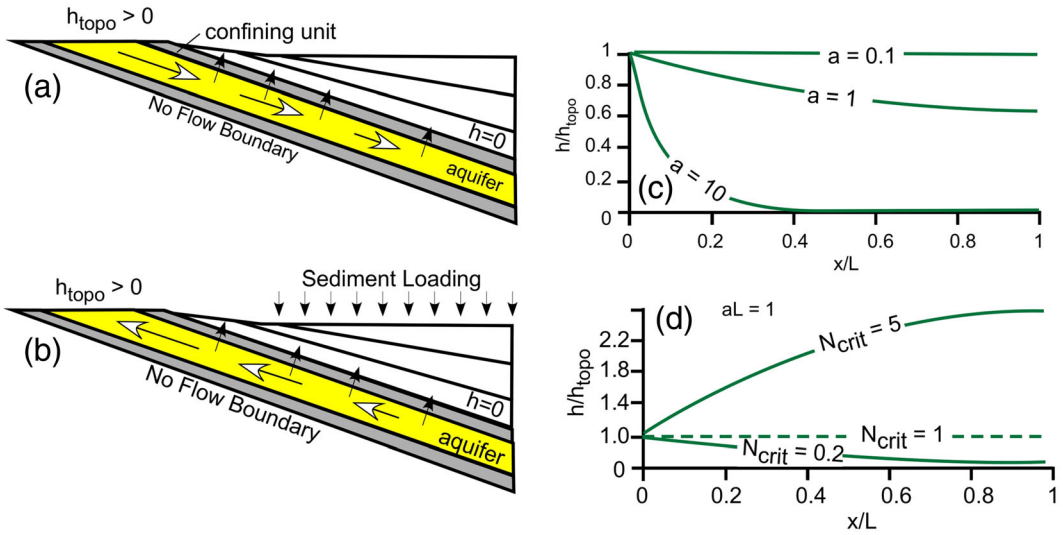


**Figure A7.** Schematic diagrams depicting shore normal (a) topography- and (b) compaction-driven flow systems on the continental shelf. (c) Results from analytical solution (Equations A25a and A26a) for topography flow considering three scenarios of confining unit permeability ranging from relatively tight ($a = 0.1$) to relatively permeable ($a = 10$). (d) Analytic results for degrees of compaction verses topography-driven flow (from Kooi, 1999).

One analytical solution presented by Kooi (1999) considers head changes due to topography-driven flow within a coastal aquifer overlain by a leaky confining unit:

$$h = \frac{h_{topo}}{[1 + \exp(-2aL)]}[\exp(a\{x - 2L\}) + \exp(-ax)] \tag{A25a}$$

$$a = \sqrt{\frac{1}{H_s H_a}}\frac{k_s}{k_a} \tag{A25b}$$

where $h_{topo}$ is the specified head boundary condition at $x = 0$, $L$ is the domain length, $x$ is lateral distance, $H_a$ is the thickness of the aquifer, and $H_s$ is the thickness of the confining unit. Small values of "$a$" denote a relatively tight confining unit with little leakage. For this scenario, heads do not change much moving offshore. This impacts the degree to which freshwater can extend offshore. Kooi (1999) also developed an analytical solution to consider the interactions between topography- and compaction-driven flow. This required including adding source term ($Q$; Equation A24b) into the analytical solution, which is given by:

$$\frac{h}{h_{topo}} = \frac{1 - N_{crit}}{[1 + \exp(-2aL)]}[\exp(a\{x - 2L\}) + \exp(-ax)] + N_{crit} \tag{A26a}$$

$$N_{crit} = \frac{C}{h_{topo}} \tag{A26b}$$

$$C = \frac{QH_sH_a}{k_s} \tag{A26c}$$

Figure A7d presents computed heads within the offshore aquifer or different values of $N_{crit.}$ When $N_{crit} = 1$, the effects of compaction-driven flow and topography-driven flow are balanced, causing hydrostatic conditions. When $N_{crit} > 1$, compaction-driven flow dominates. When $N_{crit} < 1$, topography-driven flow dominates. These analytical solutions reveal what are the important controlling parameters on compaction and topography-driven flow in continental shelf environments.

A number of studies have focused on the evolution of pore pressures in marine environments because of its relevance to petroleum exploration, environmental drilling safety, and tsunami prediction. Dugan and Flemings (2000, 2002) developed numerical models of overpressure formation that considered the two-dimensional effects of a permeable basal aquifer unit overlain by fine-grained sediments on the

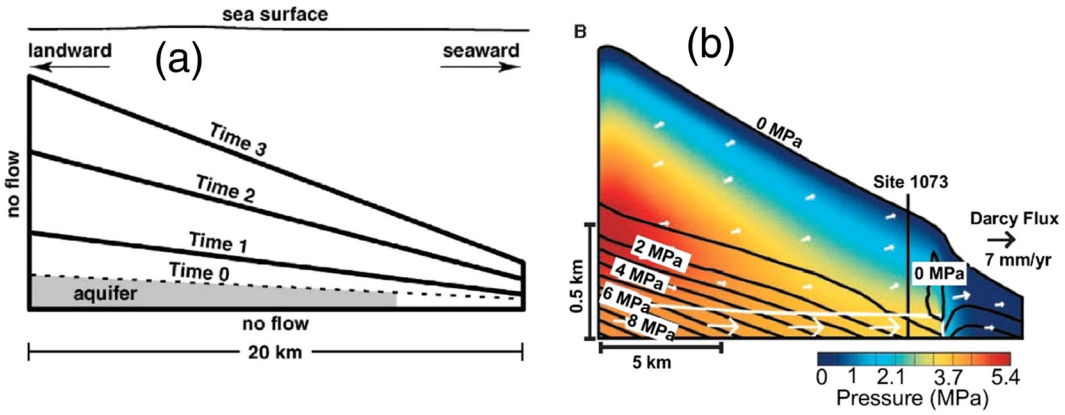


**Figure A8.** (a) Schematic diagram depicting time evolution of sediment thickness on the New Jersey continental slope. (b) Computed fluid pressures (colored patterns) and effective stress (black lines) along the New Jersey continental slope. White arrows depict groundwater flow directions (source: Dugan & Flemings, 2000).

distribution of pore pressures and slope failure (Figure A8). They solved the following Lagrangian-based groundwater flow equation:

$$\frac{DP}{Dt} = \frac{\rho_f g}{\mu_f}\frac{\left(1-\phi^2\right)}{S_s}\left\{\frac{\partial}{\partial x}\left[k\frac{\partial P}{\partial x}\right] + \frac{\partial}{\partial z}\left[k\frac{\partial P}{\partial z}\right]\right\} + \frac{\rho_f g \phi \alpha_f}{S_s(1-\phi)}\frac{D\sigma_v}{Dt} \tag{A27}$$

where $P$ is fluid pressure, $k$ is permeability, and $S_s$ is specific storage. These authors used the following failure criteria to determine slope stability:

$$FS = \frac{c + \left[\left(\sigma_v - zg\rho_f\right)\cos^2\theta - P_{Dev}\right]\tan\theta_f}{\left(\sigma_v - zg\rho_f\right)\cos\theta\sin\theta} \tag{A28}$$

where $FS$ is the factor of safety (slope failure occurs for $FS > 1$), $c$ is sediment cohesion, $\theta$ is the slope of the sediment water interface, and $\theta_f$is the internal angle of friction. This model included a dynamic mesh algorithm that grew the model domain through time (Figure A8a). These authors found that pressure redistribution due to the presence of a basal sand unit promoted continental slope instability. They concluded that high pore fluid pressures within the basal aquifer may have acted to reduce the $FS$ to unity near the top of Miocene sediments and could explain the observations of instability within Miocene sediments in submarine canyons offshore New Jersey (Hampson & Robb, 1984).

Kooi et al. (2000) assessed continental shelf aquifer salinization in response to Holocene to modern sea level rise using an idealized, sloping rectangular model domain having a width of 10 m and lateral extent of 400 m. Sea level was permitted to migrate laterally across the model domain during their numerical experiments. They used a variable-density model METROPOL-3 in their study. A sensitivity study (Figure A9) was undertaken in which they considered different layering and permeability scenarios. In some model runs, they also included a thin low-permeability upper layer, which impeded the formation of haline convection cells (sand/clay scenarios). They defined a dimensionless number group to guide the sensitivity analysis. The dimensionless number ($\Gamma$) is the ratio of the rate of lateral sea level migration ($v_{sl}$) along the top boundary divided by an estimate of the average lateral velocity of seawater migration within a rectangular aquifer ($v_{tr}^{max}$) have a slope (tilt) of $B$:

$$\Gamma = \frac{v_{sl}}{v_{Tr}^{max}} = \frac{\phi\mu_f v_{sl}}{k\rho_s g tan^2 B} \tag{A29}$$

The authors found that advection- and diffusion-dominated solute transport occurred depending on permeability conditions. Transient haline convection occurred if the rate of sea level rise was faster than the lateral saltwater velocity. They related the results from their sensitivity study to the presence of offshore freshwater

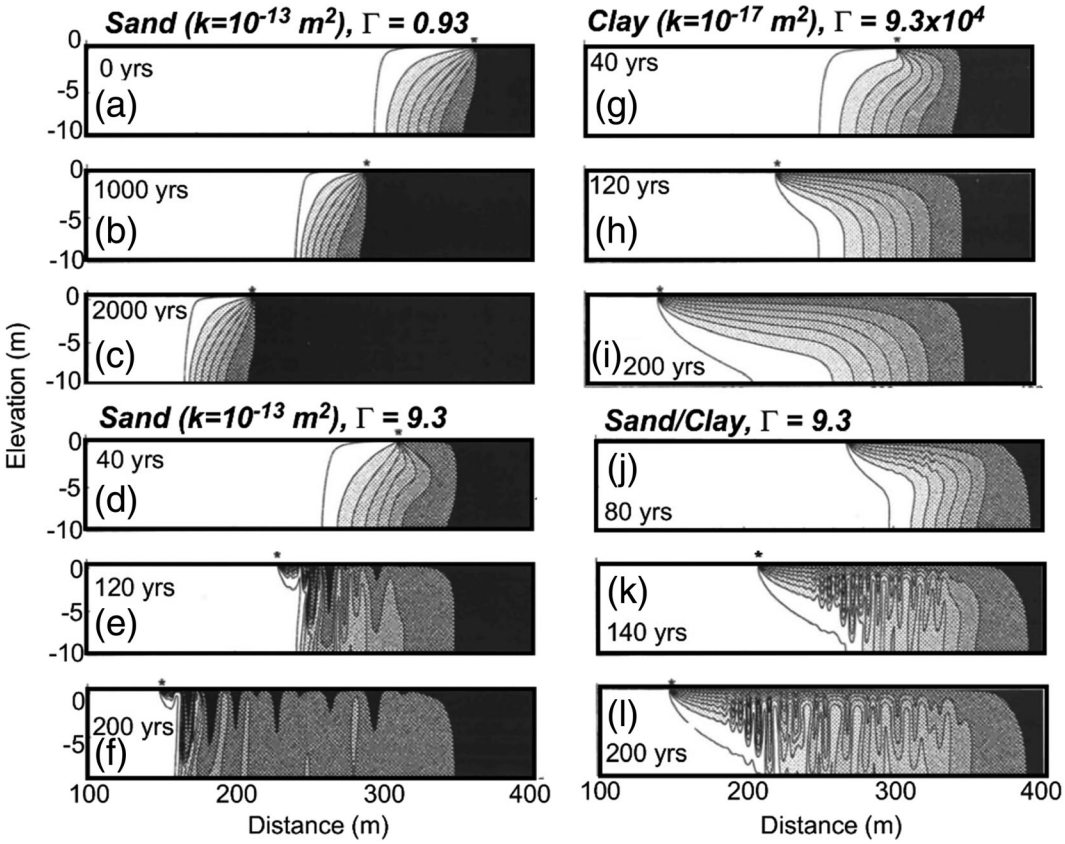


**Figure A9.** (a–l) Comparison of salinization of the thin (10 m thick) aquifer due to landward migration of sea level over a period of 2000 using different representations of sediment permeability (modified from Kooi et al., 2000).

in Suriname, South America, and New Jersey, USA. Post and Kooi (2003) conducted similar analysis of haline convection cell formation for the Dutch coastline. These authors conclude that salinization of permeable ($10^{-11}$ $m^2$) coastal aquifers about 200 m thick during sea level rise could have occurred in decades. This is similar to what was calculated by the characteristic time using Equation A15 (51 a). Both Kooi et al. (2000) and Post and Kooi (2003) emphasized the need to use very high resolution grids to accurately represent haline convection.

Meisler et al. (1984) were among the first to use a two-dimensional groundwater flow model in an attempt to reproduce the observed lateral extent of sequestered freshwater offshore New Jersey (Folger et al., 1978) by considering lower sea level conditions (45, 30, and 15 m below modern) and different representations of continental shelf hydro-stratigraphy. Rather than using a vertically layered system, these authors represented the continental shelf as having different lateral zones (A–C) within which porous media properties could be varied (Figure A10). They explored both different values of anisotropy, absolute permeability and mean Pleistocene sea level conditions. These authors concluded that the wedge of OFG denoted by the 18 parts per thousand isochlor in Figure A10 could be best matched by assuming that the average Pleistocene sea level conditions were about 30 m lower than modern conditions.

Person et al. (2003), Marksammer et al. (2007), and DeFoor et al. (2011) considered the effects of Pleistocene glaciations on the emplacement of fresh glacial meltwater in continental shelf aquifers within New England, US, and southeastern Greenland. These studies had to reconstruct the thickness and lateral extent of the Laurentide and Greenland ice sheet in their models. The role of permafrost in reducing continental shelf recharge also had to be considered in their models. These authors found that during periods of glaciation, discharge to the continental shelf was enhanced by up to a factor of 10. The formation of pro-glacial lakes on the continental shelf may have also enhanced the emplacement of freshwater (Person et al., 2012). These findings are consistent with palaeo-hydrologic models developed for North America (Lemieux et al., 2008a, 2008b, 2008c).

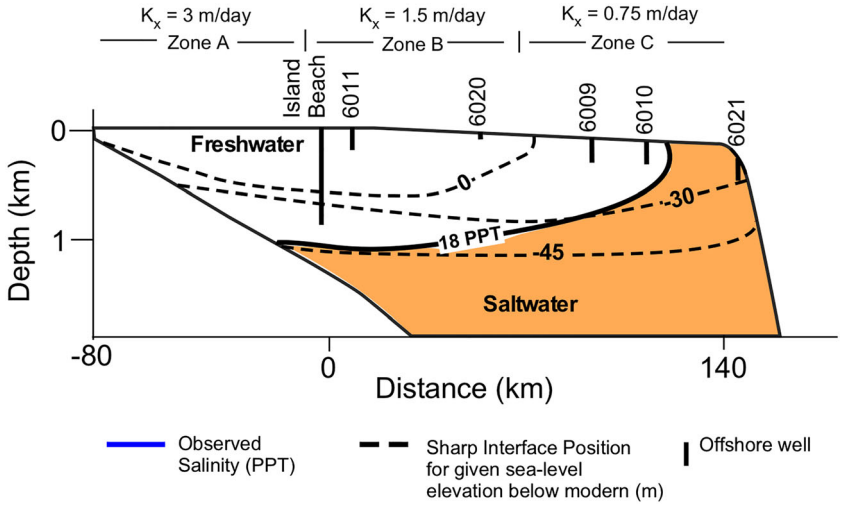


**Figure A10.** Comparison of predicted steady-state saltwater-freshwater interface locations and estimated 18-ppt (thick black line) isochlor based on well data (vertical black line). The numbers on the dashed lines indicate the steady-state sea level used in the model to predict the sharp-interface position. The anisotropy ($K_x/K_z$) in all runs was 30,000 (after Hathaway et al., 1979 and Meisler et al., 1984).

D. Cohen et al. (2010) and Siegel et al. (2014) developed a 3-D high-performance computer model called *PGEOFE* of the North Atlantic continental shelf from New Jersey to Maine, which also considered the effects of glaciations (Figures 8a–8b). These authors considered sea level fluctuations and glacial loading over the last 2 Ma in their analysis. The model was compared to salinity distributions from eleven wells from legacy continental shelf drilling campaigns on the continental shelf (Hathaway et al., 1979). D. Cohen et al. (2010) used model output to estimate the volume of sequestered freshwater (<1 PSU) was 1,300 $km^3$ for this region. D. Cohen et al. (2010) proposed that where confined aquifers crop out in submarine canyons, SGD can occur.

Over the past several years, hydrologists have addressed the paucity of offshore well data using geostatistical simulation methods in order to predict the offshore extent of SGD and OFG (Michael et al., 2016; Yu & Michael, 2019a) (Figure A11). These studies revealed that heterogeneous, anisotropic hydrostratigraphic units can be more effective in producing OFG than traditional stratigraphic or equivalent homogenous, anisotropic hydrostratigraphic framework models, even under modern sea level conditions. Thus, onshore-offshore aquifer systems need not be perfectly confined or out of equilibrium with sea level in order to contain freshened groundwater. By running dozens of simulations conditioned by well stratigraphic data, predictions of the most likely, minimum, and maximum estimates of OFG can be made (Thomas et al., 2019) (Figures 8c–8e). These geostatistical simulation methods can be used to synthesize available information for OFG systems. They can honor existing well stratigraphic data through direct conditioning and incorporate indirect data, such as seismic, probabilistically. They can also incorporate an underlying structural model derived from data or stratigraphic knowledge in the form of statistics such as variograms (two-point methods)

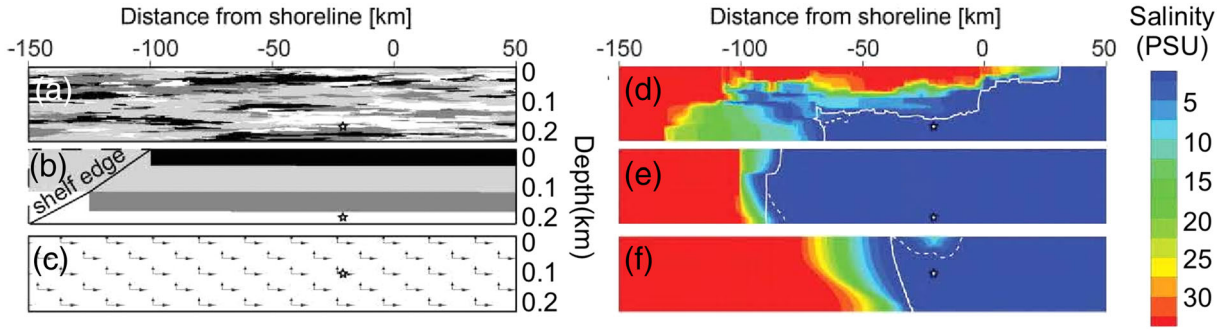


**Figure A11.** Effects of different representations of aquifer heterogeneity ([a] heterogeneous, [b] layered, and [c] homogeneous models) on OFG distribution (modified from Yu & Michael, 2019a). Flow is from right to left.

and training images (multiple-point methods). Thus, geostatistical methods are useful tools for representing the geologic heterogeneity that determines salinity distributions and their response to long- and short-time scale hydrologic forcing, particularly in OFG systems that lack the data necessary to model the geologic structure deterministically.

## Conflict of Interest

The authors declare no competing interests.

## Data Availability Statement

The global database of offshore freshened groundwater records is available in Micallef (2020).

**Acknowledgments**
This study has received funding from the European Research Council (ERC), under the European Union's Horizon 2020 research and innovation program (grant agreement No. 677898 (MARCAN) to A. M.) and the U.S. National Science Foundation (NSF FRES 1925974 to M. P.; NSF OCE 0824368 to B. D.; and NSF EAR 1151733 to H. A. M.). T. M., B. W. and Y. Z. were funded by the SMART project through the Helmholtz European Partnering Initiative (Project ID Number PIE-0004) involving GEOMAR and the University of Malta.

## References

Abegg, F., Linke, P., & GEOMAR Helmholtz-Zentrum für Ozeanforschung Kiel (2017). Remotely operated vehicle "ROV KIEL 6000". *Open Access Journal of Large-Scale Research Facilities*, *3*(A117).

Adkins, J. F., McIntyre, K., & Schrag, D. P. (2002). The salinity, temperature and $\delta^{18}O$ content of the glacial deep ocean. *Science*, *298*(5599), 1769–1773. https://doi.org/10.1126/science.1076252

Adyasari, D., Hassenrück, C., Oehler, T., Sabdaningsih, A., & Moosdorf, N. (2019). Microbial community structure associated with submarine groundwater discharge in northern Java (Indonesia). *Science of the Total Environment*, *689*, 590–601. https://doi.org/10.1016/j.scitotenv.2019.06.193

Aeshbach-Hertig, W., & Gleeson, T. (2012). Regional strategies for the accelerating global problem of groundwater depletion. *Nature Geoscience*, *5*(12), 853–861. https://doi.org/10.1038/ngeo1617

Alcalde, J., Bond, C., Johnson, G., Kloppenburg, A., Ferrer, O., Bell, R., & Ayarza Arribas, M. P. (2019). Fault interpretation in seismic reflection data: An experiment analysing the impact of conceptual model anchoring and vertical exaggeration. *Solid Earth*, *10*(5), 1651–1662. https://doi.org/10.5194/se-10-1651-2019

Amato, D. W., Bishop, J. M., Glenn, C. R., Dulai, H., & Smith, C. M. (2016). Impact of submarine groundwater discharge on marine water quality and reef biota of Maui. *PLoS ONE*, *11*(11), e0165825. https://doi.org/10.1371/journal.pone.0165825

Archie, G. E. (1942). The electrical resistivity log as an aid in determining some reservoir characteristics. *Journal of Petroleum Technology*, *5*, 1–8.

Armitage, P. J., Butcher, A. R., Churchill, J. M., Csoma, A. E., Hollis, C., Lander, R. H., et al. (2018). Reservoir quality of clastic and carbonate rocks: Analysis*, Modelling and Prediction*, The Geological Society of London.

Arroyo, J., & Shirazi, S. (2012). *Cost of brackish groundwater desalination in Texas*. Austin, TX: Texas Water Development Board.

Athy, L. F. (1930). Density, porosity and compaction of sedimentary rocks. *American Association of Petroleum Geologists Bulletin*, *14*, 1–24.

Attias, E., Thomas, D., Sherman, D., Ismail, K., & Constable, S. (2020). Marine electrical imaging reveals novel freshwater transport mechanism in Hawai'i. *Science Advances*, *6*(48), eabd4866.

Avseth, P., Mukerji, T., & Mavko, G. (2009). *Quantitative seismic interpretation: Applying rock physics to reduce interpretation risk*. Cambridge: Cambridge University Press.

Back, W., Hanshaw, B. B., Pyle, T., Plummer, L. N., & Weidie, A. E. (1979). Geological significance of groundwater discharge and carbonate dissolution to the formation of the Caleta Xel Ha, Quintana Roo, Mexico. *Water Resources Research*, *15*(6), 1521–1535. https://doi.org/10.1029/WR015i006p01521

Bailey, G. N., & King, G. C. (2011). Dynamic landscapes and human dispersal patterns: Tectonics, coastlines, and the reconstruction of human habitats. *Quaternary Science Reviews*, *30*(11–12), 1533–1553. https://doi.org/10.1016/j.quascirev.2010.06.019

Bakalowicz, M. (2014). Karst at depth below the sea level around the Mediterranean due to the Messinian crisis of salinity: Hydrological consequences and issues. *Geologica Belgica*, *17*(1), 96–101.

Bakken, T. H., Ruden, F., & Mangset, L. E. (2012). Submarine groundwater: A new concept for the supply of drinking water. *Water Resources Management*, *26*(4), 1015–1026. https://doi.org/10.1007/s11269-011-9806-1

Bakker, M. (2006). Analytic solutions for interface flow in combined confined and semi-confined, coastal aquifers. *Advances in Water Resources*, *29*(3), 417–425. https://doi.org/10.1016/j.advwatres.2005.05.009

Bakker, M., Miller, A. D., Morgan, L. K., & Werner, A. D. (2017). Evaluation of analytic solutions for steady interface flow where the aquifer extends below the sea. *Journal of Hydrology*, *551*, 660–664. https://doi.org/10.1016/j.jhydrol.2017.04.009

Bard, E., Hamelin, B., & Fairbanks, R. G. (1990). U-Th ages obtained by mass spectrometry in corals from Barbados: Sea level during the past 130,000 years. *Nature*, *346*(6283), 456–458. https://doi.org/10.1038/346456a0

Barlow, P. M. (2003). Ground water in fresh water-saltwater environments of the Atlantic coast, Geological Survey (USGS).

Barnes, A. E. (2001). Seismic attributes in your facies. *Canadian Society of Exploration Geophysicists Recorder*, *26*, 41–47.

Barnes, R. O. (1973). An in situ interstitial water sampler for use in unconsolidated sediments. *Deep Sea Research and Oceanographic Abstracts*, *20*(12), 1125–1128.

Barnes, R. O. (1988). ODP in-situ fluid sampling and measurement; A new wireline tool, Affiliation (analytic): Rosari, 110, 55.

Bar-On, Y. M., Phillips, R., & Milo, R. (2018). The biomass distribution on Earth. *Proceedings of the National Academy of Sciences of the United States of America*, *115*(25), 6506–6511. https://doi.org/10.1073/pnas.1711842115

Bates, B., Kundzewicz, Z., Wu, S., & Palutikof, J. (2008). *Climate change and water*. Geneva: IPCC Secreteriat.

Batzle, A., & Wang, C. H. (1992). Seismic properties of pore fluids. *Geophysics*, *57*(11), 1396–1408. https://doi.org/10.1190/1.1443207

Bayon, G., Henderson, G. M., & Bohn, M. (2009). U-Th stratigraphy of a cold seep carbonate crust. *Chemical Geology*, *260*(1–2), 47–56. https://doi.org/10.1016/j.chemgeo.2008.11.020

BBC News (2018). *The 11 cities most likely to run out of drinking water—Like Cape Town, edited*. UK: BBC.

Bear, J. (2012). Hydraulics of groundwater, Courier Corporation.

Bear, J., Cheng, A. H. D., Sorek, S., Ouazar, D., & Herrera, I. (Eds) (1999). *Seawater intrusion in coastal aquifers: Concepts, methods and practices*. Netherlands: Springer Science & Business Media. https://doi.org/10.1007/978-94-017-2969-7

Beck, A. J., Charette, M. A., Cochran, J. K., Gonneea, M. E., & Peucker-Ehrenbrink, B. (2013). Dissolved strontium in the subterranean estuary-implications for the marine strontium isotope budget. *Geochimica et Cosmochimica Acta*, *117*, 33–52. https://doi.org/10.1016/j.gca.2013.03.021

Beck, A. J., Rapaglia, P., Cochran, J. K., & Bokuniewicz, H. J. (2007). Radium mass-balance in Jamaica Bay, NY: Evidence for a substantial flux of submarine groundwater. *Marine Geochemistry*, *106*, 419–441.

Becker, K., & Fisher, A. T. (2008). Borehole packer tests at multiple depths resolve distinct hydrologic intervals in 3.5-Ma upper oceanic crust on the eastern flank of Juan de Fuca Ridge. *Journal of Geophysical Research*, *113*, B07105. https://doi.org/10.1029/2007JB005446

Becker, M. W., Metge, D. W., Collins, S. A., Shapiro, A. M., & Harvey, R. W. (2003). Bacterial transport experiments in fractured crystalline bedrock. *Groundwater*, *41*(5), 682–689. https://doi.org/10.1111/j.1745-6584.2003.tb02406.x

Bekins, B., McCaffrey, A. M., & Dreiss, S. J. (1994). Influence of kinetics on the smectite to illite transition in the Barbados accretionary prism. *Journal of Geophysical Research*, *99*(B9), 18,147–18,158. https://doi.org/10.1029/94JB01187

Bender, M., Martin, W., Hess, J., Sayles, F., Ball, L., & Lambert, C. (1987). A whole-core squeezer for interfacial pore-water sampling 1. *Limnology and Oceanography*, *32*(6), 1214–1225. https://doi.org/10.4319/lo.1987.32.6.1214

Bennett, P. C., Rogers, J. R., & Choi, W. J. (2001). Silicates, silicate weathering, and microbial ecology. *Geomicrobiology Journal*, *18*(1), 3–19.

Bense, V. F., & Van Balen, R. T. (2004). The effect of fault relay and clay smearing on groundwater flow patterns in the Lower Rhine Embayment. *Basin Research*, *16*(3), 397–411. https://doi.org/10.1111/j.1365-2117.2004.00238.x

Berndt, C. (2005). Focused fluid flow in passive continental margins. *Philosophical Transactions of the Royal Society A*, *363*(1837), 2855–2871. https://doi.org/10.1098/rsta.2005.1666

Berndt, C., Bunz, S., Clayton, T., Mienert, J., & Saunders, M. (2004). Seismic character of bottom simulating reflectors: Examples from the mid-Norwegian margin. *Marine and Petroleum Geology*, *21*(6), 723–733. https://doi.org/10.1016/j.marpetgeo.2004.02.003

Bertoni, C., & Cartwright, J. (2005). 3D seismic analysis of slope-confined canyons from the Plio-Pleistocene of the Ebro Continental Margin (Western Mediterranean). *Basin Research*, *17*(1), 43–62. https://doi.org/10.1111/j.1365-2117.2005.00254.x

Bertoni, C., Lofi, J., Micallef, A., & Moe, H. (2020). Seismic reflection methods in offshore groundwater research. *Geosciences*, *10*(8), 299. https://doi.org/10.3390/geosciences10080299

Bethke, C. M. (1985). A numerical model of compaction-driven groundwater flow and heat transfer and its application to the paleohydrology of intracratonic sedimentary basins. *Journal of Geophysical Research*, *90*(B8), 6817–6828. https://doi.org/10.1029/JB090iB08p06817

Bethke, C. M. (1986). Inverse hydrologic analysis of the distribution of origin of Gulf Coast-type geopressured zones. *Journal of Geophysical Research*, *91*(B6), 6535–6545. https://doi.org/10.1029/JB091iB06p06535

Blatter, D., Key, K., Ray, A., Gustafson, C., & Evans, R. (2019). Bayesian joint inversion of controlled source electromagnetic and magnetotelluric data to image fresh water aquifer offshore New Jersey. *Geophysical Journal International*, *218*(3), 1822–1837. https://doi.org/10.1093/gji/ggz253

Böhlke, J. K., & Krantz, D. E. (2003). *Isotope geochemistry and chronology of offshore ground water beneath Indian River Bay*. Reston, Virginia: Delaware US Geological Survey.

Bratton, J. F. (2007). The importance of shallow confining units to submarine groundwater flow. *IAHS Publication*, *312*, 28–34.

Bratton, J. F. (2010). The three scales of submarine groundwater flow and discharge across passive continental margins. *The Journal of Geology*, *118*(5), 565–575. https://doi.org/10.1086/655114

Bratton, J. F., Böhlke, J. K., Krantz, D. E., & Tobias, C. R. (2009). Flow and geochemistry of groundwater beneath a back-barrier lagoon: The subterranean estuary at Chincoteague Bay, Maryland, USA. *Marine Chemistry*, *113*(1–2), 78–92. https://doi.org/10.1016/j.marchem.2009.01.004

Brennwald, M. S., Hofer, M., Peeters, F., Aeschbach-Hertig, W., Strassmann, K., Kipfer, R., et al. (2003). Analysis of dissolved noble gases in the pore water of lacustrine sediments. *Limnology and Oceanography: Methods*, *1*(1), 51–62.

Brown, K. M., Saffer, D. M., & Bekins, B. A. (2001). Smectite diagenesis, pore-water freshening, and fluid flow at the toe of the Nankai wedge. *Earth and Planetary Science Letters*, *194*(1–2), 97–109. https://doi.org/10.1016/S0012-821X(01)00546-5

Browne, G. H., & Naish, T. R. (2003). Facies development and sequence architecture of a late Quaternary fluvial-marine transition, Canterbury Plains and shelf, New Zealand: implications for forced regressive deposits. *Sedimentary Geology*, *158*(1–2), 57–86. https://doi.org/10.1016/S0037-0738(02)00258-0

Buchardt, B., Israelson, C., Seaman, P., & Stockmann, G. (2001). The Ikaite tufa towers in Ikka Fjord, SW Greenland: Formation by mixing of seawater and alkaline spring water. *Journal of Sedimentary Research*, *71*(1), 176–189. https://doi.org/10.1306/042800710176

Cable, J. E., Burnett, W. C., Chanton, J. P., & Weatherly, G. (1996). Modeling groundwater flow into the ocean based on $^{222}$Rn. *Earth and Planetary Science Letters*, *144*(3–4), 591–604. https://doi.org/10.1016/S0012-821X(96)00173-2

Cartwright, J., & Santamarina, C. (2015). Seismic characteristics of fluid escape pipes in sedimentary basins: Implications for pipe genesis. *Marine and Petroleum Geology*, *65*, 126–140. https://doi.org/10.1016/j.marpetgeo.2015.03.023

Caspard, E., Rudkiewicz, J. L., Eberli, G. P., Brosse, E., & Renard, M. (2004). Massive dolomitization of a Messinian reef in the Great Bahama Bank: A numerical modelling evaluation of Kohout geothermal convection. *Geofluids*, *4*(1), 40–60. https://doi.org/10.1111/j.1468-8123.2004.00071.x

Castagna, J. P., & Smith, S. W. (1994). Comparison of AVO indicators: A modeling study. *Geophysics*, *59*(12), 1849–1855. https://doi.org/10.1190/1.1443572

Castagna, J. P., Sun, S., & Siegfried, R. W. (2003). Instantaneous spectral analysis: Detection of low-frequency shadows associated with hydrocarbons. *The Leading Edge*, *22*(2), 120–127. https://doi.org/10.1190/1.1559038

Castagna, J. P., & Swan, H. W. (1997). Principles of AVO crossplotting. *The Leading Edge*, *16*(4), 337–344. https://doi.org/10.1190/1.1437626

Chaussard, E., Amelung, F., Abidin, H., & Hong, S.-H. (2013). Sinking cities in Indonesia: ALOS PALSAR detects rapid subsidence due to groundwater and gas extraction. *Remote Sensing of Environment*, *128*, 150–161. https://doi.org/10.1016/j.rse.2012.10.015

Chen, C.-T., Hu, J.-C., Lu, C.-Y., Lee, J.-C., & Chan, Y.-C. (2007). Thirty-year land elevation change from subsidence to uplift following the termination of groundwater pumping and its geological implications in the Metropolitan Taipei Basin, Northern Taiwan. *Engineering Geology*, *95*(1–2), 30–47. https://doi.org/10.1016/j.enggeo.2007.09.001

Cheng, A. H., & Ouazar, D. (2003). *Coastal aquifer management: Monitoring, modeling, and case studies*, edited. New York: CRC Press. https://doi.org/10.1201/9780203493496

Cohen, D., Person, M., Wang, P., Gable, C. W., Hutchinson, D., Marksamer, A., et al. (2010). Origin and extent of freshwater paleowaters on the Atlantic continental shelf, USA. *Groundwater*, *48*(1), 143–158. https://doi.org/10.1111/j.1745-6584.2009.00627.x

Cohen, K. M., & Lobo, F. J. (2013). Continental shelf drowned landscapes: Submerged geomorphological and sedimentary record of the youngest cycles. *Geomorphology*, *203*, 1–5. https://doi.org/10.1016/j.geomorph.2013.09.006
Constable, S. (2013). Review paper: Instrumentation for marine magnetotelluric and controlled source electromagnetic sounding. *Geophysical Prospecting*, *61*, 505–532. https://doi.org/10.1111/j.1365-2478.2012.01117.x
Constable, S., Kannberg, P. K., & Weitemeyer, K. (2016). Vulcan: A deep-towed CSEM receiver. *Geochemistry, Geophysics, Geosystems*, *17*, 1042–1064. https://doi.org/10.1002/2015GC006174
Cronin, T. M. (2012). Rapid sea-level rise. *Quaternary Science Reviews*, *56*, 11–30. https://doi.org/10.1016/j.quascirev.2012.08.021
Cumbie, D. H., & McKay, L. D. (1999). Influence of diameter on particle transport in a fractured shale saprolite. *Journal of Contaminant Hydrology*, *37*(1–2), 139–157. https://doi.org/10.1016/S0169-7722(98)00156-9
Dählmann, A., & de Lange, G. J. (2003). Fluid-sediment interactions at Eastern Mediterranean mud volcanoes: A stable isotope study from ODP Leg 160. *Earth and Planetary Science Letters*, *212*(3–4), 377–391. https://doi.org/10.1016/S0012-821X(03)00227-9
Damania, R., Desbureaux, S., Hyland, M., Islam, A., Moore, S., Rodella, A.-S., et al. (2017). *Uncharted waters: The new economics of water scarcity and variability*. Washington, D.C.: World Bank. https://doi.org/10.1596/978-1-4648-1179-1
De Lange, G. J. (1983). Geochemical evidence of a massive slide in the southern Norwegian Sea. *Nature*, *305*(5933), 420–422. https://doi.org/10.1038/305420a0
de Marsily, G. (1986). *Quantitative hydrogeology: Groundwater hydrology for engineers*. New York: Academic Press.
DeFoor, W., Person, M., Larsen, H. C., Lizarralde, D., Cohen, D., & Dugan, B. (2011). Ice sheet-derived submarine groundwater discharge on Greenland's continental shelf. *Water Resources Research*, *47*, W07549. https://doi.org/10.1029/2011WR010536
Deng, Y., Ren, J., Guo, Q., Cao, J., Wang, H., & Liu, C. (2017). Rare earth element geochemistry characteristics of seawater and pore water from deep sea in western Pacific. *Scientific Reports*, *7*(1), 16539. https://doi.org/10.1038/s41598-017-16379-1
Desilets, D., Zreda, M., Almasi, P. F., & Elmore, D. (2006). Determination of cosmogenic $^{36}$Cl in rocks by isotope dilution: Innovations, validation and error propagation. *Chemical Geology*, *233*(3–4), 185–195. https://doi.org/10.1016/j.chemgeo.2006.03.001
Dimova, N. T., Swarzenski, P. W., Dulaiova, H., & Glenn, C. R. (2012). Utilizing multichannel electrical resistivity methods to examine the dynamics of the fresh water-seawater interface in two Hawaiian groundwater systems. *Journal of Geophysical Research*, *117*, C02012. https://doi.org/10.1029/2011JC007509
Du, Z., & Key, K. (2018). Case study: North Sea heavy oil reservoir characterization from integrated analysis of towed-streamer EM and dual-sensor seismic data. *The Leading Edge*, *37*(8), 608–615. https://doi.org/10.1190/tle37080608.1
Duffy, C. J., & Al-Hassan, S. (1988). Groundwater circulation in a closed desert basin: Topographic scaling and climatic forcing. *Water Resources Research*, *24*(10), 1675–1688. https://doi.org/10.1029/WR024i010p01675
Dugan, B., & Flemings, P. (2000). Overpressure and fluid flow in the New Jersey continental slope: Implications for slope failure and cold seeps. *Science*, *289*(5477), 288–291. https://doi.org/10.1126/science.289.5477.288
Dugan, B., & Flemings, P. B. (2002). Fluid flow and stability of the US continental slope offshore New Jersey from the Pleistocene to the present. *Geofluids*, *2*(2), 137–146. https://doi.org/10.1046/j.1468-8123.2002.00032.x
Dugan, B., & Sheahan, T. C. (2012). Offshore sediment overpressures of passive margins: Mechanisms, measurement and models. *Reviews of Geophysics*, *50*, RG3001. https://doi.org/10.1029/2011RG000379
Edelman, J. H. (1972). Groundwater hydraulics of extensive aquifers, in International Institute for Land Reclamation and Drainage Bulletin, edited, p. 216, Netherlands.
Edgcomb, V. P., Beaudoin, D., Gast, R., Biddle, J. F., & Teske, A. (2011). Marine subsurface eukaryotes: The fungal majority. *Environmental Microbiology*, *13*(1), 172–183. https://doi.org/10.1111/j.1462-2920.2010.02318.x
Edmunds, W. M., & Milne, C. J. (Eds) (2001). *Palaeowaters in coastal Europe: Evolution of groundwater since the Late Pleistocene* (pp. 289–311). London: Geological Society of London.
Edwards, B. D., Ehman, K. D., Ponti, D. J., Reichard, E. G., Tinsley, J. C., Rosenbauer, R. J., et al. (2009). Stratigraphic controls on saltwater intrusion in the Dominguez Gap area of coastal Los Angeles. *Geological Society of America Special Paper*, *454*, 375–395.
Ehlers, J., & Gibbard, P. L. (2004). *Quaternary glaciations extent and chronology*. Amsterdam: Elsevier.
Engelhardt, T., Kallmeyer, J., Cypionka, H., & Engelen, B. (2014). High virus-to-cell ratios indicate ongoing production of viruses in deep subsurface sediments. *The ISME Journal*, *8*(7), 1503–1509. https://doi.org/10.1038/ismej.2013.245
Essaid, H. I. A. (1990). A multilayered sharp interface model of coupled fresh-water and saltwater flow in coastal systems - model development and application. *Water Resources Research*, *26*(7), 1431–1454. https://doi.org/10.1029/WR026i007p01431
Evans, R. L. (2007). Using CSEM techniques to map the shallow section of seafloor: From the coastline to the edges of the continental slope. *Geophysics*, *72*(2), WA105–WA116. https://doi.org/10.1190/1.2434798
Evans, R. L., & Lizarralde, D. (2003). Geophysical evidence for karst formation associated with offshore groundwater transport: An example from North Carolina. *Geochemistry, Geophysics, Geosystems*, *4*(8), 1069. https://doi.org/10.1029/2003GC000510
Evans, R. L., & Lizarralde, D. (2011). The competing impacts of geology and groundwater on electrical resistivity around Wrightsville Beach, NC. *Continental Shelf Research*, *31*(7–8), 841–848. https://doi.org/10.1016/j.csr.2011.02.008
Faure, H., Walter, R. C., & Grant, D. R. (2002). The coastal oasis: Ice age springs on emerged continental shelves. *Global and Planetary Change*, *33*(1–2), 47–56. https://doi.org/10.1016/S0921-8181(02)00060-7
Fendorf, S., Michael, H. A., & van Geen, A. (2010). Spatial and temporal variations of groundwater arsenic in south and Southeast Asia. *Science*, *328*(5982), 1123–1127. https://doi.org/10.1126/science.1172974
Fisher, A. T. (1998). Permeability within basaltic oceanic crust. *Reviews of Geophysics*, *36*(2), 143–182. https://doi.org/10.1029/97RG02916
Fisher, A. T. (2005). Marine hydrogeology: Recent accomplishments and future opportunities. *Hydrogeology Journal*, *13*(1), 69–97. https://doi.org/10.1007/s10040-004-0400-y
Folger, D. W., Hathaway, R., Christopher, R. A., Valentine, P. C., & Poag, C. W. (1978). *Stratigraphic test well*. Massachussetts: Nantucket Island.
Foyle, A. M., Henry, V. J., & Alexander, C. R. (2002). Mapping the threat of sea-water intrusion in a regional coastal aquifer-aquitard system in the southeastern United States. *Environmental Geology*, *43*(1–2), 151–159. https://doi.org/10.1007/s00254-002-0636-6
Fulthorpe, C. S., Hoyanagi, K., Crundwell, M.P., Dinarès-Turell, J., Ding, X., George, S.C., et al. (2011). Site U1353, Proceedings of the Integrated Ocean Drilling Program, 317, 103.
Galeati, G., Gambolati, G., & Neuman, S. P. (1992). Coupled and partially coupled Eulerian-Lagrangian model of freshwater-seawater mixing. *Water Resources Research*, *28*(1), 149–165.
Gambolati, G., Gatto, P., & Ricceri, G. (1984). *Land subsidence due to gas-oil removal in layered anisotropic soils by a finite element model, paper presented at Proceedings of the III International Symposium on Land Subsidence*. Venice: International Association of Hydrological Sciences.

Garing, C., Luquot, L., Pezard, P. A., & Gouze, P. (2013). Geochemical investigations of saltwater intrusion into the coastal carbonate aquifer of Mallorca, Spain. *Applied Geochemistry*, *39*, 1–10. https://doi.org/10.1016/j.apgeochem.2013.09.011

Gehre, M., Geilmann, H., Richter, J., Werner, R. A., & Brand, W. A. (2004). Continuous flow $^{2}H/1H$ and $^{18}O/^{16}O$ analysis of water samples with dual inlet precision. *Rapid Communications in Mass Spectrometry*, *18*(22), 2650–2660. https://doi.org/10.1002/rcm.1672

Gehrmann, R. A. S., Dettmer, J., Schwalenberg, K., Engels, M., Ozmaral, A., & Dosso, S. E. (2015). Trans-dimensional Bayesian inversion of controlled-source electromagnetic data in the German North Sea. *Geophysical Prospecting*, *63*(6), 1314–1333. https://doi.org/10.1111/1365-2478.12308

Geng, X., & Michael, H. A. (2020). Preferential flow enhances pumping-induced saltwater intrusion in volcanic aquifers. *Water Resources Research*, *56*, e2019WR026390. https://doi.org/10.1029/2019WR026390

Gerber, C., Vaikmäe, R., Aeschbach, W., Babre, A., Jiang, W., Leuenberger, M., et al. (2017). Using $^{81}Kr$ and noble gases to characterize and date groundwater and brines in the Baltic Artesian Basin on the one-million-year timescale. *Geochimica et Cosmochimica Acta*, *205*, 187–210. https://doi.org/10.1016/j.gca.2017.01.033

Gerdes, M. L., Baumgartner, L. P., & Person, M. (1998). Convective fluid flow through heterogeneous country rocks during contact metamorphism. *Journal of Geophysical Research*, *103*(B10), 23,983–24,003. https://doi.org/10.1029/98JB02049

Ghaffour, N., Missimer, T. M., & Amy, G. L. (2013). Technical review and evaluation of the economics of water desalination: Current and future challenges for better water supply sustainability. *Desalinisation*, *309*, 197–207. https://doi.org/10.1016/j.desal.2012.10.015

Gleeson, T., Befus, K. M., Jasechko, S., Luijendijk, E., & Cardenas, M. B. (2016). The global volume and distribution of modern groundwater. *Nature Geoscience*, *9*(2), 161–167. https://doi.org/10.1038/ngeo2590

Glover, R. E. (1959). The pattern of freshwater flow in a coastal aquifer. *Journal of Geophysical Research*, *64*(4), 457–459. https://doi.org/10.1029/JZ064i004p00457

Godeau, N., Deschamps, P., Guihou, A., Leonide, P., Tendil, A., Gerdes, A., et al. (2018). U-Pb dating of calcite cement and diagenetic history in microporous carbonate reservoirs: Case of the Urgonian Limestone, France. *Geology*, *46*(3), 247–250. https://doi.org/10.1130/G39905.1

Goebel, M., Knight, R., & Halkjaer, M. (2019). Mapping saltwater intrusion with an airborne electromagnetic method in the offshore coastal environment, Monterey Bay, California. *Journal of Hydrology: Regional Studies*, *23*.

Goode, D. J. (1996). Direct simulation of groundwater age. *Water Resources Research*, *32*(2), 289–296. https://doi.org/10.1029/95WR03401

Gordon, D. S., Flemings, P. B., Harbaugh, J. W., Watney, W. L., Rankey, E. C., Slingerland, R., et al. (1999). Two-dimensional modeling of groundwater flow in an evolving deltaic environment. In *Numerical experiments in stratigraphy: Recent advances in stratigraphic and sedimentologic computer simulations* (pp. 301–312). Tulsa, OK: Society of Sedimentary Geology.

Grasby, S. E., Chen, Z., Issler, D., & Stasiuk, L. (2009). Evidence for deep anaerobic biodegradation associated with rapid sedimentation and burial in the Beaufort-Mackenzie basin, Canada. *Applied Geochemistry*, *24*, 532–542.

Grasshoff, K., Kremling, K., & Ehrhardt, M. (Eds) (2009). *Methods of seawater analysis*. Hoboken: John Wiley and Sons.

Greenlee, L. F., Lawler, D. F., Freeman, B. D., Marrot, B., & Moulin, P. (2009). Reverse osmosis desalination: Water sources, technology, and today's challenges. *Water Research*, *43*(9), 2317–2348. https://doi.org/10.1016/j.watres.2009.03.010

Greskowiak, J. (2014). Tide-induced salt-fingering flow during submarine groundwater discharge. *Geophysical Research Letters*, *41*, 6413–6419. https://doi.org/10.1002/2014GL061184

Groen, J. (1998). Hydrogeological investigations in Suriname. *Paper presented at Proceedings of the Koninklijke Nederlandse Akademie van Wetenschappen, The Netherlands* (pp. 129–174).

Groen, J., Kooi, H., Post, V. E. A., & de Vries, J. J. (2000). Fresh and moderately brackish groundwaters in coastal plains and continental shelves: Past and ongoing natural processes, in Proceedings of the 16th Salt Water Instrusion Meeting-SWIM, edited (pp. 73-80).

Groen, J., Velstra, J., & Meesters, A. (2000). Salinization processes in paleowaters in coastal sediments of Suriname: Evidence from $\Delta^{7}Cl$ analysis and diffusion modelling. *Journal of Hydrology*, *234*(1–2), 1–20. https://doi.org/10.1016/S0022-1694(00)00235-3

Grollimund, B., & Zoback, M. D. (2000). Post glacial lithospheric flexure and induced stresses and pore pressure changes in the northern North Sea. *Tectonophysics*, *327*(1–2), 61–81. https://doi.org/10.1016/S0040-1951(00)00162-1

Gustafson, C., Key, K., & Evans, R. L. (2019). Aquifer systems extending far offshore on the U.S. Atlantic margin. *Scientific Reports*, *9*(1), 8709. https://doi.org/10.1038/s41598-019-44611-7

Guswa, J. H., & LeBlanc, D. R. (1985). *Digital models of ground-water flow in the Cape Cod aquifer system, Massachusetts* (p. 112). New York: US Government Printing Office.

Hampson, J., & Robb, J. (1984). A geological map of the continental slope off New Jersey: Lindenkohl Canyon to Toms Canyon, U.S. Geological Survey Miscellaneous Investigations Map I-1608.

Hanebuth, T. J., Stattegger, K., & Saito, Y. (2002). The stratigraphic architecture of the central Sunda Shelf (SE Asia) recorded by shallow-seismic surveying. *Geo-Marine Letters*, *22*(2), 86–94. https://doi.org/10.1007/s00367-002-0102-1

Hansen, J. H., Sato, M., Russell, G., & Kharecha, P. (2013). Climate sensitivity, sea level and atmospheric carbon dioxide. *Philosophical Transaction of the Royal Society A: Mathematical, Physical and Engineering Sciences*, *371*(2001), 20120294. https://doi.org/10.1098/rsta.2012.0294

Hantush, M. S. (1968). Unsteady movement of fresh water in thick unconfined saline aquifers. *Hydrological Sciences Journal*, *13*(2), 40–60.

Haq, B. U., von Rad, U., O'Connell, S., Bent, A., Blome, C. D., Borella, P. E., et al. (1990). Site 763, Proceedings of the Ocean Drilling Program, 122, 289.

Haroon, A., Hölz, S., Gehrmann, R. A., Attias, E., Jegen, M., Minshull, T. A., & Murton, B. J. (2018). Marine dipole-dipole controlled source electromagnetic and coincident-loop transient electromagnetic experiments to detect seafloor massive sulphides: Effects of three-dimensional bathymetry. *Geophysical Journal International*, *215*(3), 2156–2171. https://doi.org/10.1093/gji/ggy398

Haroon, A., Hölz, S., Weymer, B. A., Tezkan, B., & Jegen, M. (2018). Calculating time-domain controlled source electromagnetic signals with MARE2DEM, paper presented at 3rd Applied Shallow Marine Geophysics Conference.

Haroon, A., Lippert, K., Mogilatov, V., & Tezkan, B. (2018). First application of the marine differential electric dipole for groundwater investigations: A case study from Bat Yam, Israel. *Geophysics*, *83*(2), 59–76.

Harrar, W. G., Williams, A. T., Barker, J. A., & Camp, M. V. (2001). Modelling scenarios for the emplacement of palaeowaters on aquifer systems. In W. M. Edmunds, & C. J. Milne (Eds.), *Palaeowaters in coastal Europe: Evolution of groundwater since the Late Pleistocene* (pp. 213–229). London: Geological Society of London.

Harrison, W. J., & Summa, L. L. (1991). Paleohydrology of the Gulf of Mexico basin. *American Journal of Science*, *291*(2), 109–176. https://doi.org/10.2475/ajs.291.2.109

Harvey, R. W., & George, L. H. (1987). Growth determinations for unattached bacteria in a contaminated aquifer. *Applied and Environmental Microbiology*, *53*(12), 2992–2996. https://doi.org/10.1128/AEM.53.12.2992-2996.1987

Harvey, R. W., Kinner, N. E., MacDonald, D., Metge, D. W., & Bunn, A. (1993). Role of physical heterogeneity in the interpretation of small-scale laboratory and field observations of bacteria, microbial-sized microsphere, and bromide transport through aquifer sediments. *Water Resources Research*, *29*(8), 2713–2721. https://doi.org/10.1029/93WR00963

Hathaway, J. C., Poag, C. W., Valentine, P. C., Manheim, F. T., Kohout, F. A., Bothner, M. H., et al. (1979). U.S Geological Survey core drilling on the Atlantic shelf. *Science*, *206*(4418), 515–527. https://doi.org/10.1126/science.206.4418.515

Heincke, B., Jegen, M., Moorkamp, M., Hobbs, R. W., & Chen, J. (2017). An adaptive coupling strategy for joint inversions that use petrophysical information as constraints. *Journal of Applied Geophysics*, *136*, 279–297. https://doi.org/10.1016/j.jappgeo.2016.10.028

Hem, J. D. (1970). Study and interpretation of the chemical characteristics of natural water, USGS Water-Supply.

Henry, H. R. (1964). Effects of dispersion on salt encroachment in coastal aquifers. In *Seawater in coastal aquifers* (pp. C1–C83). Washington, DC: US Geological Survey.

Hensen, C., Nuzzo, M., Hornibrook, E., Pinheiro, L. M., Bock, B., Magalhães, V. H., & Brückmann, W. (2007). Sources of mud volcano fluids in the Gulf of Cadiz-indications for hydrothermal imprint. *Geochimica et Cosmochimica Acta*, *71*(5), 1232–1248. https://doi.org/10.1016/j.gca.2006.11.022

Hensen, C., Wallmann, K., Schmidt, M., Ranero, C. R., & Suess, E. (2004). Fluid expulsion related to mud extrusion off Costa Rica—A window to the subducting slab. *Geology*, *32*(3), 201–204. https://doi.org/10.1130/G20119.1

Hesse, R. (2003). Pore water anomalies of submarine gas-hydrate zones as tool to assess hydrate abundance and distribution in the subsurface: What have we learned in the past decade? *Earth Science Reviews*, *61*(1–2), 149–179. https://doi.org/10.1016/S0012-8252(02)00117-4

Hesse, R., & Harrison, W. E. (1981). Gas hydrates (clathrate) causing pore-water freshening and oxygen isotope fractionation in deep-water sedimentary sections of terrigenous continental margins. *Earth and Planetary Science Letters*, *55*(3), 453–462. https://doi.org/10.1016/0012-821X(81)90172-2

Hoefs, J. (2009). *Stable isotope geochemistry*. Berlin: Springer.

Hoffmann, J. J. L., Schneider von Deimling, J., Schröder, J. F., Schmidt, M., Held, P., Crutchley, G. J., et al. (2020). Complex eyed pockmarks and submarine groundwater discharge revealed by acoustic data and sediment cores in Eckernförde Bay, SW Baltic Sea. *Geochemistry, Geophysics, Geosystems*, *21*, e2019GC008825. https://doi.org/10.1029/2019GC008825

Hofste, R. W., Kuzma, S., Walker, S., Sutanudjaja, E. H., Bierkens, M. F., Kuijper, M. J., et al. (2019). Aqueduct 3.0: Updated decision-relevant global water risk indicators, World Resources Institute, Washington D.C.

Hölz, S., Swidinsky, A., Sommer, M., Jegen, M., & Bialas, J. (2015). The use of rotational invariants for the interpretation of marine CSEM data with a case study from the North Alex mud volcano, West Nile Delta. *Geophysical Journal International*, *201*(1), 224–245. https://doi.org/10.1093/gji/ggv015

Hong, W.-L., Lepland, A., Himmler, T., Kim, J. H., Chand, S., Sahy, D., et al. (2019). Discharge of meteoric water in the eastern Norwegian Sea since the last glacial period. *Geophysical Research Letters*, *46*, 8194–8204. https://doi.org/10.1029/2019GL084237

Hooke, R. L. (1998). Principles of glacier mechanics: Englewood Cliffs, 248 pp.

Houben, G., & Post, V. E. A. (2017). The first field-based descriptions of pumping-induced saltwater intrusion and upconing. *Hydrogeology Journal*, *25*(1), 243–247. https://doi.org/10.1007/s10040-016-1476-x

Houben, G. J., Stoeckl, L., Mariner, K. E., & Choudhury, A. S. (2018). The influence of heterogeneity on coastal groundwater flow—Physical and numerical modeling of fringing reefs, dykes and structured conductivity fields. *Advances in Water Resources*, *113*, 155–166. https://doi.org/10.1016/j.advwatres.2017.11.024

Huffman, A. R. (2002). The future of pore-pressure prediction using geophysical methods. *The Leading Edge*, *21*(2), 199–205. https://doi.org/10.1190/1.1452613

Hughes, J. D., Vacher, H. L., & Sanford, W. E. (2007). Three-dimensional flow in the Florida platform: Theoretical analysis of Kohout convection at its type locality. *Geology*, *35*(7), 663–666. https://doi.org/10.1130/G23374A.1

Hughes, J. D., Vacher, H. L., & Sanford, W. E. (2009). Temporal response of hydraulic head, temperature, and chloride concentrations to sea-level changes, Floridan aquifer system, USA. *Hydrogeology Journal*, *17*(4), 793–815. https://doi.org/10.1007/s10040-008-0412-0

Hupers, A., & Kopf, A. (2012). Effect of smectite dehydration on pore water geochemistry in the shallow subduction zone: An experimental approach. *Geochemistry, Geophysics, Geosystems*, *13*, Q0AD26. https://doi.org/10.1029/2012GC004212

Ijiri, A., Tomioka, N., Wakaki, S., Masuda, H., Shozugawa, K., Kim, S., et al. (2018). Low-temperature clay mineral dehydration contributes to Porewater dilution in Bering Sea slope subseafloor. *Frontiers in Earth Science*, *6*(36). https://doi.org/10.3389/feart.2018.00036

Ingle, J. C., Jr., Suyehiro, K., von Breymann, M. T., Bristow, J. S., Burkle, L. H., Charvet, J., et al. (1989). Site 798. *Proceedings of the Ocean Drilling Program* (pp. 121–235). College Station: Ocean Drilling Program.

Jackson, P. D., Taylor-Smith, D., & Stanford, P. N. (1978). Resistivity-porosity-particle shape relationships for marine sands. *Geophysics*, *43*(6), 1250–1268. https://doi.org/10.1190/1.1440891

Jahnke, R. A. (1988). A simple, reliable, and inexpensive pore-water sampler 1. *Limnology and Oceanography*, *33*(3), 483–487. https://doi.org/10.4319/lo.1988.33.3.0483

Jahnke, R. A., Alexander, C. R., & Kostka, J. E. (2003). Advective pore water input of nutrients to the Satilla River Estuary, Georgia, USA. *Estuarine, Coastal and Shelf Science*, *56*(3–4), 641–653. https://doi.org/10.1016/S0272-7714(02)00216-0

Janssen, F., Huettel, M., & Witte, U. (2005). Pore-water advection and solute fluxes in permeable marine sediments (II): Benthic respiration at three sandy sites with different permeabilities (German Bight, North Sea). *Limnology and Oceanography*, *50*(3), 779–792. https://doi.org/10.4319/lo.2005.50.3.0779

Jiang, W., Bailey, K., Lu, Z. T., Mueller, P., O'Connor, T. P., Cheng, C. F., et al. (2012). An atom counter for measuring $^{81}$Kr and $^{85}$Kr in environmental samples. *Geochimica et Cosmochimica Acta*, *91*, 1–6. https://doi.org/10.1016/j.gca.2012.05.019

Jiang, W., Williams, W., Bailey, K., Davis, A. M., Hu, S. M., Lu, Z. T., et al. (2011). Ar 39 detection at the 10−16 isotopic abundance level with atom trap trace analysis. *Physical Review Letters*, *106*(10), 103001. https://doi.org/10.1103/PhysRevLett.106.103001

Jiao, J. J., Shi, L., Kuang, X., Ming Lee, C., Yim, W. W. S., & Yang, S. (2015). Reconstructed chloride concentration profiles below the seabed in Hong Kong (China) and their implications for offshore groundwater resources. *Hydrogeology Journal*, *23*(2), 277–286. https://doi.org/10.1007/s10040-014-1201-6

Jiráková, H., Huneau, F., Celle-Jeanton, H., Hrkal, Z., & le Coustumer, P. (2011). Insights into palaeorecharge conditions for European deep aquifers. *Hydrogeology Journal*, *19*(8), 1545–1562. https://doi.org/10.1007/s10040-011-0765-7

Johnsen, S. J., Dahl-Jensen, D., Dansgaard, W., & Gundestrup, N. (1995). Greenland palaeotemperatures derived from GRIP borehole temperature and ice core isotope profiles. *Tellus*, *47B*, 624–629.

Johnston, R. H. (1983). The salt-water-fresh-water interface in the tertiary limestone aquifer, Southeast Atlantic outer continental-shelf of the USA. *Journal of Hydrology*, *61*(1–3), 239–249. https://doi.org/10.1016/0022-1694(83)90251-2

Jones, E., Qadir, M., van Vliet, M. T. H., Smakhtin, V., & Kang, S.-M. (2019). The state of desalination and brine production: A global outlook. *Science of the Total Environment*, *657*, 1343–1356. https://doi.org/10.1016/j.scitotenv.2018.12.076

Jowett, E. C., Cathles, L. M., & Davis, B. W. (1993). Predicting depths of gypsum dehydration in evaporitic sedimentary basins. *American Association of Petroleum Geologists Bulletin*, *77*, 402–413.

Karaca, D., Hensen, C., & Wallmann, K. (2010). Controls on authigenic carbonate precipitation at cold seeps along the convergent margin off Costa Rica. *Geochemistry, Geophysics, Geosystems*, *11*, Q08S27. https://doi.org/10.1029/2010GC003062

Karagiannis, I. C., & Soldatos, P. G. (2008). Water desalination cost literature: Review and assessment. *Desalinisation*, *223*(1–3), 448–456. https://doi.org/10.1016/j.desal.2007.02.071

Kastner, M., Elderfield, H., & Martin, J. B. (1991). Fluids in convergent margins: What do we know about their composition, origin, role in diagenesis and importance for oceanic chemical fluxes? *Philosophical Transactions of the Royal Society of London*, *335*, 243–259.

Kastner, M., & Gieskes, J. M. (1983). Opal-A to opal-CT transformation: A kinetic study. *Developments in Sedimentology*, *36*, 211–227. https://doi.org/10.1016/S0070-4571(08)70092-X

Kestin, J., Khalifa, H. E., & Corriea, R. (1981). Tables of the dynamics and kinematic viscosity of aqueous NaCl solutions in the temperature range of 20–150°C and the pressure range of 0.1–35 MPa. *Journal of Physical Chemistry Reference Data*, *10*(1), 71–88. https://doi.org/10.1063/1.555641

Key, K. (2016). MARE2DEM: A 2-D inverstion code for controlled-source electromagnetic and magnetotelluric data. *Geophysical Journal International*, *207*(1), 571–588. https://doi.org/10.1093/gji/ggw290

Kirkegaard, C., Sonnenborg, T. O., Auken, E., & Jørgensen, F. (2011). Salinity distribution in heterogeneous coastal aquifers mapped by airborne electromagnetics. *Vadose Zone Journal*, *10*(1), 125–135. https://doi.org/10.2136/vzj2010.0038

Kleinberg, R., & Griffin, D. (2005). NMR measurements of permafrost: Unfrozen water assay, pore-scale distribution of ice, and hydraulic permeability of sediments. *Cold Regions Science and Technology*, *42*(1), 63–77. https://doi.org/10.1016/j.coldregions.2004.12.002

Knight, A. C., Werner, A. D., & Irvine, D. J. (2019). Combined geophysical and analytical methods to estimate offshore freshwater extent. *Journal of Hydrology*, *576*, 529–540. https://doi.org/10.1016/j.jhydrol.2019.06.059

Knight, A. C., Werner, A. D., & Morgan, L. K. (2018). The onshore influence of offshore fresh groundwater. *Journal of Hydrology*, *561*, 724–736. https://doi.org/10.1016/j.jhydrol.2018.03.028

Kohout, F. A. (1964). The flow of fresh water and salt water in the Biscayne aquifer of the Miami area, Florida. In H. H. Cooper, et al. (Eds.), *Sea water in coastal aquifers: Relation of salt water to fresh groundwater* (pp. 12–32). Washington, DC: USGS Water Supply.

Kohout, F. A. (1965). A hypothesis concerning cyclic flow of salt water related to geothermal heating in the Floridan aquifer. *New York Academy of Sciences Transactions*, *28*(2 Series II), 249–271. https://doi.org/10.1111/j.2164-0947.1965.tb02879.x

Konikow, L. F., & Grove, D. B. (1977). Derivation of equations describing solute transport in groundwater.

Kooi, H. (1999). Competition between topography- and compaction-driven flow in a confined-aquifer: Some analytical results. *Hydrogeology Journal*, *7*(3), 245–250. https://doi.org/10.1007/s100400050198

Kooi, H., & Groen, J. (2003). Geological processes and the management of groundwater resources in coastal areas. *Netherlands Journal of Geosciences*, *82*(1), 31–40. https://doi.org/10.1017/S0016774600022770

Kooi, H., Groen, J., & Leijnse, A. (2000). Modes of seawater intrusion during transgressions. *Water Resources Research*, *36*(12), 3581–3589. https://doi.org/10.1029/2000WR900243

Kooi, H., & Groen, K. (2001). Offshore continuation of coastal groundwater systems; predictions using sharp-interface approximations and variable-density flow modelling. *Journal of Hydrology*, *246*(1–4), 19–35. https://doi.org/10.1016/S0022-1694(01)00354-7

Krabbenhöft, A., Eisenhauer, A., Böhm, F., Vollstaedt, H., Fietzke, J., Liebetrau, V., et al. (2010). Constraining the marine strontium budget with natural strontium isotope fractionations ($^{87}Sr/^{86}Sr^*$, $\delta^{88/86}Sr$) of carbonates, hydrothermal solutions and river waters. *Geochimica et Cosmochimica Acta*, *74*(14), 4097–4109. https://doi.org/10.1016/j.gca.2010.04.009

Krantz, D. E., Manheim, F. T., Bratton, J. F., & Phelan, D. J. (2004). Hydrogeologic setting and ground water flow beneath a section of Indian River Bay, Delaware. *Groundwater*, *42*(7), 1035–1051. https://doi.org/10.1111/j.1745-6584.2004.tb02642.x

Kreyns, P., Geng, X., & Michael, H. A. (2020). The influence of connected heterogeneity on groundwater flow and salinity distributions in coastal volcanic aquifers. *Journal of Hydrology*, *586*, 124863. https://doi.org/10.1016/j.jhydrol.2020.124863

Kwong, H. T., & Jiao, J. J. (2016). Hydrochemical reactions and origin of offshore relatively fresh pore water from core samples in Hong Kong. *Journal of Hydrology*, *537*, 283–296. https://doi.org/10.1016/j.jhydrol.2016.03.050

Laattoe, T., Werner, A. D., & Simmons, C. T. (2013). Seawater intrusion under current sea-level rise: Processes accompanying coastline transgression. In C. E. Wetzelhuetter (Ed.), *Groundwater in the coastal zones of Asia-Pacific* (pp. 295–313). New York: Springer. https://doi.org/10.1007/978-94-007-5648-9_14

Lager, A., Webb, K. J., & Black, C. J. J. (2007). Impact of brine chemistry on oil recovery. In *IOR 2007-14th European symposium on improved oil recovery*. Cairo, Egypt.

Langevin, C. D., Thorne, D. T. Jr., Dausman, A. M., Sukop, M. C., & Guo, W. (2008). SEAWAT version 4: A computer program for simulation of multi-species solute and heat transport. In *U. S. Geological Survey techniques and methods* (p. 39). Reston, VA: US Geological Survey.

Ledoux, E., Sauvagnac, S., & Rivera, A. (1990). A compatible single-phase/two-phase numerical model: 1. Modeling the transient salt-water/fresh-water interface motion. *Groundwater*, *28*(1), 79–87. https://doi.org/10.1111/j.1745-6584.1990.tb02231.x

Legrand, H. E., & Stringfield, V. T. (1971). Development and distribution of permeability in carbonate aquifers. *Water Resources Research*, *7*(5), 1284–1294. https://doi.org/10.1029/WR007i005p01284

Lemieux, J.-M., Sudicky, E. A., Peltier, W. R., & Tarasov, L. (2008a). Simulating the impact of glaciations on continental groundwater flow systems: 1. Relevant processes and model formulation. *Journal of Geophysical Research*, *113*, F03017. https://doi.org/10.1029/2007JF000928

Lemieux, J.-M., Sudicky, E. A., Peltier, W. R., & Tarasov, L. (2008b). Dynamics of groundwater recharge and seepage over the Canadian landscape during the Wisconsinian glaciation. *Journal of Geophysical Research*, *113*, F01011. https://doi.org/10.1029/2007JF000838

Lemieux, J.-M., Sudicky, E. A., Peltier, W. R., & Tarasov, L. (2008c). Simulating the impact of glaciations on continental groundwater flow systems: 2. Model application to the Wisconsinian glaciation over the Canadian landscape. *Journal of Geophysical Research*, *113*, F03018. https://doi.org/10.1029/2007JF000929

Levi, E., Goldman, M., Tibor, G., & Herut, B. (2018). Delineation of subsea fresh water extension by marine geoelectromagnetic soundings (SE Mediterranean Sea). *Water Resources Management*, *32*(11), 3765–3779. https://doi.org/10.1007/s11269-018-2018-1

Li, X., Hu, B. X., & Tong, J. (2016). Numerical study on tide-driven submarine groundwater discharge and seawater recirculation in heterogeneous aquifers. *Stochastic Environmental Research and Risk Assessment*, *30*(6), 1741–1755. https://doi.org/10.1007/s00477-015-1200-8

Liebetrau, V., Augustin, N., Kutterolf, S., Schmidt, M., Eisenhauer, A., Garbe-Schönberg, D., & Weinrebe, W. (2014). Cold-seep-driven carbonate deposits at the Central American forearc: Contrasting evolution and timing in escarpment and mound settings. *International Journal of Earth Sciences*, *103*(7), 1845–1872. https://doi.org/10.1007/s00531-014-1045-2

Lin, I. T., Wang, C. H., You, C. F., Lin, S., Huang, K. F., & Chen, Y. G. (2010). Deep submarine groundwater discharge indicated by tracers of oxygen, strontium isotopes and barium content in the Pingtung coastal zone, southern Taiwan. *Marine Chemistry*, *122*(1–4), 51–58. https://doi.org/10.1016/j.marchem.2010.08.007

Linke, P. (2011). FS SONNE Fahrtbericht/Cruise Report SO210 ChiFlux: Identification and investigation of fluid flux, mass wasting and sediments in the forearc of the central Chilean subduction zone, Valparaiso - Valparaiso, 23.09.-01.11.2010, 103 pp, IFM-GEOMAR, Kiel.

Lippert, K., & Tezkan, B. (2020). On the exploration of a marine aquifer offshore Israel by long-offset transient electromagnetics. *Geophysical Prospecting*, *68*(3), 999–1015. https://doi.org/10.1111/1365-2478.12875

Liu, C.-H., Huang, X., Xie, T. N., Duan, N., Xue, Y. R., Zhao, T. X., et al. (2017). Exploration of cultivable fungal communities in deep coal-bearing sediments from ∼1.3 to 2.5 km below the ocean floor. *Environmental Microbiology*, *19*(2), 803–818. https://doi.org/10.1111/1462-2920.13653

Lofi, J., Berné, S., Tesson, M., Seranne, M., & Pezard, P. A. (2012). Giant solution-subsidence structure in the Western Mediterranean related to deep substratum dissolution. *Terra Nova*, *24*(3), 181–188. https://doi.org/10.1111/j.1365-3121.2011.01051.x

Lofi, J., Inwood, J., Proust, J. N., Monteverde, D. H., Loggia, D., Basile, C., et al. (2013). Fresh-water and salt-water distribution in passive margin sediments: Insights from Integrated Ocean Drilling Program Expedition 313 on the New Jersey margin. *Geosphere*, *9*(4), 1–16.

Lofi, J., Pezard, P., Bouchette, F., Raynal, O., Sabatier, P., Denchik, N., et al. (2013). Integrated onshore-offshore investigation of a Mediterranean layered coastal aquifer. *Groundwater*, *51*(4), 550–561.

Lunne, T., & Long, M. (2006). Review of long seabed samplers and criteria for new sampler design. *Marine Geology*, *226*(1–2), 145–165. https://doi.org/10.1016/j.margeo.2005.07.014

Magnabosco, C., Lin, L. H., Dong, H., Bomberg, M., Ghiorse, W., Stan-Lotter, H., et al. (2018). The biomass and biodiversity of the continental subsurface. *Nature Geoscience*, *11*(10), 707–717. https://doi.org/10.1038/s41561-018-0221-6

Malinverno, A., Kastner, M., Torres, M. E., & Wortmann, U. G. (2008). Gas hydrate occurrence from pore water chlorinity and downhole logs in a transect across the northern Cascadia margin (Integrated Ocean Drilling Program Expedition 311). *Journal of Geophysical Research*, *113*, B08103. https://doi.org/10.1029/2008JB005702

Manda, A. K., & Gross, M. R. (2006). Identifying and characterizing solution conduits in karst aquifers through geospatial (GIS) analysis of porosity from borehole imagery: An example from the Biscayne aquifer, South Florida (USA). *Advances in Water Resources*, *29*(3), 383–396. https://doi.org/10.1016/j.advwatres.2005.05.013

Marksammer, A. J., Person, M. A., Day-Lewis, F. D., Lane, J. W., Cohen, D., Dugan, B., et al. (2007). Integrating geophysical, hydrochemical, and hydrologic data to understand the freshwater resources on Nantucket Island, Massachusetts. In D. W. Hyndman, F. D. Day-Lewis, K. Singha, et al. (Eds.), *Subsurface Hydrology: Data Integration for Properties and Processes*, *AGU Water Resources Monograph* (pp. 143–159). Washington, DC: American Geophysical Union.

Martin-Nagle, R. (2020). *Governance of offshore fresh water resources*. Leiden: Brill Nijhoff Publishers. https://doi.org/10.1163/9789004421042

Martin-Nagle, R. (2016). *Transboundary Offshore Aquifers: A Search for a Governance Regime*. Lieden: Brill.

Mavko, G., Mukerji, T., & Dvorkin, J. (2003). *The rock physics handbook: Tools for seismic analysis in porous media*. Cambridge: Cambridge University Press.

Mazzullo, S. J. (2004). Overview of porosity evolution in carbonate reservoirs. *Kansas Geological Society Bulletin*, *79*(1–2), 22–28.

McAuley, S. D., Barringer, J. L., Paulachok, G. N., Clark, J. S., & Zapecza, O. S. (2001). Groundwater flow and quality in the Atlantic City 800 Foot Sand, New Jersey (p. 86).

McKenzie, J. M., & Voss, C. I. (2013). Permafrost thaw in a nested groundwater-flow system. *Hydrogeology Journal*, *21*(1), 299–316. https://doi.org/10.1007/s10040-012-0942-3

Meisler, H., Leahy, P. P., & Knobel, L. L. (1984). Effect of eustatic sea-level changes on saltwater-freshwater relations in the Northern Atlantic coastal plain, U.S. Geological Survey.

Meissl, S., & Behrmann, J. H. (2010). Data report: Preliminary assessment of Pleistocene sediment strength in the Ursa Basin (Gulf of Mexico continental slope) from triaxial and ring shear test data, Proceedings of the Integrated Ocean Drilling Program, 308.

Micallef, A. (2020). Global database of offshore freshened groundwater records, Creative Commons Attribution 4.0 International, https://doi.org/10.5281/zenodo.4247833

Micallef, A., Berndt, C., Berndt, J., Jegen, M., Schwalenberg, K., Wollatz-Vogt, M., et al. (2018). Cruise report RV Hercules [MARCAN Malta 2018], Valletta-Valletta, 1.-10.10.2018 (p. 37). University of Malta, Malta.

Micallef, A., Mountjoy, J., Schwalenberg, K., Jegen, M., Weymer, B., Woelz, S., et al. (2018). How offshore groundwater shapes the seafloor. *Eos, Transactions of the American Geophysical Union*, *99*. https://doi.org/10.1029/2018EO090691

Micallef, A., Person, M., Haroon, A., Weymer, B. A., Jegen, M., Schwalenberg, K., et al. (2020). 3D characterisation and quantification of an offshore freshened groundwater system in the Canterbury bight. *Nature Communications*, *11*(1), 1372. https://doi.org/10.1038/s41467-020-14770-7

Michael, H. A., Mulligan, A. E., & Harvey, C. F. (2005). Seasonal oscillations in water exchange between aquifers and the coastal ocean. *Nature*, *436*(7054), 1145–1148. https://doi.org/10.1038/nature03935

Michael, H. A., Scott, K. C., Koneshloo, M., Yu, X., Khan, M. R., & Li, K. (2016). Geologic influence on groundwater salinity drives large seawater circulation through the continental shelf. *Geophysical Research Letters*, *43*, 10,782–10,791. https://doi.org/10.1002/2016GL070863

Middelburg, J. J., & de Lange, G. J. (1989). The isolation of Kau Bay during the last glaciation: Direct evidence from interstitial water chlorinity. *Netherlands Journal of Sea Research*, *24*(4), 615–622. https://doi.org/10.1016/0077-7579(89)90138-5

Miller, K. G., Mountain, G. S., Browning, J. V., Kominz, M., Sugarman, P. J., Christie-Blick, N., et al. (1998). Cenozoic global sea level, sequences, and the New Jersey transect: Results from coastal plain and slope drilling. *Reviews of Geophysics*, *36*(4), 569–601. https://doi.org/10.1029/98RG01624

Mitchum, R. M., Vail, P. R., & Thompson, S. (1977). The depositional sequence as a basic unit for stratigraphic analysis. *AAPG Memoir*, *26*, 53–62.

Moore, J. C., & Saffer, D. M. (2001). Updip limit of the seismogenic zone beneath the accretionary prism of southwest Japan: An effect of diagenetic to low-grade metamorphic processes and increasing effective stress. *Geology*, *29*(2), 183–186. https://doi.org/10.1130/0091-7613(2001)029<0183:ULOTSZ>2.0.CO;2

Moore, W. S. (1976). Sampling $^{228}$Ra in the deep ocean. *Deep Sea Research and Oceanographic Abstracts*, *23*(7), 647–651. https://doi.org/10.1016/0011-7471(76)90007-3

Moore, W. S. (1996). Large groundwater inputs to coastal waters revealed by $^{226}$Ra enrichments. *Nature*, *380*(6575), 612–614. https://doi.org/10.1038/380612a0

Moore, W. S. (2010). The effect of submarine groundwater discharge on the ocean. *Annual Review of Marine Science*, *2*, 345–374.

Moorkamp, M., Roberts, A. W., Jegen, M., Heincke, B., & Hobbs, R. W. (2013). Verification of velocity-resistivity relationships derived from structural joint inversion with borehole data. *Geophysical Research Letters*, *40*, 3596–3601. https://doi.org/10.1002/grl.50696

Moosdorf, N., & Oehler, T. (2017). Societal use of fresh submarine groundwater discharge: An overlooked water resource. *Earth-Science Reviews*, *171*, 338–348. https://doi.org/10.1016/j.earscirev.2017.06.006

Mora, G. (2005). Isotope-tracking of pore water freshening in the fore-arc basin of the Japan Trench. *Marine Geology*, *219*(2–3), 71–79. https://doi.org/10.1016/j.margeo.2005.06.020

Morgan, L. K., Werner, A. D., & Patterson, A. E. (2018). A conceptual study of offshore fresh groundwater behaviour in the Perth Basin (Australia): Modern salinity trends in a prehistoric context. *Journal of Hydrology: Regional Studies*, *19*, 318–334.

Morgera, E., Webster, E., Hamley, G., Sindico, F., Robbie, J., Switzer, S., et al. (2020). *The right to water for food and agriculture*. Rome: FAO.

Morley, C., Maczak, A., Rungprom, T., Ghosh, J., Cartwright, J. A., Bertoni, C., & Panpichityota, N. (2017). New style of honeycomb structures revealed on 3D seismic data indicate widespread diagenesis offshore Great South Basin, New Zealand. *Marine and Petroleum Geology*, *86*, 140–154. https://doi.org/10.1016/j.marpetgeo.2017.05.035

Morrissey, S. K., Clark, J., Bennett, M., Richardson, E., & Stute, M. (2010). Groundwater reorganization in the Floridan aquifer following Holocene sea-level rise. *Nature Geoscience*, *3*(10), 683–687. https://doi.org/10.1038/ngeo956

Moshier, O. S. (1989). Microporosity in micritic limestones: A review. *Sedimentary Geology*, *63*(3–4), 191–213. https://doi.org/10.1016/0037-0738(89)90132-2

Mottl, M. J., & Hayashi, T. (2009). Fresh and salty: Chemistry of sediment pore water from the New Jersey shallow shelf: IODP Exp313, in AGU Fall Meeting, edited, San Francisco.

Mountain, G. S., Proust, J. N., McInroy, D., Cotterill, C., & Expedition 313 Scientists (2010). Proceedings of the Integrated Ocean Drilling Program.

Mozley, P. S., & Burns, S. J. (1993). Oxygen and carbon isotopic composition of marine carbonate concretions: An overview. *Journal of Sedimentary Petrology*, *63*(1), 73–83.

Müller, H., von Dobeneck, T., Nehmiz, W., & Hamer, K. (2011). Near-surface electromagnetic, rock magnetic, and geochemical fingerprinting of submarine fresh water seepage at Eckernförde Bay (SW Baltic Sea). *Geo-Marine Letters*, *31*(2), 123–140. https://doi.org/10.1007/s00367-010-0220-0

Müller, T., Osenbrück, K., Strauch, G., Pavetich, S., Al-Mashaikhi, K. S., Herb, C., et al. (2016). Use of multiple age tracers to estimate groundwater residence times and long-term recharge rates in arid southern Oman. *Applied Geochemistry*, *74*, 67–83. https://doi.org/10.1016/j.apgeochem.2016.08.012

Mulligan, A., & Uchupi, E. (2003). New interpretation of glacial history of Cape Code may have important implications for groundwater contaminant transport. *Eos, Transactions of the American Geophysical Union*, *84*(19), 177–183. https://doi.org/10.1029/2003EO190001

Mulligan, A. E., Evans, R. L., & Lizarralde, D. (2007). The role of paleochannels in groundwater/seawater exchange. *Journal of Hydrology*, *335*(3–4), 313–329. https://doi.org/10.1016/j.jhydrol.2006.11.025

Myhre, A. M., Thiede, J., & Firth, J. V. (1995). Site 912. In J. A. McKenzie, et al. (Eds.), *Proceedings of ODP 151 Initial Reports* (pp. 319–343). College Station: Ocean Drilling Program. https://doi.org/10.2973/odp.proc.ir.151.1995

Neumann, B., Vafeidis, A. T., Zimmermann, J., & Nicholls, R. J. (2015). Future coastal population growth and exposure to sea-level rise and coastal flooding—A global assessment. *PLoS ONE*, *10*(3), e0118571. https://doi.org/10.1371/journal.pone.0118571

Neuzil, C. E. (2003). Hydromechanical coupling in geologic processes. *Hydrogeology Journal*, *11*(1), 41–83. https://doi.org/10.1007/s10040-002-0230-8

Nicholls, R. J., & Cazenave, A. (2010). Sea-level rise and its impacts on coastal zones. *Science*, *328*(5985), 1517–1520. https://doi.org/10.1126/science.1185782

Nigro, O. D., Jungbluth, S. P., Lin, H.-T., Hsieh, C.-C., Miranda, J. A., Schvarcz, C. R., et al. (2017). Viruses in the oceanic basement, mBio, 8, e02129–02116.

Ong, D. M. (2002). The New Timor Sea Arrangement 2001: Is joint development of common offshore oil and gas deposits mandated under international law? *International Journal of Marine and Coastal Law*, *17*(1), 79–122. https://doi.org/10.1163/157180802X00279

Oteri, A. U. (1988). Electric log interpretation for the evaluation of salt water intrusion in the eastern Niger Delta. *Hydrological Sciences Journal*, *33*(1), 19–30. https://doi.org/10.1080/02626668809491219

Paldor, A., Katz, O., Aharonov, E., Weinstein, Y., Roditi-Elasar, M., Lazar, A., & Lazar, B. (2020). Deep Submarine Groundwater Discharge—Evidence from Achziv Submarine Canyon at the Exposure of the Judea Group Confined Aquifer, Eastern Mediterranean. *Journal of Geophysical Research: Oceans*, *125*, e2020RG000706. https://doi.org/10.1029/2019JC015435

Paldor, A., Shalev, E., Katz, O., & Aharonov, E. (2019). Dynamics of saltwater intrusion and submarine groundwater discharge in confined coastal aquifers: A case study in northern Israel. *Hydrogeology Journal*, *27*(5), 1611–1625. https://doi.org/10.1007/s10040-019-01958-5

Pan, D., Morono, Y., Inagaki, F., & Takai, K. (2019). An improved method for extracting viruses from sediment: Detection of far more viruses in the subseafloor than previously reported. *Frontiers in Microbiology*, *10*. https://doi.org/10.3389/fmicb.2019.00878

Paola, C., Mullin, J., Ellis, C., Mohrig, D. C., Swenson, J. B., Parker, G., et al. (2001). Experimental stratigraphy. *GSA Today*, *11*(7), 4–9. https://doi.org/10.1130/1052-5173(2001)011<0004:ES>2.0.CO;2

Park, S., Wolanin, P. M., Yuzbashyan, E. A., Lin, H., Darnton, N. C., Stock, J. B., et al. (2003). Influence of topology on bacterial social interaction. *Proceedings of the National Academy of Sciences of the United States of America*, *100*(24), 13,910–13,915. https://doi.org/10.1073/pnas.1935975100

Paull, C. K., Spiess, F. N., Curry, J. R., & Twichell, D. C. (1990). Origin of Florida Canyon and the role of spring sapping on the formation of submarine mass box canyons. *Geological Society of America Bulletin*, *102*(4), 502–515. https://doi.org/10.1130/0016-7606(1990)102<0502:OOFCAT>2.3.CO;2

Perkin, R. G., & Lewis, E. L. (1980). The practical salinity scale 1978: Fitting the data. *IEEE Journal of Oceanic Engineering*, *OE-5*(9).

Person, M., Dugan, B., Swenson, J. B., Urbano, L., Stott, C., Taylor, J., & Willett, M. (2003). Pleistocene hydrogeology of the Atlantic continental shelf, New England. *Geological Society of America Bulletin*, *115*(11), 1324–1343. https://doi.org/10.1130/B25285.1

Person, M., Marksamer, A., Dugan, B., Sauer, P. E., Brown, K., Bish, D., et al. (2012). Use of a vertical $\delta^{18}O$ profile to constrain hydraulic properties and recharge rates across a glacio-lacustrine unit, Nantucket Island, Massachusetts, USA. *Hydrogeology Journal*, *20*(2), 325–336. https://doi.org/10.1007/s10040-011-0795-1

Person, M., McIntosh, J., Bense, V. F., & Remenda, V. H. (2007). Pleistocene hydrology of North America: The role of ice sheets in reorganizing groundwater flow systems. *Reviews of Geophysics*, *45*, RG3007. https://doi.org/10.1029/2006RG000206

Person, M., Wilson, J. L., Morrow, N., & Post, V. E. A. (2017). Continental-shelf freshwater water resources and improved oil recovery by low-salinity waterflooding. *AAPG Bulletin*, *101*(01), 1–18. https://doi.org/10.1306/05241615143

Pewe, T. L. (1983). The periglacial environment in North America during Wisconsin time. *Late Quaternary Environments of the United States*, *1*, 157–189.

Pezard, P., & Lovell, M. (1990). Downhole images: Electrical scanning reveals the nature of subsurface oceanic crust. *Eos, Transactions American Geophysical Union*, *71*(20), 709–718. https://doi.org/10.1029/90EO00178

Phillips, F. M. (2013). Chlorine-36 dating of old groundwater. In International Atomic Energy Agency (Ed.), *Isotope methods for dating old groundwater* (pp. 125–152). Vienna: International Atomic Energy Agency.

Plummer, L. N., & Glynn, P. D. (2013). Radiocarbon dating in groundwater systems. In International Atomic Energy Agency (Ed.), *Isotope methods for dating old groundwater* (pp. 33–90). Vienna: International Atomic Energy Agency.

Post, V. E., Vandenbohede, A., Werner, A. D., & Teubner, M. D. (2013). Groundwater ages in coastal aquifers. *Advances in Water Resources*, *57*, 1–11. https://doi.org/10.1016/j.advwatres.2013.03.011

Post, V. E. A., Groen, J., Kooi, H., Person, M., Ge, S., & Edmunds, W. M. (2013). Offshore fresh groundwater reserves as a global phenomenon. *Nature*, *504*(7478), 71–78. https://doi.org/10.1038/nature12858

Post, V. E. A., & Kooi, H. (2003). Rates of salinization by free convection in high-permeability sediments: Insights from numerical modeling and application to the Dutch coastal area. *Hydrogeology Journal*, *11*(5), 549–559. https://doi.org/10.1007/s10040-003-0271-7

Purkl, S., & Eisenhauer, A. (2004). Determination of radium isotopes and $^{222}Rn$ in a groundwater affected coastal area of the Baltic Sea and the underlying sub-sea floor aquifer. *Marine Chemistry*, *87*(3–4), 137–149. https://doi.org/10.1016/j.marchem.2004.02.005

Purtschert, R., Yokochi, R., & Sturchio, N. C. (2013). Krypton-81 dating of old groundwater. In International Atomic Energy Agency (Ed.), *Isotope methods for dating old groundwater*, edited by (pp. 91–124). Vienna: International Atomic Energy Agency.

Putnam, A. E., & Broecker, W. S. (2017). Human-induced changes in the distribution of rainfall. *Science Advances*, *3*(5), e1600871. https://doi.org/10.1126/sciadv.1600871

Razin, P., Taati, F., & van Buchem, F. S. P. (2010). Sequence stratigraphy of Cenomanian–Turonian carbonate platform margins (Sarvak Formation) in the high Zagros, SW Iran: An outcrop reference model for the Arabian plate. In F. S. P. van Buchem, et al. (Eds.), *Mesozoic and Cenozoic carbonate systems of the Mediterranean and the Middle East: Stratigraphic and diagenetic reference models* (pp. 187–218). London: Geological Society of London Special Publications.

Reijenstein, H. M., Posamentier, H. W., & Bhattacharya, J. P. (2011). Seismic geomorphobgy and high-resolution seismic stratigraphy of inner-shelf fluvial, estuarine, deltaic, and marine sequences. Gulf of Thailand. *American Association of Petroleum Geologists Bulletin*, *95*(11), 1959–1990. https://doi.org/10.1306/03151110134

Rittenberg, S. C., Emery, K. O., Hulsemann, J., Degens, E. T., Fay, R. C., Reuter, J. H., et al. (1963). Biogeochemistry of sediments in experimental Mohole. *Journal of Sedimentary Research*, *33*(1), 140–172.

Ritterbusch, F., Ebser, S., Welte, J., Reichel, T., Kersting, A., Purtschert, R., et al. (2014). Groundwater dating with atom trap trace analysis of $^{39}Ar$. *Geophysical Research Letters*, *41*, 6758–6764. https://doi.org/10.1002/2014GL061120

Rivera, A., Ledoux, E., & Sauvagnac, S. (1990). A compatible single-phase/two-phase numerical model: 2. Application to a coastal aquifer in Mexico. *Groundwater*, *28*(2), 215–223. https://doi.org/10.1111/j.1745-6584.1990.tb02249.x

Roberts, N., Drost, K., Horstwood, M., Condon, D., Drake, H., Milodowski, A., et al. (2020). LA-ICP-MS U-Pb carbonate geochronology: strategies, progress, and application to fracture-fill calcite, Geochronology Discussions.

Ruden, F. (2009). Freshwater entrapment in offshore Zanzibar basins. In *International symposium on efficient groundwater resources management*, edited by T.. Bangkok: Department of Groundwater Resources.

Russoniello, C. J., Fernandez, C., Bratton, J. F., Banaszak, J. F., Krantz, D. E., Andres, A. S., et al. (2013). Geologic effects on groundwater salinity and discharge into an estuary. *Journal of Hydrology*, *498*, 1–12. https://doi.org/10.1016/j.jhydrol.2013.05.049

Saager, P. M., Sweerts, J. P., & Ellermeijer, H. J. (1990). A simple pore-water sampler for coarse, sandy sediments of low porosity. *Limnology and Oceanography*, *35*(3), 747–751. https://doi.org/10.4319/lo.1990.35.3.0747

Saffer, D. M., & McKiernan, A. W. (2009). Evaluation of in situ smectite dehydration as a pore water freshening mechanism in the Nankai Trough, offshore southwest Japan. *Geochemistry, Geophysics, Geosystems*, *10*, Q02010. https://doi.org/10.1029/2008GC002226

Salem, H. S., & Chilingarian, G. V. (1999). The cementation factor of Archie's equation for shaly sandstone reservoirs. *Journal of Petroleum Science and Engineering*, *23*(2), 83–93. https://doi.org/10.1016/S0920-4105(99)00009-1

Sanford, W. E., & Buapeng, S. (1996). Assessment of a groundwater flow model of the Bangkok Basin, Thailand, using carbon-14-based ages and paleohydrology. *Hydrogeology Journal*, *4*(4), 26–40. https://doi.org/10.1007/s100400050083

Sanford, W. E., & Konikow, L. F. (1989). Porosity develoment of coastal carbonate aquifers. *Geology*, *17*(3), 249–252. https://doi.org/10.1130/0091-7613(1989)017<0249:PDICCA>2.3.CO;2

Sanford, W. E., & Pope, J. P. (2010). Current challenges using models to forecast seawater intrusion: Lessons from the Eastern Shore of Virginia, USA. *Hydrogeology Journal*, *18*(1), 73–93. https://doi.org/10.1007/s10040-009-0513-4

Sanford, W. E., & Wood, W. W. (2001). Hydrology of the coastal sabkhas of Abu Dhabi, United Arab Emirates. *Hydrogeology Journal*, *9*(4), 358–366. https://doi.org/10.1007/s100400100137

Santoro, A. E., Boehm, A. B., & Francis, C. A. (2006). Denitrifier community composition along a nitrate and salinity gradient in a coastal aquifer. *Applied and Environmental Microbiology*, *72*(3), 2102–2109. https://doi.org/10.1128/AEM.72.3.2102-2109.2006

Santoro, A. E., Francis, C. A., Sieyes, N. R. D., & Boehm, A. B. (2008). Shifts in the relative abundance of ammonia-oxidizing bacteria and archaea across physicochemical gradients in a subterranean estuary. *Environmental Microbiology*, *10*(4), 1068–1079. https://doi.org/10.1111/j.1462-2920.2007.01547.x

Sayers, C. M., Woodward, M. J., & Bartman, R. C. (2002). Seismic pore-pressure prediction using reflection tomography and 4-C seismic data. *The Leading Edge*, *21*(2), 188–192. https://doi.org/10.1190/1.1452611

Schaefer, M. V., Ying, S. C., Benner, S. G., Duan, Y., Wang, Y., & Fendorf, S. (2016). Aquifer arsenic cycling induced by seasonal hydrologic changes within the Yangtze River Basin. *Environmental Science & Technology*, *50*, 3521–3529.

Schlüter, M., Sauter, E. J., Andersen, C. E., Dahlgaard, H., & Dando, P. R. (2004). Spatial distribution and budget for submarine groundwater discharge in Eckernförde Bay (Western Baltic Sea). *Limnology and Oceanography*, *49*(1), 157–167. https://doi.org/10.4319/lo.2004.49.1.0157

Schneider, F., & Hay, S. (2001). Compaction model for quartzose sandstones application to the Garn Formation, Haltenbanken, mid-Norwegian continental shelf. *Marine and Petroleum Geology*, *18*(7), 833–848. https://doi.org/10.1016/S0264-8172(01)00032-0

Scholz, F., Hensen, C., Reitz, A., Romer, R. L., Liebetrau, V., Meixner, A., et al. (2009). Isotopic evidence ($^{87}Sr/^{86}Sr$, $\delta^{7}Li$) for alteration of the oceanic crust at deep-rooted mud volcanoes in the Gulf of Cadiz, NE Atlantic Ocean. *Geochimica et Cosmochimica Acta*, *73*(18), 5444–5459. https://doi.org/10.1016/j.gca.2009.06.004

Schrum, H. N., Murray, R. W., & Gribsholt, B. (2012). Comparison of Rhizon sampling and whole round squeezing for marine sediment pore water. *Scientific Drilling*, *13*, 47–50. https://doi.org/10.5194/sd-13-47-2012

Schubert, M., Kopitz, J., & Chalupnik, S. (2014). Sample volume optimisation for radon-in-water detection by liquid scintillation counting. *Journal of Environmental Radioactivity*, *134*, 109–113. https://doi.org/10.1016/j.jenvrad.2014.03.005

Scott, K. (2015). Integrated Ocean management. In D. R. Rothwell, et al. (Eds.), *The Oxford Handbook of the Law of the Sea* (pp. 467–490). Oxford: Oxford University Press.

Screaton, E. J. (2010). Recent advances in subseafloor hydrogeology: Focus on basement-sediment interactions, subduction zones, and continental slopes. *Hydrogeology Journal*, *18*(7), 1547–1570. https://doi.org/10.1007/s10040-010-0636-7

Seeberg-Elverfeldt, J., Schlüter, M., Feseker, T., & Kölling, M. (2005). Rhizon sampling of pore waters near the sediment-water interface of aquatic systems. *Limnology and Oceanography: Methods*, *3*(8), 361–371.

Seifert, D., & Jensen, J. L. (1999). Using sequential indicator simulatino as a tool in reservoir description: Issues and uncertainties. *Mathematical Geology*, *31*(5), 527–550. https://doi.org/10.1023/A:1007563907124

Serra, O. (1984). *Fundamental of well log interpretation: The acquisition of logging data*. Amsterdam: Elsevier.

Sherman, D., Kannberg, P., & Constable, S. (2017). Surface towed electromagnetic system for mapping of subsea Arctic permafrost. *Earth and Planetary Science Letters*, *460*, 97–104. https://doi.org/10.1016/j.epsl.2016.12.002

Siegel, J., Dugan, B., Lizzarlde, D., Person, M., DeFoor, W., & Miller, N. (2012). Geophysical evidence of a late Pleistocene glaciation and paleo-ice stream on the Atlantic Continental Shelf offshore Massachusetts, USA. *Marine Geology*, *303–306*, 63–74. https://doi.org/10.1016/j.margeo.2012.01.007

Siegel, J., Person, M., Dugan, B., Cohen, D., Lizarralde, D., & Gable, C. W. (2014). Influence of late Pleistocene glaciations on the hydrogeology of the continental shelf offshore Massachusetts, USA. *Geochemistry, Geophysics, Geosystems*, *15*, 4651–4670. https://doi.org/10.1002/2014GC005569

Siemon, B., Christiansen, A. V., & Auken, E. (2009). A review of helicopter-borne electromagnetic methods for groundwater exploration. *Near Surface Geophysics*, *7*(5–6), 629–646. https://doi.org/10.3997/1873-0604.2009043

Siever, R. (1962). A squeezer for extracting interstitial water from modern sediments. *Journal of Sedimentary Research*, *32*(2), 329–331. https://doi.org/10.1306/74D70CC2-2B21-11D7-8648000102C1865D

Solorzano-Rivas, S. C., & Werner, A. D. (2018). On the representation of subsea aquitards in models of offshore fresh groundwater. *Advances in Water Resources*, *112*, 283–294. https://doi.org/10.1016/j.advwatres.2017.11.025

Sommer, S., Linke, P., Pfannkuche, O., Schleicher, T., Deimling, J. S. V., Reitz, A., et al. (2009). Seabed methane emissions and the habitat of frenulate tubeworms on the Captain Arutyunov mud volcano (Gulf of Cadiz). *Open Access Marine Ecology Progress Series*, *382*, 69–86. https://doi.org/10.3354/meps07956

Soulet, G., Delaygue, G., Vallet-Coulomb, C., Böttcher, M. E., Sonzogni, C., Lericolais, G., & Bard, E. (2010). Glacial hydrologic conditions in the Black Sea reconstructed using geochemical pore water profiles. *Earth and Planetary Science Letters*, *296*(1–2), 57–66. https://doi.org/10.1016/j.epsl.2010.04.045

Southgate, H. N., & Möller, N. K. (2000). Fractal properties of coastal profile evolution at Duck, North Carolina. *Journal of Geophysical Research*, *105*(C5), 11,489–11,507. https://doi.org/10.1029/2000JC900021

Souza, W. R., & Voss, C. I. (1987). Analysis of an anisotropic coastal aquifer system using variable-density flow and solute transport simulation. *Journal of Hydrology*, *92*(1–2), 17–41.

Spagnioli, G., Finkenzeller, S., Freudenthal, T., Hoekstra, T., Woolard, M., Storteboom, O., et al. (2015). First deployment of the underwater drill rig MeBo200 in the North Sea and its applications for the geotechnical exploration. In *SPE offshore Europe conference and exhibition*. Aberdeen.

Spechler, R. M. (1994). Saltwater intrusion quality of water in Floridan aquifer system, northeastern Florida (p. 76).

Spinelli, G. A., Giambalvo, E. R., & Fisher, A. T. (2004). Sediment permeability, distribution, and influence on fluxes in oceanic basement. In E. E. Davis, & H. Elderfield (Eds.), *Hydrogeology of the oceanic lithosphere* (pp. 151–188). Cambridge: Cambridge University Press.

Sprenger, M., Stumpp, C., Weiler, M., Aeschbach, W., Allen, S. T., Benettin, P., et al. (2019). The demographics of water: A review of water ages in the critical zone. *Reviews of Geophysics*, *57*, 800–834. https://doi.org/10.1029/2018RG000633

Stakes, D. S., Orange, D., Paduan, J. B., Salamy, K. A., & Maher, N. (1999). Cold-seeps and authigenic carbonate formation in Monterey Bay, California. *Marine Geology*, *159*(1–4), 93–109. https://doi.org/10.1016/S0025-3227(98)00200-X

Stein, S., Russak, A., Sivan, O., Yechieli, Y., Rahav, E., Oren, Y., & Kasher, R. (2016). Saline groundwater from coastal aquifers as a source for desalination. *Environmental Science and Technology*, *50*(4), 1955–1963. https://doi.org/10.1021/acs.est.5b03634

Steiner, Z., Lazar, B., Erez, J., & Turchyn, A. V. (2018). Comparing Rhizon samplers and centrifugation for pore-water separation in studies of the marine carbonate system in sediments. *Limnology and Oceanography: Methods*, *16*(12), 828–839.

Stewart, M., Trompetter, V., & van der Raaij, R. (2002). Age and source of Canterbury plains groundwater, Environment Canterbury.

Stigall, J., & Dugan, B. (2010). Overpressure and earthquake initiated slope failure in the Ursa region, northern Gulf of Mexico. *Journal of Geophysical Research*, *115*, B04101. https://doi.org/10.1029/2009JB006848

Strassmann, K. M., Brennwald, M. S., Peeters, F., & Kipfer, R. (2005). Dissolved noble gases in the pore water of lacustrine sediments as palaeolimnological proxies. *Geochimica et Cosmochimica Acta*, *69*(7), 1665–1674. https://doi.org/10.1016/j.gca.2004.07.037

Strebelle, S. (2002). Conditional simulation of complex geological structures using multiple-point statistics. *Mathematical Geology*, *34*(1), 1–21. https://doi.org/10.1023/A:1014009426274

Sturchio, N. C., Du, X., Purtschert, R., Lehmann, B. E., Sultan, M., Patterson, L. J., et al. (2004). One million year old groundwater in the Sahara revealed by krypton-81 and chlorine-36. *Geophysical Research Letters*, *31*, L05503. https://doi.org/10.1029/2003GL019234

Stuyfzand, P. J., & Raat, K. J. (2010). Benefits and hurdles of using brackish groundwater as a drinking water source in the Netherlands. *Hydrogeology Journal*, *18*(1), 117–130. https://doi.org/10.1007/s10040-009-0527-y

Swart, P. K., Isern, A., & lderfield, H., & McKenzie, J. A. (1993). A summary of interstitial-water geochemistry of Leg 133. In J. A. McKenzie, et al. (Eds.), *Proceedings of ODP 133 scientific results* edited by (pp. 705–721). College Station: Ocean Drilling Program. https://doi.org/10.2973/odp.proc.sr.133.258.1993

Swarzenski, P., Reich, C., Spechler, R., Kindinger, J., & Moore, W. (2001). Using multiple geochemical tracers to characterize the hydrogeology of the submarine spring off crescent beach, Florida. *Chemical Geology*, *179*(1–4), 187–202. https://doi.org/10.1016/S0009-2541(01)00322-9

Swarzenski, P. W., & Reich, C. D. (2000). Re-examining submarine spring off Crescent Beach, FL, US Geological Survey.

Szymczycha, B., Kłostowska, Ż., Kuliński, K., Winogradow, A., Jakacki, J., Klusek, Z., et al. (2018). Deep submarine groundwater discharge indicated by pore water chloride anomalies in the Gulf of Gdańsk, southern Baltic Sea, E3S Web of Conference, 54, 00035.

Talwani, M. (2009). Integrated Ocean Drilling Program (IODP). In V. Gornitz (Ed.), *Encyclopedia of paleoclimatology and ancient environments* (pp. 473–476). Dordrecth: Springer. https://doi.org/10.1007/978-1-4020-4411-3_114

Taniguchi, M., Dulai, H., Burnett, K. M., Santos, I. R., Sugimoto, R., Stieglitz, T., et al. (2019). Submarine groundwater discharge: Updates on its measurement techniques, geophysical drivers, magnitudes and effects. *Frontiers in Environmental Science*, *7*(141). https://doi.org/10.3389/fenvs.2019.00141

Tarasov, L., & Peltier, W. R. (2004). A geophysically constrained large ensemble analysis of the deglacial history of the North American ice-sheet complex. *Quaternary Science Reviews*, *23*(3–4), 359–388. https://doi.org/10.1016/j.quascirev.2003.08.004

Teasdale, P. R., Batley, G. E., Apte, S. C., & Webster, I. T. (1995). Pore water sampling with sediment peepers. *TrAC Trends in Analytical Chemistry*, *14*(6), 250–256. https://doi.org/10.1016/0165-9936(95)91617-2

Thomas, A. T., Reiche, S., Riedel, M., & Clauser, C. (2019). The fate of submarine fresh groundwater reservoirs at the New Jersey shelf, USA. *Hydrogeology Journal*, *27*(7), 2673–2694. https://doi.org/10.1007/s10040-019-01997-y

Tobin, H. J., & Saffer, D. M. (2009). Elevated fluid pressure and extreme mechanical weakness of a plate boundary thrust, Nankai Trough subduction zone. *Geology*, *37*(8), 679–682. https://doi.org/10.1130/G25752A.1

Tomaru, H., Torres, M. E., Matsumoto, R., & Borowski, W. S. (2006). Effect of massive gas hydrate formation on the water isotopic fractionation of the gas hydrate system at Hydrate Ridge, Cascadia margin, offshore Oregon. *Geochemistry, Geophysics, Geosystems*, *7*, Q10001. https://doi.org/10.1029/2005GC001207

Tomonaga, Y., Brennwald, M. S., & Kipfer, R. (2013). Using helium and other noble gases in ocean sediments to characterize active methane seepage off the coast of New Zealand. *Marine Geology*, *344*, 34–40. https://doi.org/10.1016/j.margeo.2013.07.010

Torgersen, T., & Stute, M. (2013). Helium (and other noble gases) as a tool for understanding long timescale groundwater transport. In *Isotope methods for dating old groundwater* (pp. 179–216). Vienna: International Atomic Energy Agency.

Tucker, M. E., & Wright, V. P. (1990). *Carbonate sedimentology* (p. 482). Oxford: Blackwell. https://doi.org/10.1002/9781444314175

Uchupi, E., Driscoll, N., Ballard, R. D., & Bolmer, S. T. (2001). Drainage of late Wisconsin glacial lakes and the morphology and late Quaternary stratigraphy of the new Jersey-southern New England continental shelf and slope. *Marine Geology*, *172*(1–2), 117–145. https://doi.org/10.1016/S0025-3227(00)00106-7

United Nations (2015). World Water Development Report 2015, United Nations.

UN-Water (2020). UN-Water Analytical Brief on Unconventional Water Resources, United Nations, Geneva.

Vail, P. R., Mitchum, R. M., & Thompson, S. (1977). Seismic stratigraphy and global changes of sea level; Part 4, Global cycles of relative changes of sea level. In C. E. Payton (Ed.), *Memoir: American Association of Petroleum Geologists* (pp. 83–97). Tulsa, OK: American Association of Petroleum Geologists.

Van Engelen, J., Oude Essink, G. H. P., Kooi, H., & Bierkens, M. F. P. (2018). On the origins of hypersaline groundwater in the Nile Delta aquifer. *Journal of Hydrology*, *560*, 301–317. https://doi.org/10.1016/j.jhydrol.2018.03.029

van Geldern, R., Baier, A., Subert, H. L., Kowol, S., Balk, L., & Barth, J. A. C. (2014). Pleistocene paleo-groundwater as a pristine fresh water resource—Evidence from stable and radiogenic isotopes. *Science of the Total Environment*, *496*, 107–115. https://doi.org/10.1016/j.scitotenv.2014.07.011

van Geldern, R., & Barth, J. A. (2012). Optimisation of instrument setup and post-run corrections for oxygen and hydrogen stable isotope measurements of water by isotope ratio infrared spectroscopy (IRIS). *Limnology and Oceanography: Methods*, *10*(2), 1024–1036.

van Geldern, R., Hayashi, T., Bottcher, M. E., Mottl, M., Barth, J. A. C., & Stadler, S. (2013). Stable isotope geochemistry of pore waters and marine sediments from the New Jersey shelf: Methane formation and fluid origin. *Geosphere*, *9*(1), 96–112. https://doi.org/10.1130/GES00859.1

Varma, S., & Michael, K. (2012). Impact of multi-purpose aquifer utilisation on a variable-density groundwater flow system in the Gippsland Basin, Australia. *Hydrogeology Journal*, *20*(1), 119–134. https://doi.org/10.1007/s10040-011-0800-8

Villarreal, D., & LeVoy, L. (2010). Oil and gas exploration and development agreements. *Energy & Mineral Law Institute*, *31*, 323–375.

Voris, H. K. (2000). Maps of Pleistocene sea levels in Southeast Asia: Shorelines, river systems and time durations. *Journal of Biogeography*, *27*(5), 1153–1167. https://doi.org/10.1046/j.1365-2699.2000.00489.x

Voss, C. I., & Souza, W. R. (1987). Variable density flow and solute transport simulation of regional aquifers containing a narrow freshwater-saltwater transition zone. *Water Resources Research*, *23*(10), 1851–1866. https://doi.org/10.1029/WR023i010p01851

Vrolijk, P., Fisher, A., & Gieskes, J. (1991). Geochemical and geothermal evidence for fluid migration in the Barbados Accretionary Prism (ODP leg 110). *Geophysical Research Letters*, *18*(5), 947–950. https://doi.org/10.1029/91GL00913

Water Reuse Association (2012). Seawater desalinisation costs.

Waxman, M. H., & Smits, L. J. M. (1968). Electrical conductivities in oil-bearing shaly sands. *Society of Petroleum Engineers Journal*, *8*(02), 107–122. https://doi.org/10.2118/1863-A

Wentworth, C. K. (1939). Specific gravity of sea-water and the Ghyben-Herzberg ratio in Hawaii. *Eos, Transactions of the American Geophysical Union*, *20*(4), 690–692. https://doi.org/10.1029/TR020i004p00690

Werner, A. D., Bakker, M., Post, V. E., Vandenbohede, A., Lu, C., Ataie-Ashtiani, B., et al. (2013). Seawater intrusion processes, investigation and management: Recent advances and future challenges. *Advances in Water Resources*, *51*, 3–26. https://doi.org/10.1016/j.advwatres.2012.03.004

Werner, A. D., & Robinson, N. I. (2018). Revisiting analytical solutions for steady interface flow in subsea aquifers: Aquitard salinity effects. *Advances in Water Resources*, *116*, 117–126. https://doi.org/10.1016/j.advwatres.2018.01.002

Weymer, B. A., Wernette, P. A., Everett, M. E., Pondthai, P., Jegen, M., & Micallef, A. (2020). Multi-layered high permeability conduits connecting onshore and offshore coastal aquifers. *Frontiers in Marine Science*, *7*(903). https://doi.org/10.3389/fmars.2020.531293

Whiticar, M. J. (2002). Diagenetic relationships of methanogenesis, nutrients, acoustic turbidity, pockmarks and freshwater seepages in Eckernförde Bay. *Marine Geology*, *182*(1–2), 29–53. https://doi.org/10.1016/S0025-3227(01)00227-4

Wieck, J., Person, M., & Strayer, L. (1995). A finite element method for simulating fault block motion and hydrothermal fluid flow within rifting basins. *Water Resources Research*, *31*(12), 3241–3258. https://doi.org/10.1029/95WR02114

Wilson, A. M. (2003). The occurrence and chemical implications of geothermal convection of seawater in continental shelves. *Geophysical Research Letters*, *30*(21), 2127. https://doi.org/10.1029/2003GL018499

Wilson, A. M. (2005). Fresh and saline groundwater discharge to the ocean: A regional perspective. *Water Resources Research*, *41*, W02016. https://doi.org/10.1029/2004WR003399

Wood, A. B. (1941). *A textbook of sound*. New York: Macmillan.

Xu, Z., Bassett, S. W., Hu, B., & Dyer, S. B. (2016). Scientific reports (2016). Long distance seawater intrusion through a karst conduit network in the Woodville Karst Plain, Florida. *Scientific Reports*, *6*(1), 32235. https://doi.org/10.1038/srep32235

Xu, Z., Hu, B. X., & Ye, M. (2018). Numerical modeling and sensitivity analysis of seawater intrusion in a dual-permeability coastal karst aquifer with conduit networks. *Hydrology and Earth System Sciences*, *22*(1), 221–239. https://doi.org/10.5194/hess-22-221-2018

Yehudai, M., Lazar, B., Bar, N., Kiro, Y., Agnon, A., Shaked, Y., & Stein, M. (2017). U-Th dating of calcite corals from the Gulf of Aqaba. *Geochimica et Cosmochimica Acta*, *198*, 285–298. https://doi.org/10.1016/j.gca.2016.11.005

You, Y., & Person, M. (2008). Role of pore pressure generation in sediment transport within half-grabens. *Basin Research*, *20*(3), 419–429. https://doi.org/10.1111/j.1365-2117.2008.00357.x

Yu, X., & Michael, H. A. (2019a). Offshore pumping impacts onshore groundwater resources and land subsidence. *Geophysical Research Letters*, *46*, 2553–2562. https://doi.org/10.1029/2019GL081910

Yu, X., & Michael, H. A. (2019b). Mechanisms, configuration typology, and vulnerability of pumping-induced seawater intrusion in heterogeneous aquifers. *Advances in Water Resources*, *128*, 117–128. https://doi.org/10.1016/j.advwatres.2019.04.013

Yuan, J., & Edwards, R. N. (2000). The assessment of marine gas hydrates through electrical remote sounding: Hydrate without a BSR? *Geophysical Research Letters*, *27*(16), 2397–2400. https://doi.org/10.1029/2000GL011585

Zamrsky, D., Karssenberg, M. E., Cohen, K. M., Bierkens, M. F. P., & Oude Essink, G. H. P. (2020). Geological heterogeneity of coastal unconsolidated groundwater systems worldwide and its influence on offshore fresh groundwater occurrence. *Frontiers in Earth Science*, *7*(339). https://doi.org/10.3389/feart.2019.00339

Zecchin, M., & Catuneanu, O. (2013). High-resolution sequence stratigraphy of clastic shelves I: Units and bounding surfaces. *Marine and Petroleum Geology*, *39*(1), 1–25. https://doi.org/10.1016/j.marpetgeo.2012.08.015

Zecchin, M., & Catuneanu, O. (2015). High-resolution sequence stratigraphy of clastic shelves III: Applications to reservoir geology. *Marine and Petroleum Geology*, *62*, 161–175. https://doi.org/10.1016/j.marpetgeo.2014.08.025

Zhang, Y., Person, M., Voller, V., Cohen, D., McIntosh, J., & Grapenthin, R. (2018). Hydromechanical impacts of Pleistocene glaciations on pore fluid pressure evolution, rock failure, and brine migration within sedimentary basins and the crystalline basement. *Water Resources Research*, *54*, 7577–7602. https://doi.org/10.1029/2017WR022464

Zwinger, T., Hartikainen, J., & Cohen, D. (2019). A high-resolution coupled permafrost-ice sheet model, Geophysical Research Abstracts, 21.